THE EFFECTS OF NONEXCITABLE REGIONS ON SIGNAL PROPAGATION IN EXCITABLE MEDIA: PROPAGATION FAILURE AND REFLECTION

by

Timothy J. Lewis

A dissertation submitted to the faculty of
The University of Utah
in partial fulfillment of the requirements for the degree of

Doctor of Philosophy

Department of Mathematics

The University of Utah

December 1998

Copyright © Timothy J. Lewis 1998

All Rights Reserved

THE UNIVERSITY OF UTAH GRADUATE SCHOOL

SUPERVISORY COMMITTEE APPROVAL

of a dissertation submitted by

Timothy J. Lewis

This dissertation has been read by each member of the following supervisory committee and by majority vote has been found to be satisfactory.

	Chair: James P. Keener
	Peter W. Alfeld
	David J. Eyre
	Aaron L. Fogelson
	Mark A. Lewis

THE UNIVERSITY OF UTAH GRADUATE SCHOOL

FINAL READING APPROVAL

To the Graduate Council of the University of Utah:

I have read the dissertation of Timothy J. Lewis in its final form and have found that (1) its format, citations, and bibliographic style are consistent and acceptable; (2) its illustrative materials including figures, tables, and charts are in place; and (3) the final manuscript is satisfactory to the Supervisory Committee and is ready for submission to The Graduate School.

Date

James P. Keener
Chair, Supervisory Committee

Approved for the Major Department

James A. Carlson
Chair/Dean

Approved for the Graduate Council

David S. Chapman
Dean of The Graduate School

ABSTRACT

Most physical excitable media have regions of depressed excitability and in many of these systems, the interaction of waves of excitation and these region is of the utmost interest. In the heart, regions of this nature can disrupt the normal wave of electrical excitation and trigger the onset of dangerous arrhythmias. In order to get insight into the effects of regions of reduced excitability, we consider a model in which the regions are idealized as nonexcitable. We show that the arrhythmia-generating phenomena of propagation failure and reflection occur in the model and attempt to elucidate the dynamical mechanisms underlying these behaviors.

We study propagation failure using the one-dimensional scalar bistable equation with a passive "gap" region. By applying ordering principles for this type of equation, the problem of finding conditions for block is reduced to finding conditions for the existence of steady states solutions. We present a geometrical method that allows one to easily compute the critical gap length above which a steady state solution, and thus block, first occurs. The method also helps uncover the general bifurcation structure of the problem including the stability of the steady state solutions. In obtaining these results, we characterize the relationship between the properties of the system and propagation failure.

Again, we consider wavefront propagation in the one-dimensional reaction diffusion equation with a passive gap region; however we now include recovery dynamics. We numerically explore the behavior of the system for various gap lengths and discover exotic reflection behavior. We introduce a new one variable model for excitable systems and by studying coupled cells described by these dynamics, we demonstrate that reflection is associated with transient dynamics around an unstable periodic orbit. This unstable periodic orbit is shown to be a continuation of the antiphase orbit of coupled oscillators. Also, we suggest two ways that stable echo

oscillations can arise in spatially coupled excitable media and conjecture that some tachycardias in the atrioventricular node could be explained by these oscillations.

Finally, we show simulations of activity in a two-dimensional excitable medium with a region of passive diffusion and describe a novel mechanism for the generation of spiral waves that involves reflection. This mechanism appears to be the most physiologically viable mechanism for the induction of the potentially fatal arrhythmias associated with spiral wave dynamics that has been proposed to date.

To Mouse

CONTENTS

LIST OF FIGURES

ACKNOWLEDGEMENTS

I would like to thank:

My committee members Peter Alfeld, David Eyre, Aaron Fogelson, Mark Lewis and Jim Keener for comments on this manuscript.

The people in the CNLD at McGill, especially MG, for getting me started.

Everyone, past and present, permanent and transient, in the Math Biology group who has helped make my stay in Utah a very enjoyable and profitable experience.

My distinguished coauthors on the other things: Terrible Topo II Timmy [25], Pretty Pattern Pejman and Dangerous Danny G [58], and the one I now call Jim [38].

Jim Keener for providing excellent teaching, a great research environment, countless value discussions (academic and otherwise) ... and a most formidable biking companion.

Brad Peercy for doing all the last minute things.

My family and friends for their never-ending love, support ... and amusement.

Svetlana die Gewaltige for providing the spark when it was (so often) needed ... and for so much more.

This work was supported in part by NSF Grants #9303502 and #9626334 to James P. Keener.

CHAPTER 1

INTRODUCTION

1.1 The Gap Model

This thesis concerns wave propagation in excitable media that contain local regions of reduced excitability. Specifically, we study the reaction diffusion equations

$$\begin{cases} u_t = (D(x)u_x)_x + s(x)f(u,w), \\ w_t = s(x)g(u,w). \end{cases} \tag{1.1}$$

In this system of equations, u is a diffusing excitability variable and w (in general a vector) is a slow recovery variable. The spatial inhomogeneity that will be considered is an abrupt decrease in the magnitudes of the excitability reaction term and diffusion coefficient followed by an abrupt return to the original magnitudes. Specifically, the functions D and s are defined piecewise as follows:

$$D(x) = \begin{cases} D, & 0 \le x < L, \\ 1, & \text{otherwise}, \end{cases} \tag{1.2}$$

and

$$s(x) = \begin{cases} \delta, & 0 \le x < L, \\ 1, & \text{otherwise}. \end{cases} \tag{1.3}$$

We will often refer to the region of low excitability ($0 \le x < L$) as the "gap" and the full model as the "gap" model. For almost all cases considered, δ will be zero corresponding to purely passive diffusion in the gap.

Local inhomogeneities such as the one described above occur in most physical excitable systems and in many of these systems, the ability of waves of excitation to be successfully transmitted over spatial regions with depressed excitability

and/or increased axial resistance is of the utmost interest. Examples appear in neurophysiology [53, 18], calcium dynamics (CICR) of muscle cells [62], population genetics [20], ecology and combustion dynamics [68]. Although the results presented in this thesis are quite general, the motivating application comes from cardiac electrophysiology. Regions of decreased excitability occur in the heart in both sickness and health and it is suggested here that understanding the interaction of waves of excitability with these regions is essential to understanding transitions between normal and pathological electrical behavior in the heart.

1.2 Applications to Cardiac Electrophysiology

1.2.1 The heart as an excitable medium

Although there is no precise definition of excitable media, they can be characterized by their behavior under external stimulation or perturbation [45]. When a perturbation above a small but sufficient amplitude is delivered to an excitable medium in a quiescent state, an autocatalytic process is activated that induces a large excursion in the state variable(s) (i.e., variables describing the state of the system). This is followed by a decay back to the quiescent state. If a smaller perturbation is given, the system will remain close to the quiescent state. This is known as threshold behavior, and reflects the nonlinearity of excitable systems. In spatially distributed systems where the excitability variable can diffuse down its gradient, local excitation can spread and waves of excitation can propagate through the medium.

One of the most important features of most cardiac cells is that they are electrically excitable. Another important feature is that cells are electrically coupled, so that the electrical activity in one cell can spread to its neighbors via electrical diffusion and lead to their excitation. These features imply that heart tissue is an excitable reaction-diffusion system. In fact, when nondimensionalized, equations describing the electrical activity of cardiac tissue, which can be derived by first principles, are of the form of system (1.1). The variable u can be thought of as the electrical potential across the cell membrane. The reaction term f would then be

the sum of the ionic currents that flow through the membrane and drive changes in the transmembrane potential, and the variable w would describe the gating dynamics that modulate the ionic currents.

Because heart tissue is excitable, it exhibits the threshold behavior described above. At rest, cardiac tissue is polarized, however when electrically perturbed, the cells undergo a large change in transmembrane potential. This change is driven by an autocatalytic activation of excitability currents that rapidly depolarize the cell membrane. These depolarizing currents then turn off and recovery currents (of the opposite sign) take over and repolarize the membrane. In electrophysiology, the full process is called an action potential. Normally, about once per second, an action potential propagates as a wave of excitation through the entire heart in an orderly fashion. This leads to the contraction of the cardiac muscle tissue (myocardium) and the pumping of blood.

1.2.2 The normal activation sequence in the heart

The ability of the heart to pump blood to the body relies on the rhythmic and staggered, but well-timed, contractions of the atrial and ventricular myocardium. A contraction is a result of electrical excitation spreading through the heart in a coordinated manner. The normal sequence of activation (i.e., electrical excitation) begins at the sino-atrial (SA) node, which is located high in the right atrium. The SA node acts as a pacemaker: it spontaneously depolarizes in a periodic fashion, and thus initiates the wave of cardiac excitation. From the SA node, the excitation spreads through the right atrium to the left atrium (both of which contract, and pump blood into the relaxed ventricles) and to the atrioventricular (AV) node. The AV node is the sole electrical link between the atria and the ventricles and exhibits slow conduction. Following this slow conduction through the AV node, the wave of excitation reaches the top of a highly ramified specialized conduction system. The initial branch of this system is called the bundle of His and the subsequent branching structure is composed of tissue called Purkinje fibers. The wave of excitation rapidly propagates through the multiple branching generations of

the His-Purkinje system, which generally line the surface of and are embedded in the ventricular endocardium. Excitation then spreads to the ventricular endocardium and propagates through the myocardium to the epicardium, causing a ventricular contraction that pumps blood to the body. Disruptions of this normal spread of excitation can result in cardiac arrhythmias that encompass a wide variety of complex behavior. Some of these cardiac arrhythmias can be benign, while others can be fatal.

1.2.3 Where's the gap?

When a person has a heart attack, a coronary artery is occluded. Occlusions substantially reduce or entirely cut off blood flow to a region of cardiac tissue, and thus this tissue becomes ischemic (sick) and begins to die. One of the properties of ischemic tissue is that there is an accumulation of extracellular potassium resulting in the decrease in the normal polarization of the cell membrane of the tissue in the ischemic region. This, in turn, causes an increase in the resting level of inactivation of the sodium current, the primary current for excitation, and thus leads to a reduction in excitability. If the region remains cut off from its blood flow for an extended period of time, the tissue will die and scar tissue known as an infarct will form. Infarcted regions have very little, if any, viable excitable tissue and cells are largely electrically decoupled from one another. It is thought that current is only allowed to flow passively through the extracellular space in the region. Generally, ischemic and infarcted regions are surrounded by healthy tissue, and thus both situations fall into the framework of our gap model. In fact, the fibrous structure of heart muscle and the truly cable-like structure of the Purkinje fibres makes the one spatial dimension in the model a good approximation in many situations.

Also, the gap model is a good simple model to study dynamics of wave propagation through the atrioventricular (AV) node. The slow conduction in the AV node is a manifestation of high resistivity (small D) and low excitability, which can become even lower under conditions such as increased heart rate, increased parasympathetic (vagal) tone, etc. On the other hand, the atrial tissue on the

proximal side of the AV node and the tissue in the bundle of His on the distal side of the AV node are highly excitable, thus the framework agrees with the gap model.

1.2.4 Effects of gaps

The main reason the systems mentioned above are of extreme interest is that inhomogeneities can disrupt waves of activation in heart tissue. In fact, the interactions of incoming waves of excitation and local inhomogeneities are thought to be involved in wave block and the induction of cardiac arrythmias.

In pathological situations, the AV node only lets a fraction of waves of excitation through to the ventricles (e.g., Wenckebach rhythms) and thus the cardiac output can drop substantially. In fact, sometimes all signals stemming from the SA node are blocked resulting in a behavior known as AV dissociation. In this case, a region below the AV node must become spontaneously active and take over the pacemaking responsibility. When this happens, the heart rate is extremely low, there is little or no nervous control of heart rate, and there is no coordination between the atrial contractions and ventricular contractions. This, of course, results in a very low cardiac output, which changes little in response to increased oxygen demand and other metabolic variations.

The effects of the interaction of waves of excitation and ischemic or infarcted regions of tissue following a heart attack can be even worse than AV nodal arrhythmias. Although the exact mechanism is unresolved, it is thought that this interaction results in the induction of persistent disorganized reentrant rhythms known as tachycardia and fibrillation. When this behavior occurs in the ventricles, it causes nonsynchronous contraction of the ventricular muscle and very little blood can be pumped into the circulatory system. If these rhythms are not terminated, the death of the victim can occur within minutes.

1.2.5 An experimental gap model

It should be noted that the AV node and infarcted and ischemic tissue are quite heterogeneous in themselves; however the gap model seems to be a simple, yet reasonable, model to study in order to gain insight to the dynamics of the much

more complicated physiological systems. A more direct application of the gap model to systems in cardiac electrophysiology is found when the model is compared to an experimental preparation known as the sucrose gap experiment [7, 31, 29]. The sucrose gap preparation is used as a simple experimental model for infarcted or ischemic tissue as well as the AV node, and exhibits much of the same behavior as these. The preparation consists of a Purkinje fibre or strip of ventricular tissue lying in a bath that is composed of three distinct sections. In the outer two sections, the bath consists of a solution that mimics the extracellular medium in healthy tissue, thus the portions of tissue in these section retain their normal excitation properties. The middle section contains an ion-free, high glucose solution that extinguishes or at least greatly limits the excitability of the portion of tissue in this section. A variable resistor that connects the outer two sections of the bath is used to vary the level of resistance across the gap. Thus, the gap model mathematically describes the sucrose gap experiment quite well.

1.3 Outline

The work in this thesis deals with two aspects of the gap problem. One aspect is the study of conduction block. In this study, we use the scalar version of system (1.1) that ignores recovery. The other aspect that we consider is the study of an exotic behavior known as reflection that can be seen under certain conditions when recovery is included.

Often the time-scales involved in recovery dynamics are much slower than those for excitation, therefore we can address questions concerning the propagation of waves of excitation by ignoring recovery dynamics (i.e., taking w to be constant) and using only the equation for u. This scalar partial differential equation is much easier to handle than the nonscalar case that we have when recovery is included. In Chapter 2, we consider the problem when recovery is not included in the gap model and describe conditions that lead to failure of wavefronts to be transmitted across the gap (conduction block). Finally, we discuss the implications of our results to cardiac dynamics.

The scalar case, where recovery dynamics are not included, fails to encompass a great deal of interesting behavior that the full system can exhibit. In Chapter 3, we study a behavior that the system can produce only when recovery dynamics are present. We describe a situation in which a wave of excitation traveling towards that gap not only successfully traverses the gap, but also starts a wave in the retrograde direction. This behavior is known as reflection. Reflection is seen in sucrose gap experiments and is thought to be responsible for triggering AV nodal tachycardias as well as reentrant cardiac arrhythmias. Chapter 3 attempts to uncover the dynamical mechanism underlying this behavior and suggests how the behavior can give rise to the arrhythmias mentioned above.

CHAPTER 2

PROPAGATION FAILURE

2.1 The Scalar Gap Problem

When considering a situation where waves of excitation are propagating through an inhomogeneous medium, it is important to address the questions: when is a region of inexcitability or depressed excitability large enough to prevent a wave of excitation from being successfully transmitted through the region and how do the properties of the excitable medium affect this? For instance, in the heart, wave block itself can be a serious arrhythmia or it can lead to fatal arrhythmias.

In order to gain insight into this issue, we study a simple spatially distributed excitable system, the bistable reaction-diffusion equation with a passive "gap" region

$$u_t = (D(x)u_x)_x + s(x)f(u), \tag{2.1}$$

where the functions D and s are piecewise defined as follows

$$D(x) = \begin{cases} D, & 0 \le x < L, \\ 1, & \text{otherwise}, \end{cases} \tag{2.2}$$

and

$$s(x) = \begin{cases} 0, & 0 \le x < L, \\ 1, & \text{otherwise}. \end{cases} \tag{2.3}$$

In the examples provided throughout this chapter, the reaction term f will be idealized to be the cubic function

$$f(u) = u(1-u)(u-\alpha), \qquad 0 < \alpha < \frac{1}{2}. \tag{2.4}$$

However, it should be noted that the results directly apply to the more general case $f \in C^1(R)$ satisfying

$$\begin{array}{c} f(0) = f(\alpha) = f(1) = 0,\ 0 < \alpha < 1, \\ f(u) < 0, \quad 0 < u < \alpha, \\ f(u) > 0, \quad \alpha < u < 1, \\ f'(0) \neq 0 \neq f'(1), \\ \int_0^1 f(u)\, du > 0. \end{array} \tag{2.5}$$

Also, the results need only be slightly modified to apply to different restrictions on f (e.g., a change of sign in the integral constraint).

The partial differential equation (PDE) (2.1) is one of the simplest caricatures of the physical system under consideration, because it has no recovery variables and has simple dynamics in the gap. However, this simplicity is the key to gaining an understanding of many aspects of the more detailed problem, because one can analyze the simple system much more easily than the full system, and therefore get useful insight into the much more complicated physical problem.

The scalar gap problem has been studied by Sneyd and Sherratt [62] in the context of Calcium-induced Calcium Release (CICR). However, they only consider the very special case of a piecewise linear discontinuous reaction term f and do not push the analysis very far. On the other hand, Fife and Peletier [20] considered a more general case of the above problem, which was inspired by population genetics. They model "gap" dynamics as a region with a decreased non-constant reaction term. By considering a special case of the Fife and Peletier problem and a more general case of Sneyd and Sherratt, both of their results can be extended. These results will be discussed later in the chapter; however now we turn to the case of a homogeneous cable for background needed to understand the gap problem.

2.2 The Homogeneous Cable

Before attacking the problem of how inhomogeneities effect signal propagation in a one-dimensional bistable system, it will be useful to start by considering the case of a uniform cable and describe classical results concerning steady state solutions, traveling wave dynamics, and threshold properties. The results themselves are

of interest here, but more importantly, an understanding of the techniques with which the results are obtained will be essential for understanding results for the inhomogeneous cable. Specifically, the type of phase plane analysis and super- and subsolution techniques that are used in the analysis of the homogeneous cable will be used extensively in the analysis of the inhomogeneous system. For this reason, we will state pertinent theorems and sketch their proofs. More detail will be provided when it is applicable to the inhomogeneous case.

The equation describing a scalar one-dimensional homogeneous excitable medium is

$$u_t = Du_{xx} + f(u). \tag{2.6}$$

where f is as described above. Without loss of generality, we will set $D = 1$, because we can rescale space as $x/\sqrt{D}$.

2.2.1 Steady state solutions

Steady state solutions to equation (2.6) can be found by setting $u_t = 0$ and studying the resulting second order ordinary differential equation

$$u_{xx} + f(u) = 0. \tag{2.7}$$

Obviously there exists three spatially uniform ($u_x = 0$) steady states where $f(u) = 0$. These are $u(x) = 0$ and $u(x) = 1$, which are stable as in the nonspatial case, and $u(x) = \alpha$, which is unstable. However, there are nonuniform steady states as well. The nonuniform steady state solutions of interest here have $u_x(\pm\infty) = 0$ and $0 \leq u \leq 1$. Up to translation invariance (and reflection invariance in case (ii)), there is exactly one of these solutions for a given reaction term, f.

Theorem 2.1 *The following lists the cases for nonuniform steady state solutions to equation (2.6):*
(i) There exists a family of steady states, $u(x - \xi)$, with boundary conditions $u(\pm\infty) = 0$, $u_x(\pm\infty) = 0$ if and only if $\int_0^1 f(u)du > 0$. Furthermore, u is

symmetric around $x = \xi$, $0 < u < 1$, $u_x > 0$ *for* $x < \xi$ *and* $u_x < 0$ *for* $x > \xi$. *The maximum of* $|u_x|$ *occurs when* $u = \alpha$. *Here and below* ξ *is arbitrary; this implies that the solutions are translation invariant.*

(ii) There exists a family of steady states, $u(x - \xi)$, *with boundary conditions* $u(\infty) = 1$ *and* $u(-\infty) = 0$ *and* $u_x(\pm\infty) = 0$, *if and only if* $\int_0^1 f(u)du = 0$ *(the equal area condition). Furthermore,* u *is monotonically increasing and* $0 < u < 1$. *The maximum of* $|u_x|$ *occurs when* $u = \alpha$. *(note that a mirror image of this solution can be found by substituting* $-x$ *for* x*).*

(iii) There exists a family of steady states, $u(x - \xi)$, *with boundary conditions* $u(\pm\infty) = 1$, $u_x(\pm\infty) = 0$ *if and only if* $\int_0^1 f(u)du < 0$. *Furthermore,* u *is symmetric around* $x = \xi$, $0 < u < 1$, $u_x < 0$ *for* $x < \xi$ *and* $u_x > 0$ *for* $x > \xi$. *The maximum of* $|u_x|$ *occurs when* $u = \alpha$.

Figure 2.1 shows examples of these three types of solutions for a cubic f with $\alpha = 0.3$. Before considering any of the individual cases, notice the following algebraic fact about equation (2.7). By multiplying equation (2.7) by $u_x dx$ and integrating, we get

$$\int_{-\infty}^{\bar{x}} u_{xx} u_x dx = -\int_{-\infty}^{\bar{x}} f(u) u_x dx.$$

Assuming u is monotonic in x (a technical condition that can usually be worked around by piecing solutions together), there is a change of variables $u_x dx = du$ that results in the equation

$$\frac{u_x^2}{2}\Big|_{-\infty}^{\bar{x}} = -\int_0^{u(\bar{x})} f(u)du = -F(u(\bar{x})),$$

$$u_x^2(x) = -2F(u(x)). \tag{2.8}$$

The solutions in the above theorem can easily be shown to exist for the appropriate conditions by using this property and examining the $w - u$ phase plane of the system

$$\begin{cases} u_x = w, \\ w_x = -f(u), \end{cases} \tag{2.9}$$

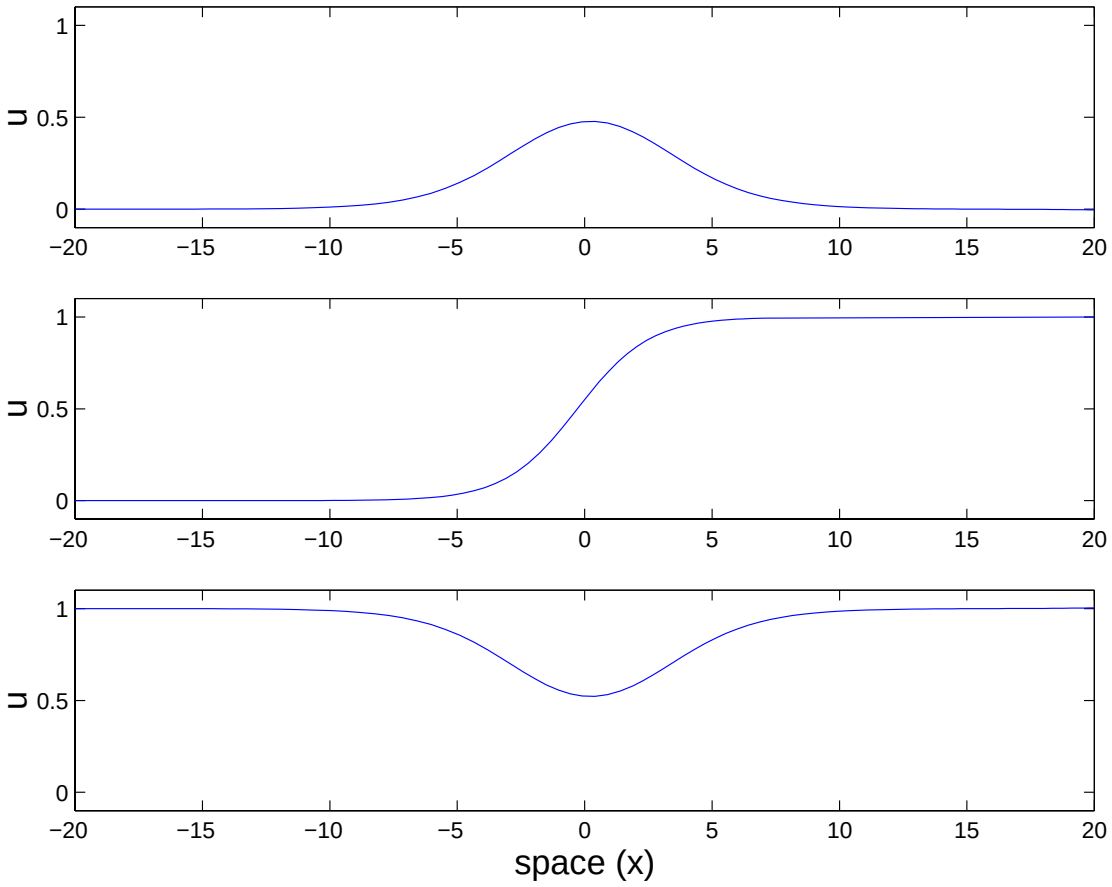

Figure 2.1. Three types of steady state solutions for $\int_0^1 f(u)du > 0$ (top), $\int_0^1 f(u)du = 0$ (middle), $\int_0^1 f(u)du < 0$ (bottom). Specifically, f is cubic with $\alpha = 0.3$, 0.5 and 0.7 from top to bottom.

which is equivalent to equation (2.7). This system has fixed points at $(0,0)$, $(\alpha,0)$, and $(1,0)$ corresponding to the uniform steady states. The fixed points at $(0,0)$ and $(1,0)$ are saddle points and the fixed point at $(\alpha,0)$ is a center.

Now let us consider the case (i). The example of the phase plane for cubic f is shown in Figure 2.2, but the phase plane for any f of the form (2.5) is qualitatively the same. Note that the boundary condition at $x = -\infty$ is associated with the point (0,0). Recall that (0,0) is a saddle point, and therefore it is required that the solution lives on the portion of unstable manifold of (0,0) projecting into the region where $w > 0$. The boundary condition at $x = \infty$ is also associated with (0,0) and this requires the solution to live on the stable manifold of $(0,0)$. Thus, we are searching for a homoclinic orbit.

Integrating forward along the unstable manifold of (0,0), w increases until $u = \alpha$ and then begins to decreases (as a result of the sign of f). By property (2.8), the trajectory hits $w = 0$ at $u = \bar{u}_A < 1$ where $\int_0^{\bar{u}_A} f(u)du = 0$. However, this can happen if and only if $\int_0^1 f(u)du > 0$. Because $u < 1$ at this crossing point, the symmetry of the equations requires that this trajectory asymptotically approaches its starting point $(0,0)$ as $x \to \infty$ and thus we have found the homoclinic orbit. In doing so, we have constructed a case (i) solution.

The proof for the existence of the solutions in case (iii) is identical to that for case (i) after applying the change of variable $u \to (1-u)$.

For the intermediate case (ii), solutions were first shown to exist by Kanel [35] by using property (2.8). Suppose $u(x)$ is a case (ii) solution. If the upper limit of x in property (2.8) is set to ∞, then the left-hand side of equation (2.8) is 0, since $u_x(\pm\infty) = 0$. Thus, because $u = 1$ is associated with the upper limit we have chosen, it follows that $\int_0^1 f(u)du = 0$.

On the other hand, if $\int_0^1 f(u)du = 0$, then by an argument similar to that for the existence of case (i), we see that the unstable manifold of (0,0) hits $w = 0$ at $u = 1$. This trajectory perfectly describes a case (ii) solution. □

In case (ii), the steady state is manifested as a heteroclinic connection between $(0,0)$ and $(1,0)$ in the phase plane (see an example of this in Figure 2.3). This

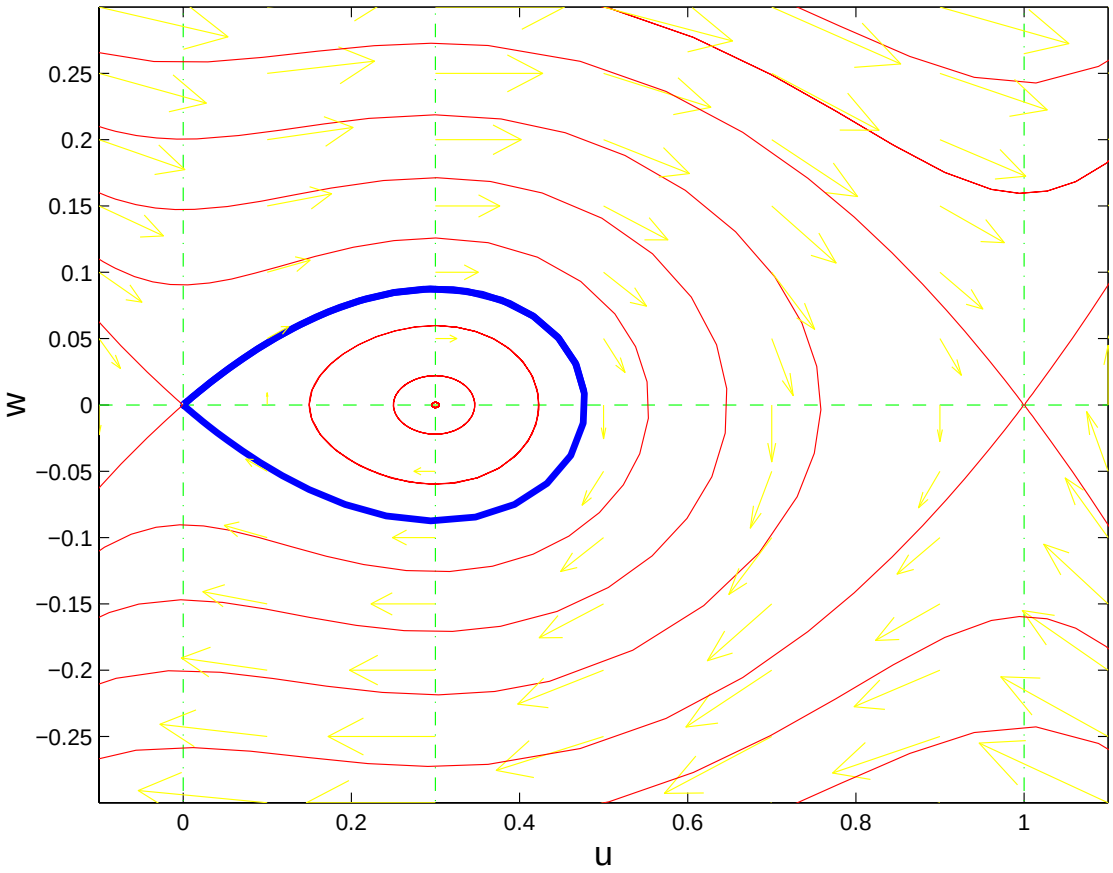

Figure 2.2. Phase plane for equation (2.7) with $\int_0^1 f(u)du > 0$ (cubic f with $\alpha = 0.3$). The thick trajectory is the homoclinic orbit. Thin lines show other trajectories and light arrows give the vector field for the flow.

solution is known as a standing wave and is a special case of traveling waves, which are discussed below.

2.2.2 Traveling wavefronts

In the absence of any inhomogeneities, signal transmission over long distances occurs entirely as a propagated wavefront in the excitable medium. Figure 2.4 shows an example of this. Initially, the medium is excited $u = 1$ for $x > 25$ and at rest $u = 0$ for $x < 25$. The sharp transition in u causes u to diffuse down its gradient into the region of the medium immediately in front (to the left) of the excited region. This increases u in this region past threshold, $u > \alpha$. Above threshold, an autocatalytic production of u is initiated and u rapidly increases towards the excited state $u = 1$. Thus, the sharp transition in u, which is the wavefront, is shifted to the left (although smoothed). This process is repeated continuously and the wavefront propagates through the medium.

The wavefronts can be understood mathematically as a traveling wave solutions of equation (2.6). These solutions are of the form $u(x,t) = U(x + ct - \xi)$ such that $U(\infty) = 1$ and $U(-\infty) = 0$ (see Figure 2.4). The parameter c is the speed of the traveling wavefront and is determined by the reaction term f.

Theorem 2.2 *For fixed $f(u)$ of form (2.5), there is a unique speed c for which there is a unique traveling wave solution to equation (2.6). The traveling wave solution is of the form $u(x,t) = U(x + ct - \xi)$ with arbitrary ξ and provides a transition between $u = 0$ and $u = 1$ such that $0 \leq U \leq 1$ and $U(\infty) = 1$ and $U(-\infty) = 0$ with $U_x(\pm\infty) = 0$.*

This theorem is due to Aronson and Weinberger [3], who also showed that U is strictly increasing and that the wave speed c is positive for $\int_0^1 f(u)du > 0$ and negative for $\int_0^1 f(u)du < 0$. The intermediate case were $\int_0^1 f(u)du = 0$ is a zero speed wave or standing wave described above. The following provides the basis of their proof for the case $\int_0^1 f(u)du > 0$.

When the independent variables, (x,t), are changed to traveling wave coordi-

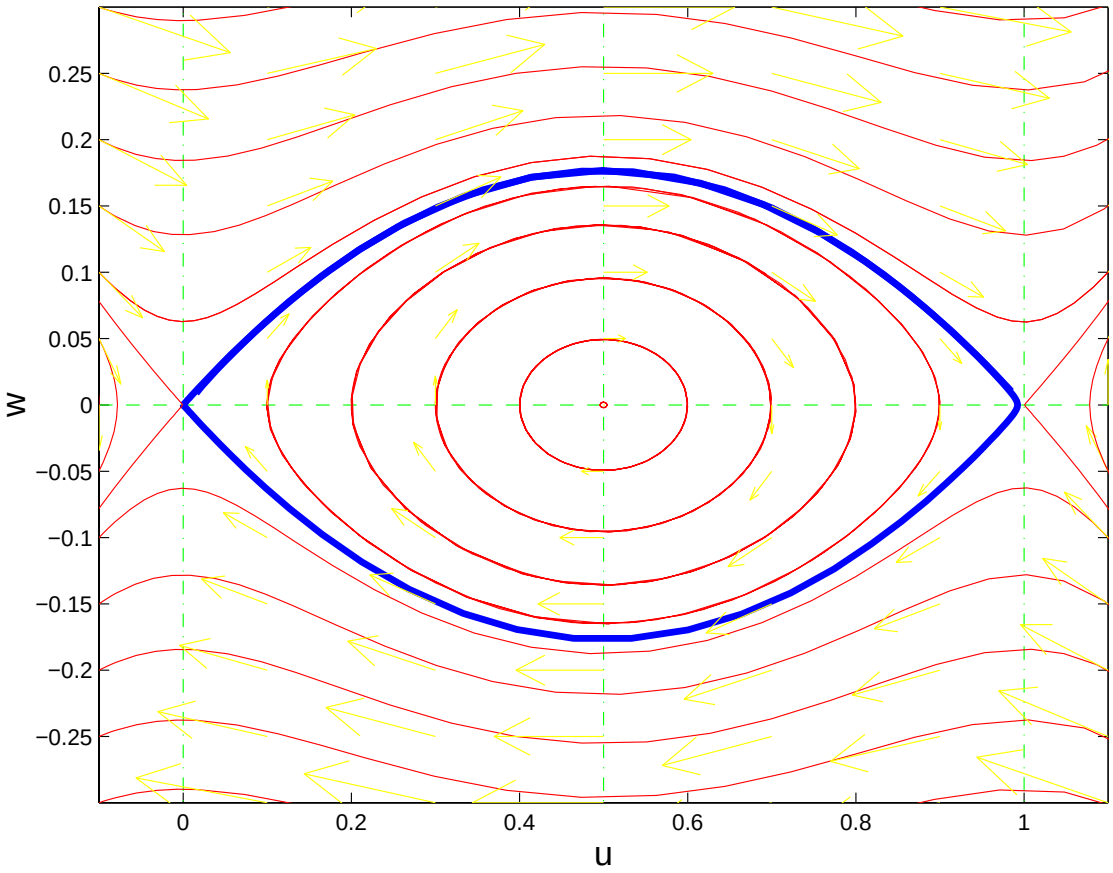

Figure 2.3. Phase plane for equation (2.7) with $\int_0^1 f(u)du = 0$ (cubic f with $\alpha = 0.5$). The thick trajectory is the heteroclinic orbit. Thin lines show other trajectories and light arrows give the vector field for the flow.

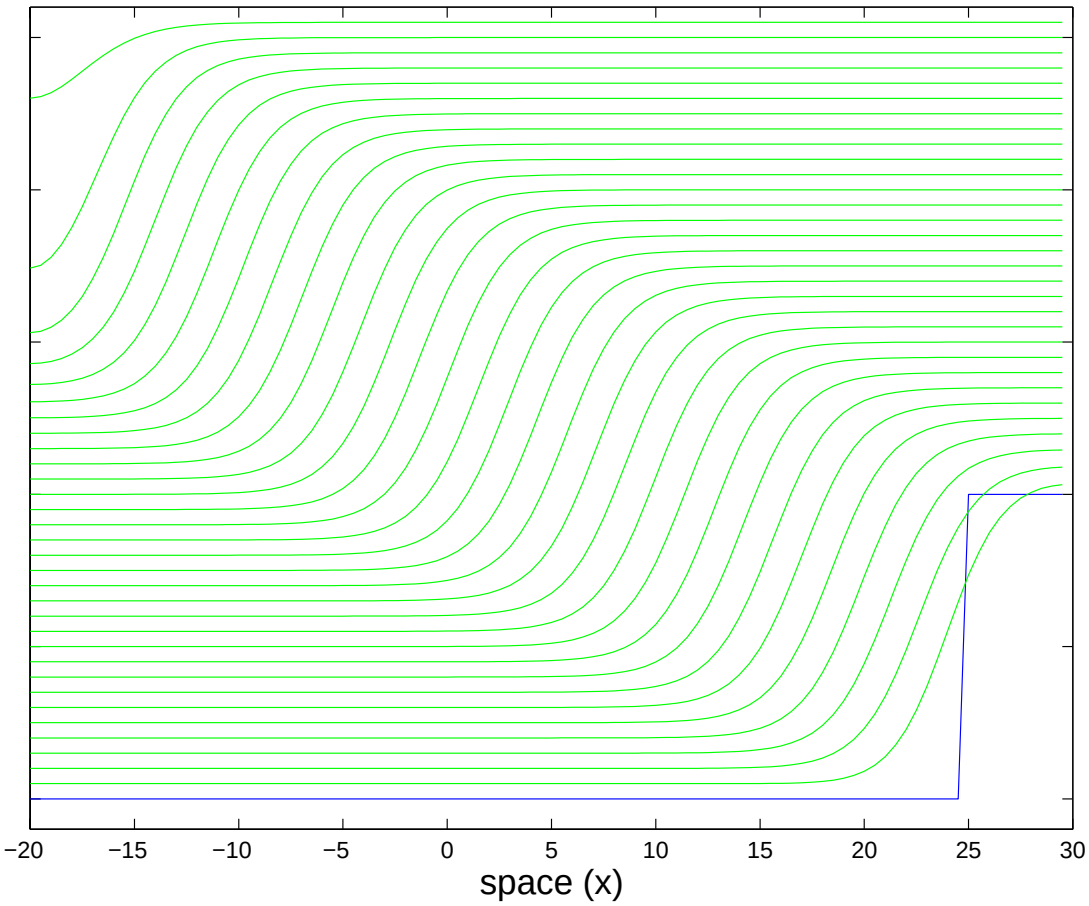

Figure 2.4. Numerical simulation of a traveling wave in (2.1) with for cubic f with $\alpha = 0.3$. u vs. space (x) is plotted. Each curve is the solution at a fixed time (every 5 time units) and as time progresses the curves are lifted slightly. The wave speed is approximately 0.28. This simulation was performed using the implicit-explicit method of Hines [26] with $\Delta t = 0.001$ and $\Delta x = 0.01$.

nates, $z = x + ct - \xi$, equation (2.6) becomes

$$U_{zz} - cU_z + f(U) = 0. \tag{2.10}$$

(Note that any translation of U satisfies equation (2.10), i.e., ξ is arbitrary). This equation is a nonlinear eigenproblem, since c is unknown a priori. Similar to the steady state equations, this equation is best studied in the phase plane given by the system of equation

$$\begin{cases} U_z = W, \\ W_z = cW - f(u), \end{cases} \tag{2.11}$$

Notice that the steady state equations are a special case of this system ($c = 0$). Again, this system has fixed points at $(0,0)$, $(\alpha,0)$, and $(1,0)$. The fixed points at $(0,0)$ and $(1,0)$ are saddle points and the fixed point at $(\alpha,0)$ is a center. We are looking for solutions $U(\infty) = 1$ and $U(-\infty) = 0$ as previously mentioned, but also $U_x(\infty) = U_x(-\infty) = 0$. That is, we are looking for a trajectory in the phase plane that connects $(0,0)$ to $(1,0)$. This trajectory will appear as a heteroclinic connection, which is both the unstable manifold of $(0,0)$ and the stable manifold of $(1,0)$.

Aronson and Weinberger showed that this heteroclinic connection exists for a unique value of c using a shooting argument. When $c = 0$, the system is identical to the system in case (i) steady state case. The unstable manifold of $(0,0)$ in this case (i.e., the homoclinic orbit) undershoots the fixed point at $(1,0)$. On the other hand, it can be analytically shown that, when c is chosen to be sufficiently large, the unstable manifold of $(0,0)$ overshoots the fixed point at $(1,0)$ crossing the line $U = 1$ at a value of $W > 0$. By continuous dependence of trajectories of system (2.11) on parameters, we are guaranteed that there exists at least one value of c for which the trajectory emanating from $(0,0)$ (the unstable manifold with $U_x > 0$) hits the point $(0,0)$, thus forming a heteroclinic connection. Furthermore, slopes of trajectories in the first quadrant of the $W - U$ plane are monotonically increasing functions of c, therefore a heteroclinic orbit exists for a unique c. $\square$

Figures 2.5–2.7 show the phase portraits for $f = -u(u-\alpha)(u-1)$ with $\alpha = 0.3$ and different values of c. Figure 2.5 is for $c = 0$ and Figure 2.6 is for $c = 0.32$. The trajectories emanating as the unstable manifold of (0,0) undershoot and overshoot the point (1,0), respectively. In Figure 2.7, c is chosen $0.4/\sqrt{2}$, so that there the unstable manifold of (0,0) hits (1,0) and thus a heteroclinic orbit exist. This trajectory corresponds to the wavefront of equation (2.6) shown in Figure 2.7. This wavefront of course has a speed of $0.4/\sqrt{2}$. (This speed can actually be calculated analytically, because f is cubic).

Fife and McLeod [19] showed that the travelling wave solution for equation (2.6) is stable. Their proof will not be given here, but it should be pointed out that it uses sub- and supersolution techniques that will be introduced in the next chapter and will be an integral part of our analysis of the inhomogeneous problem (2.1).

2.2.3 Threshold results

This subsection gives a summary of threshold results. These results tell us when local perturbations are sufficient to produce propagated wavefronts of excitation. However, the main reason that we include the results is that the theorems used to obtain them will be used to determine when propagated wavefronts are blocked in the case of an inhomogeneous medium. The results presented in this section are due to Aronson and Weinberger [3] and are based on comparison principles that in turn rely on the maximum principle for scalar parabolic partial differential operators (see Protter and Weinberger [55]).

Theorem 2.3 *(COMPARISON PRINCIPLE) Let $u(x)$ and $v(x)$ satisfy the inequalities*

$$u_t - u_{xx} - f(u) \geq v_t - v_{xx} - f(v),$$
$$0 \leq v(x,0) \leq u(x,0) \leq 1.$$

Then $u(x,t) \geq v(x,t)$ for all $t > 0$ and if $u(x,0) > v(x,0)$ then $u(x,t) > v(x,t)$ for all $t > 0$.

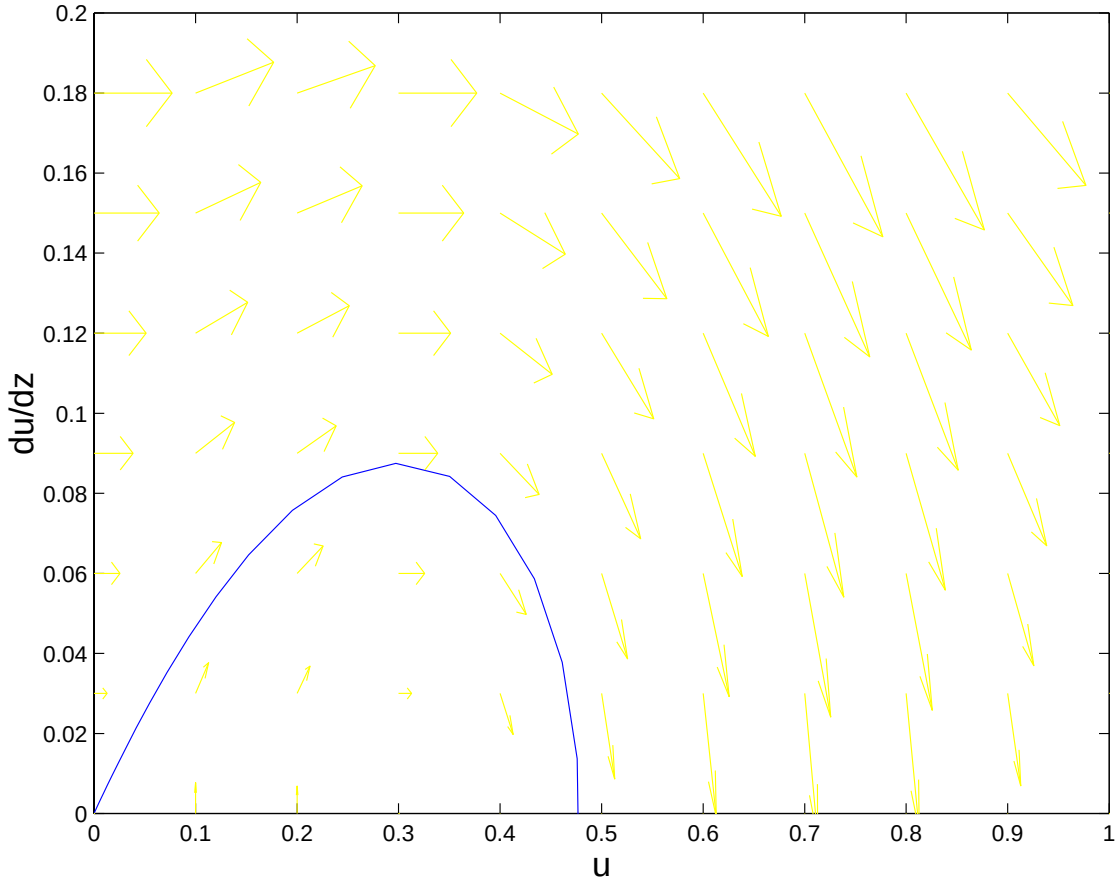

Figure 2.5. Phase plane for (2.11) with $c = 0$ (cubic f with $\alpha = 0.3$). The trajectory emanating from (0,0) undershoots (1,0).

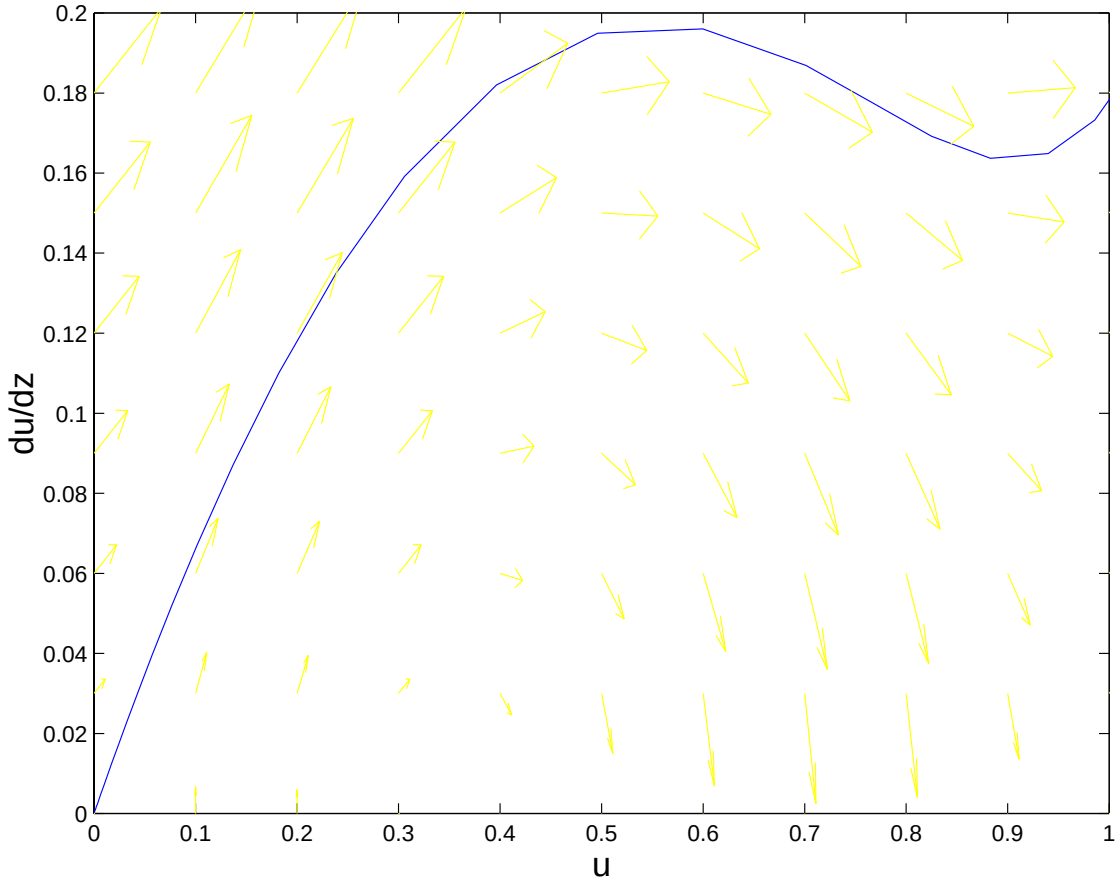

Figure 2.6. Phase plane for (2.11) with $c = 0.32$ (cubic f with $\alpha = 0.3$). The trajectory emanating from (0,0) overshoots (1,0).

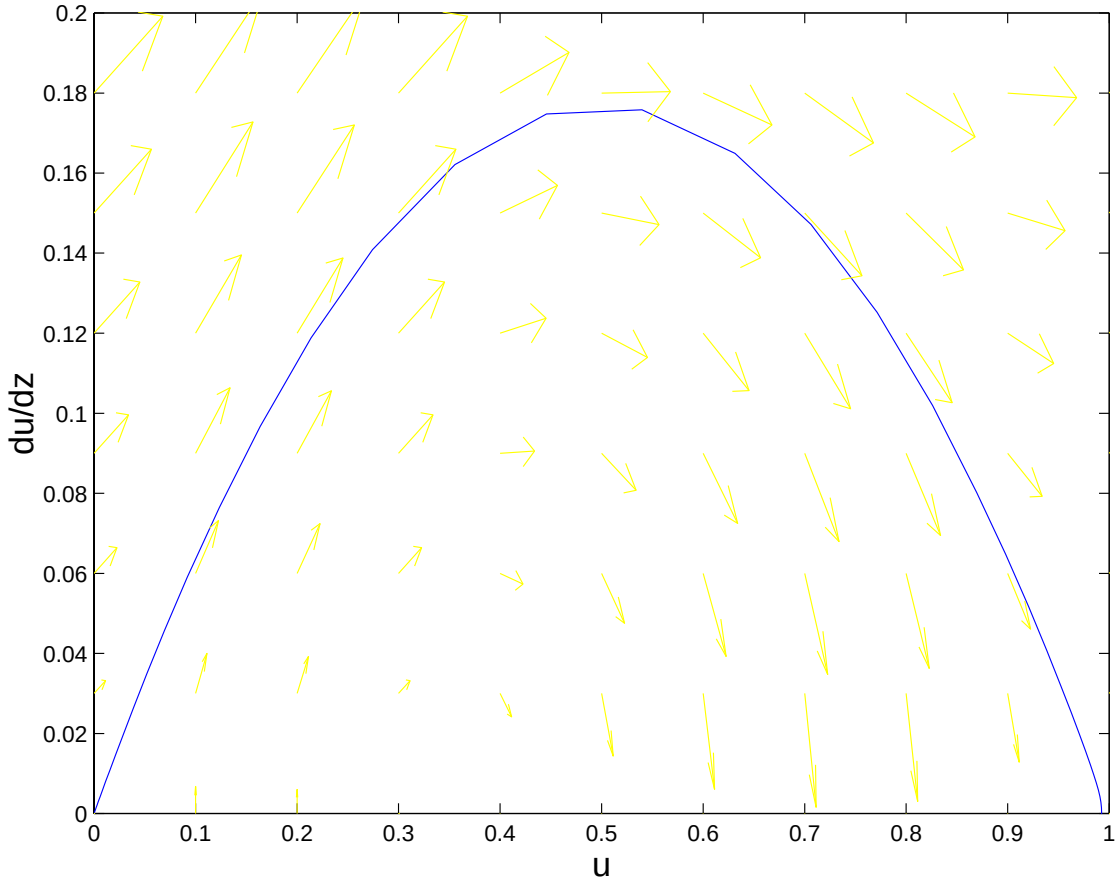

Figure 2.7. Phase plane for (2.11) with $c = 0.2828$ (cubic f with $\alpha = 0.3$). The trajectory emanating from (0,0) hits (1,0), thus forming a heteroclinic connection.

Rearranging the first inequality and applying the mean value theorem, we get

$$(u-v)_t \geq (u-v)_{xx} + (f(u)-f(v)) = (u-v)_{xx} + f'(v+\theta(u-v))(u-v)$$

for some $0 < \theta < 1$. If we define β to be the maximum of f' on [0,1] and $w = (u-v)e^{-\beta t}$, then

$$w_t \geq w_{xx} + [f'(v+\theta(u-v)) - \beta]w = w_{xx} - \gamma w.$$

where $\gamma = f'(v+\theta(u-v)) - \beta \geq 0$. By the strong maximum principle for linear parabolic partial differential inequalities, this inequality and the fact that $w(x,0) = u(x,0) - v(x,0) \geq 0$ implies that $w(x,t) \geq 0$, and thus $u(x,t) \geq v(x,t)$. Note that strict inequalities carry through in the argument where needed. □

Definition 2.4 *Suppose that* $\phi \in C^{2,1}(R \setminus \{x_j, j = 1, \ldots, N\} \times (0,T))$ *(i.e., continuous and piecewise differentiable).*
$\phi(x,t)$ *is a* **subsolution** *of equation (2.6), if* $\phi_t - \phi_{xx} - f(\phi) \leq 0$ *on differentiable segments of* ϕ *and* $\phi_x(x_j^+, t) - \phi_x(x_j^-, t) \geq 0$ *where* ϕ_x *has discontinuities.*
$\phi(x,t)$ *is a* **supersolution** *of equation (2.6), if* $\phi_t - \phi_{xx} - f(\phi) \geq 0$ *on differentiable segments of* ϕ *and* $\phi_x(x_j^+, t) - \phi_x(x_j^-, t) \leq 0$ *where* ϕ_x *has discontinuities.*

The next theorem follows from the above comparison principle and the definitions of super- and subsolutions. This theorem will be the key to understanding propagation failure in the heterogeneous cable that we will study in the next section.

Theorem 2.5 *(ORDERING PRINCIPLE) Let* $\bar{\phi}(x)$ *be a time-independent supersolution of equation (2.6) and* $u(x,t)$ *be the solution to equation (2.6) with the initial condition* $\bar{\phi}(x)$*. Then* $u(x,t)$ *is a nonincreasing function of* t *and approaches the largest steady state solution* $u^*(x)$ *of equation (2.6) such that* $u^*(x) \leq \bar{\phi}(x)$*.*
Similarly, Let $\underline{\phi}(x)$ *be a time-independent subsolution of equation (2.6) and* $u(x,t)$ *be the solution to equation (2.6) with the initial condition* $\underline{\phi}(x)$*. Then* $u(x,t)$ *is a nondecreasing function of* t *and approaches the smallest steady state solution* $u^*(x)$ *of equation (2.6) such that* $u^*(x) \geq \underline{\phi}(x)$*.*

By definition, we have that

$$\bar{\phi}_t - \bar{\phi}_{xx} - f(\bar{\phi}) \geq 0 = u_t - u_{xx} - f(u),$$
$$0 \leq u(x,0) = \bar{\phi}(x) \leq 1.$$

Theorem 2.5 implies, $\bar{\phi}(x) = u(x,0) \geq u(x,t)$ for all $t > 0$. Now, we will apply the theorem again to $u(x,t)$ and $u(x,t+\delta)$. Note that both are solutions of equation (2.6)), and therefore $u(x,t)$ can play the role of the supersolution, while $u(x,t+\delta)$ plays the role of the initial condition. We conclude that $u(x,t) \geq u(x,t+\delta)$. By following this procedure recursively, we see that $u(x,t)$ must be a nonincreasing function of t. Further argument that uses properties of parabolic equations along with the fact that $0 \leq u \leq 1$ is an invariant region guarantees that $u(x,t)$ converges to the largest steady state solution of equation (2.6) that is smaller than $\bar{\phi}(x)$.

A similar argument justifies the second portion of the theorem. □

We now present a theorem that gives conditions for when a local disturbance with compact support has sufficiently large magnitude over a sufficiently large interval to grow to $u = 1$ everywhere. That is, it gives conditions necessary for local perturbations to be superthreshold.

Before stating the theorem, we first will construct a function that will be used as the superthreshold initial conditions for the PDE (2.6). Let us construct this function $q(x)$ in a piecewise fashion. To do this, once again consider the $u - u_x$ phase plane of the steady state equations (2.7). Let us construct the function $q(x)$ in a piecewise fashion. For $-l_b < x < l_b$, $q(x)$ sketches out a trajectory that circumnavigates the homoclinic orbit associated with (0,0) such that the trajectory starts with $u = 0$, hits $u_x = 0$ at $u = b$ and ends when $u = 0$ (see Figure 2.2). This requires that $\bar{u}_A < b < 1$ where $\int_0^{\bar{u}_A} f(u)du = 0$. For all other x, $q(x) = 0$. Therefore, on $-l_b < x < l_b$, $q(x)$ satisfies $q'' + f(q) = 0$ with $q(0) = b$, $q'(0) = 0$. The length l_b can be found by using a property similar to equation (2.8)

$$\left.\frac{q_x^2}{2}\right|_{\bar{x}}^{0} = -\int_b^{q(\bar{x})} f(u)du = -F(q(\bar{x})) + F(b),$$

$$\frac{dq}{dx}(x) = -\sqrt{2(F(b) - F(q))},$$

$$l_b = -\int_{-l_b}^{0} dx = \int_0^b \frac{dq}{\sqrt{2(F(b) - F(q))}}.$$

Theorem 2.6 *Let $u(x,t)$ be the solution to equation (2.6) with the initial condition $q(x)$ as defined above. Then $\lim_{t\to\infty} u(x,t) = 1$.*

Note that $q(x)$ is a solution to equation (2.6) everywhere except at $x = \pm l_b$. Also, $q(-l_b^+) - q(-l_b^-) = q(-l_b^+) > 0$ and $q(l_b^+) - q(l_b^-) = -q(l_b^-) > 0$. Therefore, $q(x)$ is a time-independent subsolution of equation (2.6). By theorem 2.6, $u(x,t)$ must evolve to the smallest steady state that is larger than $q(x)$. By inspection of the $u - u_x$ phase plane, the only steady state that is greater than $q(x)$ and in $0 \le u \le 1$ is $u = 1$. □

There are theorems that give conditions that ensure subthreshold disturbances as well, but they will not be presented here, because we have already illustrated how theorem 2.6 can be used. In the next section, we will use theorem 2.6 to demonstrate that, when certain nonuniform steady states exist in the inhomogeneous problem, a wave of excitation cannot be transmitted through the entire medium and thus the wave is blocked.

2.3 The Inhomogeneous Cable: The Gap Model

Now we move to the scalar gap problem described in section 2.1 and study the effects of specific type of a local inhomogeneity on wave propagation. Inhomogeneities make the problem harder in many respects, however in special cases such as the problem described by equation (2.1) analytical results can still be obtained.

2.3.1 Numerical solution of the PDE

In order to become familiar with the system, it is useful to present some numerical results. For these simulations, the excitability term f is taken to be cubic with $\alpha = 0.3$ and in the gap, $D = 1$. A wavefront of excitation is started far away from the gap so that it travels towards the gap. When the wavefront reaches the proximal side of the gap it stalls, because there is no excitability in the gap. It does, however, begin to source u to the distal side of the gap via diffusion. For

"small" L, the wavefront is able to source enough u through the gap to excite the distal side of the gap, and thus after a slight delay, the wavefront is able to "jump" the gap. As L is increased, the delay increases, but the wavefront is still able to jump the gap. This behavior continues until L is increased above a critical value, L^*, after which the wavefront completely stalls. For these "large" values of L, the solution appears to approach a nonuniform steady state solution and thus there is block. Figure 2.8 shows examples of both successful transmission of the wavefront across the gap (top) and wavefront block (bottom). The critical gap length L^* is approximately 6.5 in this case. These simulations are very similar to the those of Sharp and Joyner [60] in a one-dimensional cable model using detailed ionic models and a gap consisting of zero sodium current.

Long delays before successful jumping of the gap make it difficult to compute L^* precisely without effort. Furthermore, obtaining anything more than a critical gap length for a specific excitability function at a specific set of parameters by doing only numerical simulations of the PDE is difficult. For this reason, we turn to the analytical methods to help us gain further insight into our problem.

2.3.2 Steady state solutions and block

Although no true traveling wave solutions exist for inhomogeneous problems, the ordering principles for solutions will be shown to apply. Thus, the plan of attack is to look for the existence of nonuniform steady state solutions $u^*(x)$ of the equation (2.1) for which $u, u_x \to 0$ as $x \to -\infty$ and $u \to 1$, $u_x \to 0$ as $x \to \infty$ (see Figure 2.4).

The key idea here is that $u^*(x)$ acts as time-independent supersolution of equation (2.1), and therefore if the solution starts below $u^*(x)$, then it will remain below for all time. If such a steady state exists, a wave front traveling towards the gap will asymptotically approach this steady state (or a similar, but smaller, nonuniform steady state), and hence the wavefront will be blocked by the gap. If no such steady state exists, the solution will approach $u = 1$, the smallest steady state greater than the initial conditions, and hence the wave front necessarily successfully jumps the gap. Our numerical simulations hint at this (see Figure 2.4). When block does

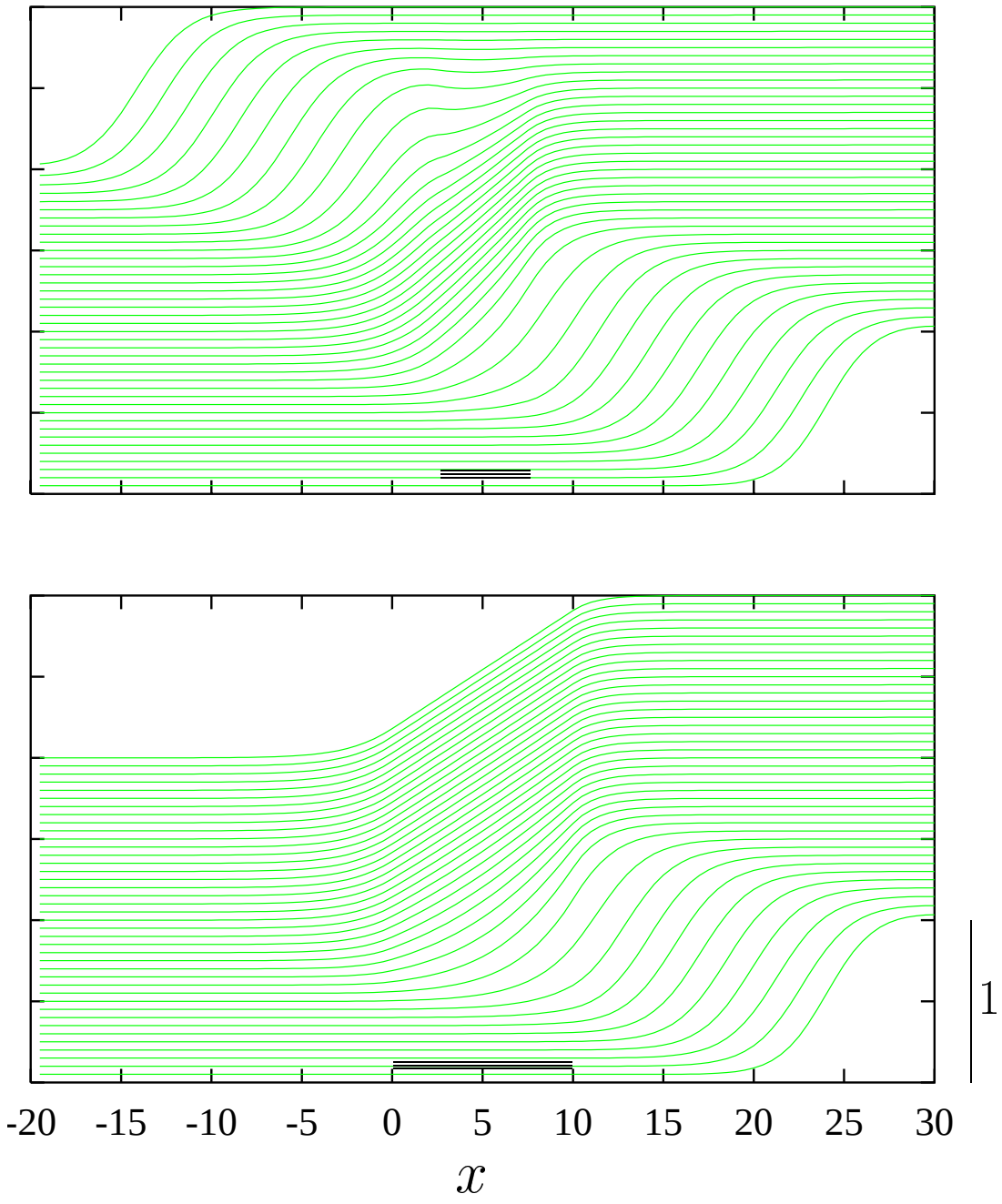

Figure 2.8. Numerical simulations of the PDE with $D = 1$, $\alpha = 0.3$. Plots are of u vs. space (x). Each curve is the solution at a fixed time (every 5 time units) and as time progresses the curves are lifted slightly. The position of the gap is marked by the a black bar on each figure. The wavefront propagates towards the gap from the right. In the top figure, there is successful transmission across the gap ($L = 5.0$), whereas in the bottom figure, the wavefront is blocked ($L = 10.0$). These simulation were performed using the implicit-explicit method of Hines [26] with $\Delta t = 0.001$ and $\Delta x = 0.01$.

occur, the solution appears to approach a steady state of this form.

The argument above is summarized in the following theorem:

Proposition 2.7 *Consider the system described in section 2.1. A wave propagating towards a diffusive gap fails to cross the gap, if and only if a nonuniform steady state solution $u^*(x)$ of the equation (2.1) exists for which $u, u_x \to 0$ as $x \to -\infty$ and $u \to 1$, $u_x \to 0$ as $x \to \infty$.*

For constant diffusion coefficient, this result follows directly from theorem 2.7, since the multiplicative factor $s(x)$ does not affect the argument used to prove this ordering principle. When diffusion constant $D(x)$ varies but is continuous, this result follows directly from a change of variables and applying theorem 2.7. Furthermore, an extension of the theorem by Pauwelussen [53, 54] includes the case of discontinuities in the diffusion coefficient. □

2.3.3 Calculating steady state solutions

Theorem 2.7 reduces the problem of looking for block to simply looking for steady state solutions. These steady state solutions must obey the equation

$$0 = \begin{cases} u_{xx} + f(u), & x \in (-\infty, 0) \\ Du_{xx} & x \in (0, L) \\ u_{xx} + f(u), & x \in (L, \infty) \end{cases} \tag{2.12}$$

with the boundary conditions mentioned above. Also, matching conditions must be satisfied for u (continuity)

$$\begin{aligned} \lim_{x \to 0^-} u &= \lim_{x \to 0^+} u, \\ \lim_{x \to L^+} u &= \lim_{x \to L^-} u, \end{aligned}$$

and for u_x (the jump condition or conservation of current)

$$\lim_{x \to 0^-} u_x = \lim_{x \to 0^+} Du_x,$$

$$\lim_{x\to L^+} u_x \;=\; \lim_{x\to L^-} Du_x.$$

Let $u_0 = u(0)$ and $u_L = u(L)$. Using the continuity condition for u, the solution in the gap $(0, L)$ must be the linear function

$$u(x) = \frac{D(u_L - u_0)}{L}x + u_0.$$

In the excitable regions of equation (2.12), we can use the same calculus trick that we used in the discussion of steady states for the homogeneous medium (section 2.2.1). Multiplying by $u_x dx$ and integrating, we obtain

$$\int_{x_0}^{x_1} u_{xx}u_x dx = -\int_{x_0}^{x_1} f(u)u_x dx$$

and assuming u is monotonic in x, the change of variables $u_x dx = du$ gives

$$\int_{x_0}^{x_1} (\frac{u_x^2}{2})_x dx = -\int_{u(x_0)}^{u(x_1)} f(u)du$$

$$\frac{u_x^2}{2}\bigg|_{x_0}^{x_1} = -F(u)|_{u(x_0)}^{u(x_1)}$$

where F is the antiderivative of f (i.e., $F(u) = \int_0^u f(v)dv$). By taking $x_1 = 0$, $x_0 = -\infty$ and $x_1 = \infty$, $x_0 = L$ and applying the appropriate boundary conditions, we respectively get

$$u_x(0^-) = \sqrt{-2F(u_0)}$$

$$u_x(L^+) = \sqrt{2(F(1) - F(u_L))}.$$

Using these two equations above, the slope of solution in the gap, and the matching conditions for u_x, we get the nonlinear system of algebraic equations for (u_0, u_L) with L as a parameter

$$\begin{cases} F(u_0) = F(u_L) - F(1), \\ D(u_L - u_0) = L\sqrt{-2F(u_0)}. \end{cases} \tag{2.13}$$

For each solution of this system, there exists a (monotonic) steady state of the original PDE (2.1). Thus, the problem of studying block has been reduced to a bifurcation problem for a nonlinear system of algebraic equations. Note that the bifurcation parameter of interest here can be thought of as L/D, therefore usually we will take $D = 1$ in what follows without loss of generality.

2.3.4 Piecewise linear reaction terms

Sneyd and Sherratt [62] obtained equations similar to system (2.13) in the context of calcium induced calcium release (CICR). However, they were able to obtain tight results but limited results, because their calculations were for the simple case of a piecewise linear discontinuous bistable equation

$$f(u) = \begin{cases} -u & u \leq \alpha, \\ -(u-1) & u > \alpha. \end{cases}$$

In their work, they set $u(0) = \alpha$ in equation (2.13) and calculate that a steady state with this condition exists for

$$L_\alpha = \frac{1}{\alpha} - 2.$$

Throughout this section, we will take L_α to be defined as the minimum value of L for which there exists a steady state with $u(0) = \alpha$.

Sneyd and Sherratt hypothesize that L_α marks a sharp delineation between guaranteed block for $L > L_\alpha$ and guaranteed successful transmission across the gap for $L < L_\alpha$. For the case of piecewise linear discontinuous f, their claim turns out to be correct (i.e., $L^* = L_\alpha$). This can be proven by trying to construct all possible piecewise defined solutions types and getting conditions for their existence. This will be omitted, because it is rather tedious and not too instructive. A much nicer proof will be given later.

On the other hand, their claim does not carries over to general f. For any f, there necessarily exists a steady state solution with $u(0) = \alpha$ for some L. Indeed, this makes sense physically, because α is the threshold for the spatially constant bistable equation. (A simple proof for this will be given later.) However, steady state solutions for more general f (e.g., continuous) exist on either side of L_α in L space. Therefore, although L_α may be used as an approximation of the critical gap length, it is only an upper bound of L^* above which there is existence of steady state solutions and guaranteed block.

To demonstrate this, consider a piecewise linear continuous reaction term

$$f(u) = \begin{cases} -u & , u \leq \frac{\alpha}{2}, \\ u - \alpha & , \frac{\alpha}{2} < u < \frac{\alpha+1}{2}, \\ -(u-1) & , u > \frac{\alpha+1}{2}. \end{cases}$$

As for the previous case, we can construct piecewise defined solutions and calculate the critical value of L below which steady state solutions do not exist,

$$L^* = \sqrt{2(\frac{1}{\alpha} - 1)^2 - 1} - 1.$$

If we were to immediately set $u(0) = \alpha$ as Sneyd and Sherratt do, then we would find

$$L_\alpha = \sqrt{2}(\frac{1}{\alpha} - 1) - 1.$$

Again, this is a tedious calculation, hence the details will be omitted. There actually is very easy way to find the L^* using ideas that will be developed in the following sections. These functions L^* and L^α are plotted in Figure 2.9. Note that both L^* and L_α are decreasing functions of the threshold α as one would expect. For sufficiently small α, L_α approximates L^* well. The normalized difference between the two functions is shown in Figure 2.10. This difference goes to 0 as $\alpha \to 0$, but as *alpha* increases and the critical gap length gets smaller, the approximation of L_α to L^* becomes increasingly worse.

Sneyd and Sherratt admit that, for f more general than the piecewise linear discontinuous case, solutions exist on either side of L_α in L space, but then conjecture that solutions for $L < L_\alpha$ must be unstable and their existence in this case does not correspond to block. This is false. According to Proposition 2.7, the existence of any steady state solution (of the appropriate form) guarantees block, because the steady state solution acts as a time-independent supersolution regardless of its stability.

Calculations from the piecewise linear continuous reaction term suggest a general bifurcation structure for solutions of the steady state equation (2.12). They show that in fact two steady state solutions can be constructed for every $L > L*$ and as L decreased to L^*, the solutions coalesce and vanish in a tangent bifurcation. For values of $L < L^*$, no solutions exist.

For nonlinear f, it is hard to find the bifurcation structure and critical gap length algebraically, even for a simple cubic f. This is true even when attempting to approximate L^* by setting $u(0) = \alpha$. Thus, in order to address the problem of

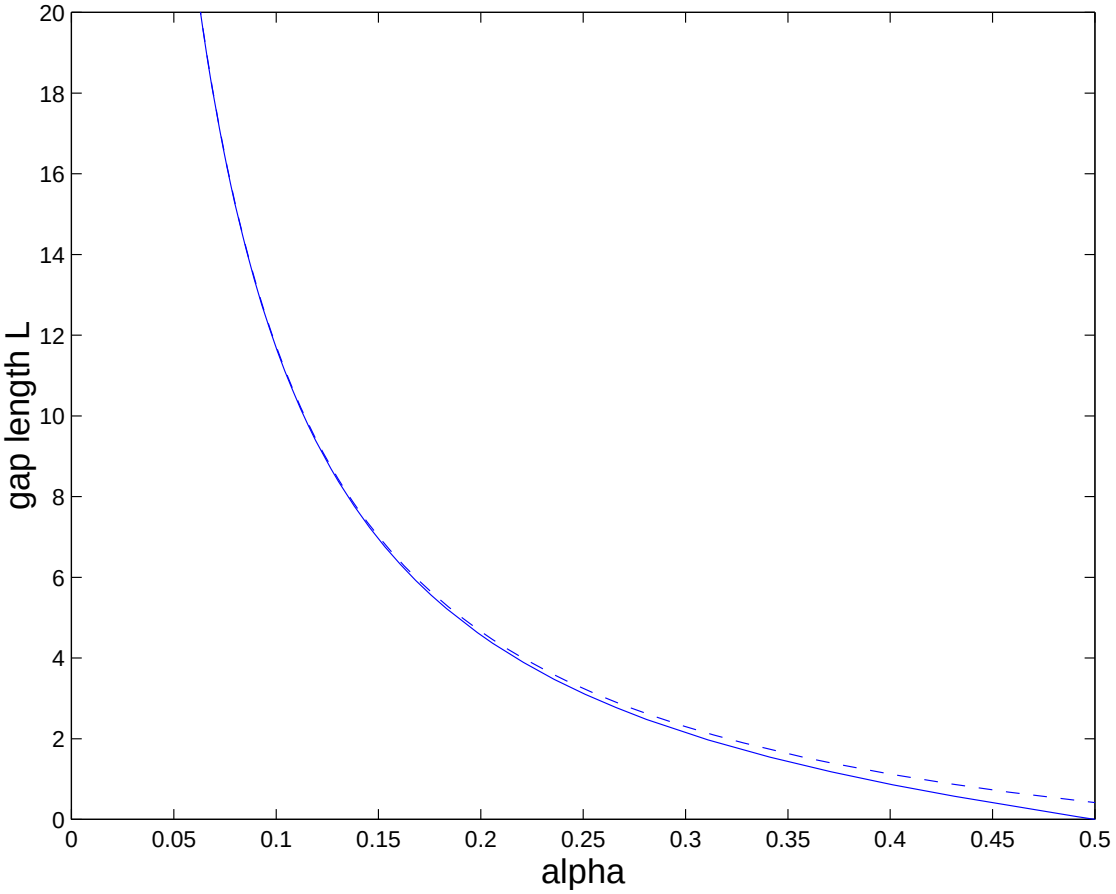

Figure 2.9. Graphs of L^* (solid line) and L_α (dashed line) as a function of α for the piecewise linear continuous reaction term described in text.

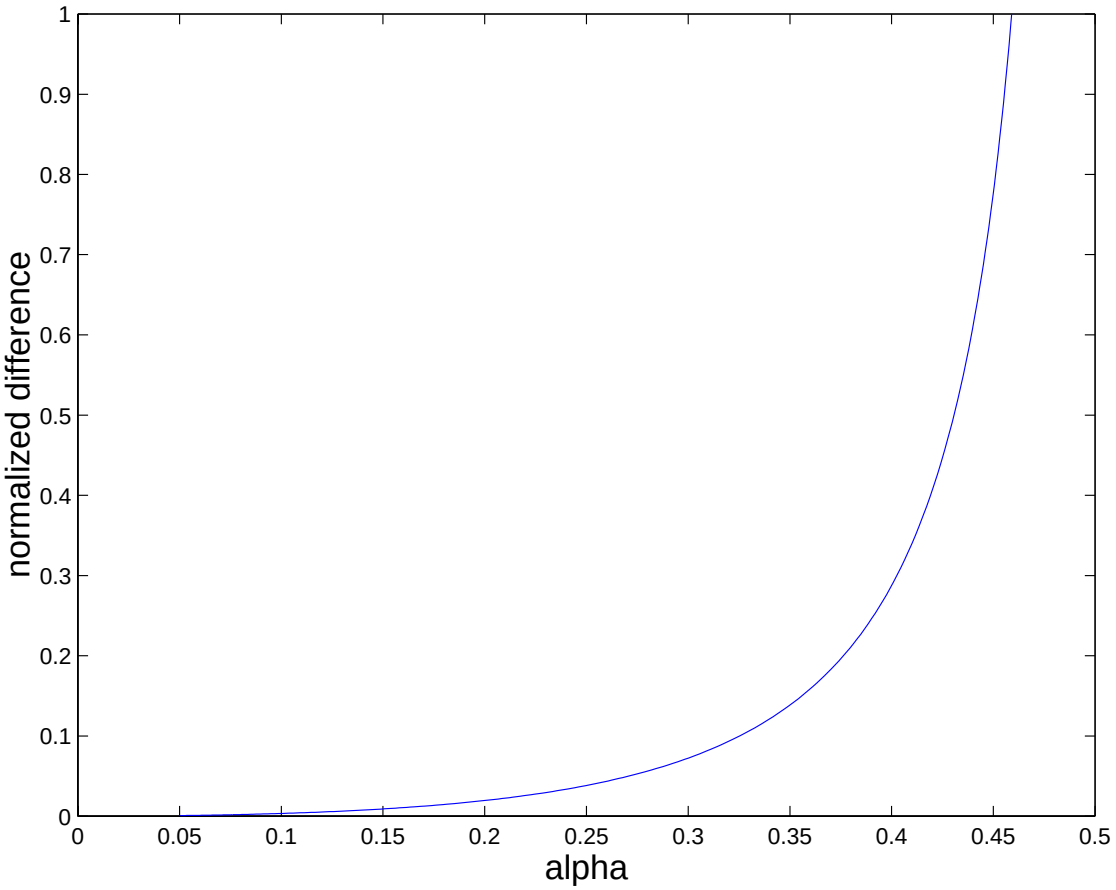

Figure 2.10. Graph of $(L_\alpha - L^*)/L^*$ as a function of α for the piecewise linear continuous reaction term described in the text.

calculating critical gap length and uncovering the general structure for nonlinear f, one must either consider the problem numerically or turn to other methods to obtain analytical insight into the behavior of the system.

2.3.5 A geometrical interpretation

Before, or even instead of, pursuing this bifurcation problem numerically (either equation (2.12) directly or system (2.13)), it is enlightening to consider a geometrical interpretation of the problem.

Consider the phase portrait of $u_{xx} + f(u) = 0$ as discussed in section 2.2 (Figure 2.2) and shown again in Figure 2.11. Two important trajectories are plotted in the phase plane: curve A is a portion of the homoclinic orbit emanating from the saddle point ($u = 0$,$u_x = 0$), and curve B is the stable manifold of the saddle point ($u = 1$,$u_x = 0$). Note that on trajectory A, $u, u_x \to 0$ as $x \to -\infty$. This is exactly the left boundary condition of steady state equations. On trajectory B, $u \to 1$, $u_x \to 0$ as $x \to \infty$, which is the boundary condition on the right. Thus, we see that the steady state solution $u^*(x)$ to the left of the gap ($x \leq 0$) lives on trajectory A, and therefore so does $(u(0), u_x(0))$. Similarly, $u^*(x)$ to the right of the gap ($x \geq L$) lives on trajectory B, and therefore so does $(u(L), u_x(L))$.

Next, we note that the "flow" in the gap (on $0 < x < L$) is governed by the differential equation $Du_{xx} = 0$. Let us take all points on curve A to be a family of initial conditions ($x = 0$) and flow forward using this differential equation to $x = L$. If any trajectory stemming from a point on A, say point a, matches up with a point on curve B, say point b, then we have found a solution. This solution can be reconstructed by considering the (u, u_x) coordinates and tracing out the following trajectory. Starting at $(0, 0)$ ($x = -\infty$), move along curve A to point a. Because curve A is a homoclinic orbit, the x value is arbitrary at this point, so we can set it to $x = 0$. From point a, follow the flow of $Du_{xx} = 0$, which is horizontal in the u_x, u-phase plane (u_x constant) until $x = L$. By design this will be point b on curve B. The remaining portion of the solution is obtained by following curve B, the stable manifold of (1,0), into the steady state (1,0) while x increases from L to ∞. This idea of piecing flows of phase planes together is somewhat similar to

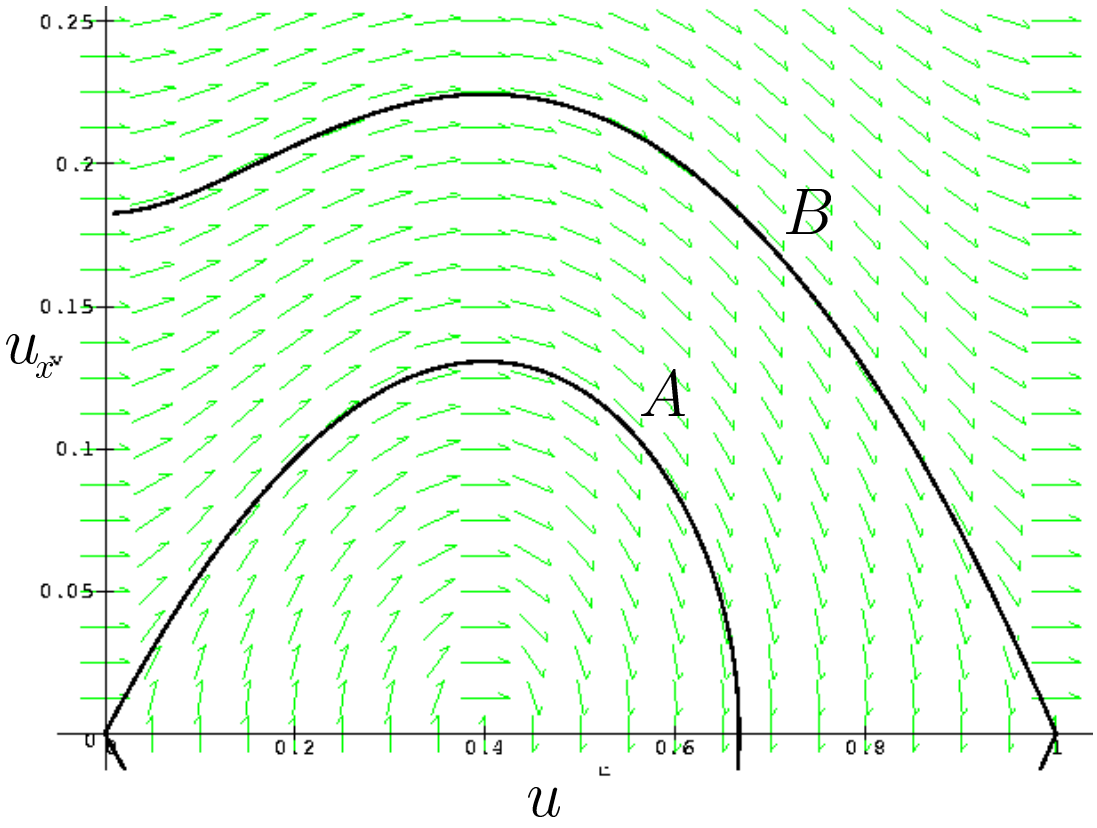

Figure 2.11. The u, u_x-phase portrait of $u_{xx} + f(u) = 0$ with vector field. f is cubic with $\alpha = 0.4$. Curve A is the homoclinic orbit associated with (0,0) and curve B is the stable manifold of (1,0).

techniques used in [53] and [37].

The description above suggests an easy way to find these solutions. As before, consider points on curve A as all possible $x = 0$ values for our solution. We can derive a map by the flow in the gap ($Du_{xx} = 0$) and map these points on curve A, $(u(0), u_x(0))$, to points on a new curve $\psi_L(A)$, which will be called$(v(L), v_x(L))$

$$\psi_L : [u(0), u_x(0)] \mapsto [v(L), v_x(L)] = [u_x(0)\frac{L}{D} + u(0), u_x(0)].$$

Any intersection of this new curve $\psi_L(A)$ and curve B corresponds to a steady state solution of the partial differential equation (2.1).

The map ψ_L is continuous and has fixed points where $u_x = 0$, which occurs at two points along the trajectory A. When $L = 0$, the map is the identity map (curve $\psi_L(A)$ is exactly curve A). However, when L is positive, the map effectively shifts curve A to the right towards trajectory B for $u_x > 0$. The map shifts curve A to the left away from trajectory B for $u_x < 0$, thus no intersections can occur on this portion of A. The shift is linear in L and the greater u_x is, the larger the shift.

2.3.6 Results

An example of the mapping described in the previous section is given for the cubic f with $\alpha = 0.3$ in Figure 2.12. One can be see that for small L, there are no intersections of $\psi_L(A)$ and curve B. However, as L increases, a critical value of L, L^*, is reached where there is one intersection, and thus one steady state solution to equation (2.1). For L greater than this critical value, two intersections, and thus two steady state solutions, exist. This suggests that the solutions arise via a saddle node bifurcation. A bifurcation diagram for this system is shown in Figure 2.13. This bifurcation structure is similar to that found in the case of an abrupt change in diffusion coefficient [53, 28], however we will show that more than two solutions can arise in the gap problem, which is not the case for the abrupt change in diffusion coefficient.

Figure 2.14 shows the actual steady state solutions of equation (2.1) for $L > L^*$. These solutions were constructed using the values at the intersection points in Figure 2.12. It will be shown that the smaller of the two solutions is stable (with

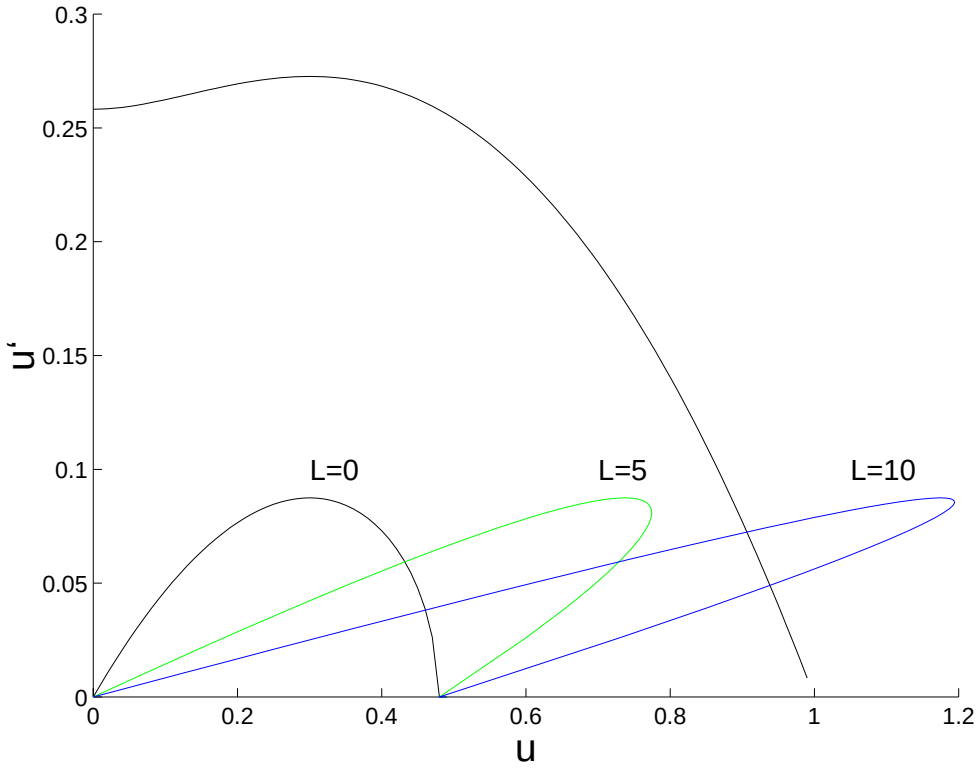

Figure 2.12. u, u_x-phase portrait of $u_{xx} + f(u) = 0$ (as in previous figure) with images of the homoclinic orbit (curve A) under the map ψ_L. Intersections with the stable manifold of $(1, 0)$ (curve B) correspond to steady state solutions of the PDE. $\alpha = 0.1$, $D = 1$. The first intersection is at $L^* = 6.40$.

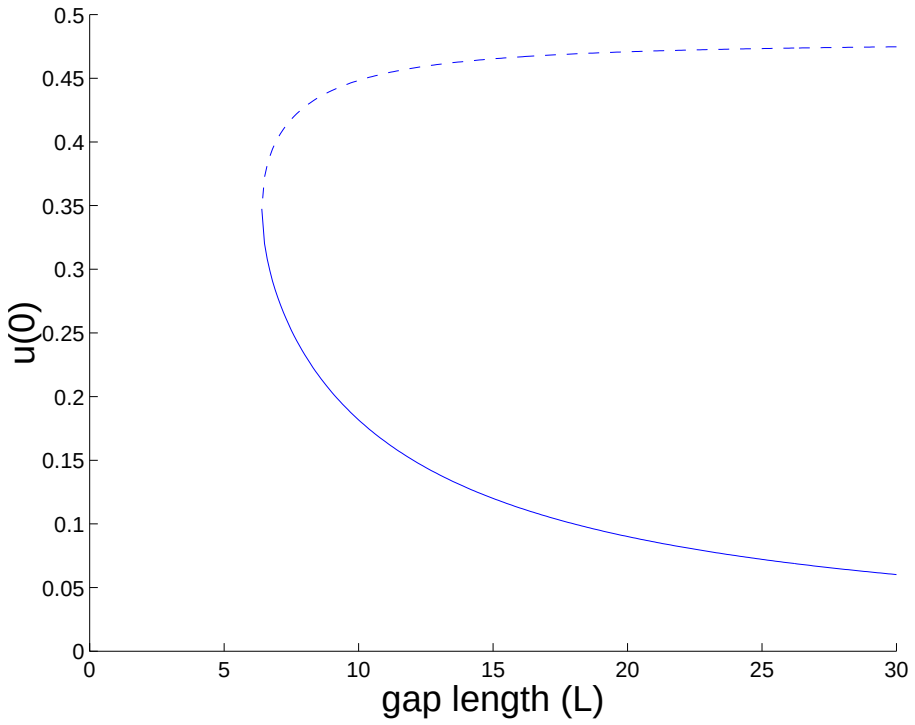

Figure 2.13. Bifurcation diagram: $u(0)$ of the steady state solution vs. gap length (L). The solid line represent stable solutions and the dashed line represent unstable solutions. The critical gap length is $L^* = 6.40$. The parameters are $\alpha = 0.3$, $D = 1$.

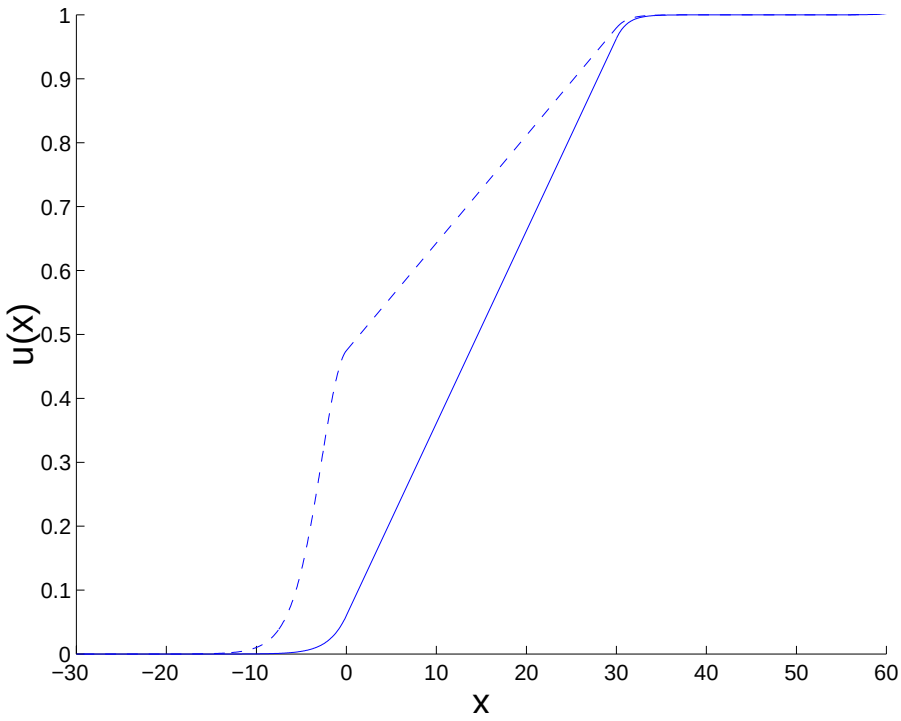

Figure 2.14. The steady state solutions or "clines" of equation (2.1) for $L = 20.0$. The solid line represent the stable solution and the dashed line represent the unstable solution. Parameters are $\alpha = 0.3$, $D = 1$.

respect to time) and the larger is unstable. The "distance" of the stable solution from the unstable solution gives an idea of the size of the basin of attraction of the stable solution. In this light, the unstable solution can be interpreted as a threshold for jumping the gap, and one can begin to address the question of how noise or other perturbations could affect the signal blocking properties of the gap. That is, if a perturbation moves the solution $u(x,t)$ above the unstable steady state solution, then a wavefront will form on the distal side of the gap. (Note that a threshold result similar to theorem thethreshthm could be derived in which the perturbation need only make $u(x,t)$ sufficiently greater than the unstable steady state over a large enough region.)

Another interesting aspect of this graphical representation is that it immediately shows the portions of f that determine whether or not block occurs. The maximal value that u attains on curve A is $\bar{u}_A$, and curve A attains a maximal value of u_x, $\bar{w}_A$, when $u = \alpha$. A steady state solution lives on curve A on the distal side of the gap, therefore $0 \leq u \leq \bar{u}_A$ on this side. Futhermore, because points on curve A are mapped horizontally in the u, u_x-phase plane by ψ_L, $\bar{w}_A$ is the maximal value of u_x that a steady state solution can attain. A steady state solution on the proximal side of the gap lives on curve B, and thus $\bar{u}_B \leq u \leq 1$ on the proximal side of the gap, where $\bar{u}_B$ is the value of u on curve B associated with $u_x = \bar{w}_A$. This potentially leaves the interval $u \in (\bar{u}_A, \bar{u}_B)$, and the corresponding portion of f, unrepresented.

For instance, for $\alpha = 0.3$, we can see in Figure 2.12 that the values of f in $u \in (0.5, 0.9)$ are inconsequential with respect to any possible steady state and therefore whether there is block or not. That is, two different reaction terms that are the same on $0 < u < 0.5$ and $0.9 < u < 1.0$ could be extremely different between 0.5 and 0.9, yet the corresponding gap problem would exhibit a identical L^* and the same steady state solutions for $L \geq L^*$. Note that as α decreases, the size of this 'inconsequential' region increases substantially.

Figure 2.15 shows the critical gap length as a function of the threshold parameter α. As intuition would predict, the critical gap length L^*, and therefore the first

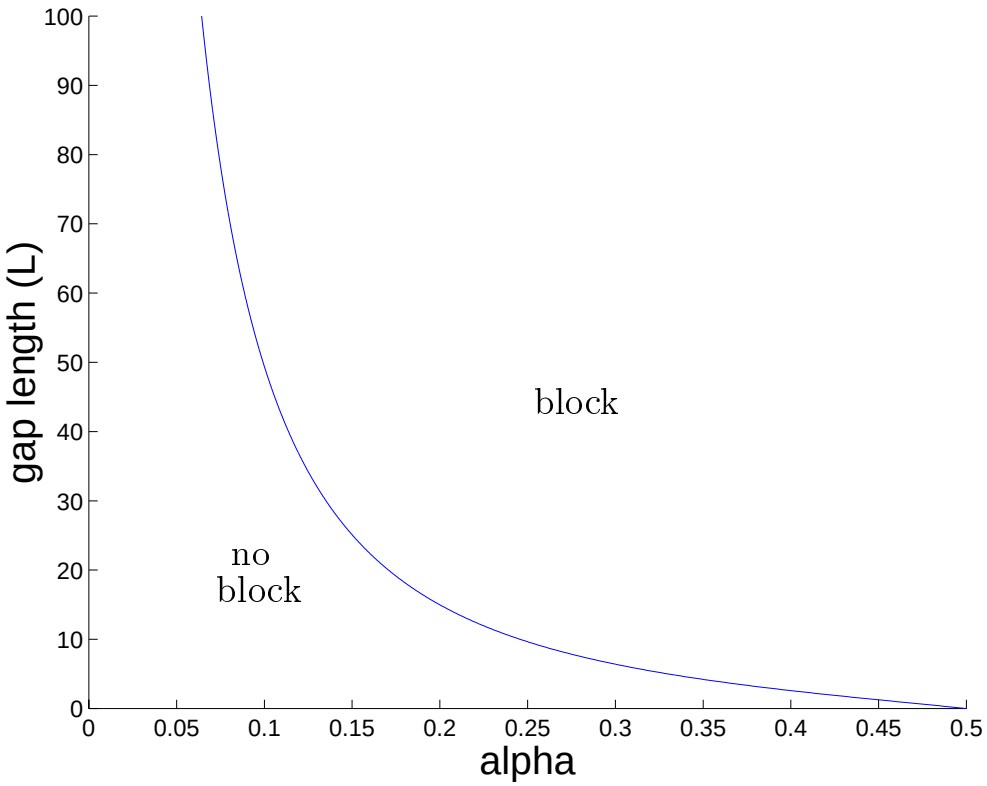

Figure 2.15. Critical gap length (L^*) vs. α for a cubic reaction term F. This curve plots the locus of the fold, as in Figure 2.13, as the parameter α is changed. The curve was calculated using AUTO [16].

point of block as gap length increases, decreases as α increases. $L^* = 0$ at $\alpha = 0.5$, which corresponds to a standing wave in the homogeneous cable. As α approaches 0 from above, L^* goes to ∞. The $\alpha = 0$ case corresponds to a Fisher-like equation [21] where the slightest perturbations away from the resting state leads to traveling wavefronts, thus for any finite gap length and nonzero diffusion in the gap, a wavefront will be able to jump the gap. Qualitatively, this curve is identical to the L^* vs. α curve analytically computed for the continuous piecewise linear reaction case (see Figure 2.9).

By using the geometric interpretation of the problem, we can now extend and solidify the ideas generated from the example above and easily prove the following existence proposition.

Proposition 2.8 *Consider the scalar gap problem (2.1) with $L \geq 0$. There exists a critical value of L, L^*, such that system has no solutions for $L < L^*$, exactly one solution at $L = L^*$ (generically), and at least two solution for $L > L^*$. Furthermore, solutions arise disappear via tangent (saddle-node) bifurcations.*

By our restrictions on f, there is a homoclinic orbit, curve A, which is associated with $(0, 0)$. For $w > 0$, it lies entirely below the stable manifold of $(1, 0)$, B. Thus, because the map ψ_L is the identity map for $L = 0$, there are no intersections of curve B and $\psi_L(A)$ and therefore no solution to system exists.

Note that the map ψ_L shifts points (u, u_x) on curve A such that the u_x values remain unchanged and u values are increased by the amount $u_x L$. That is, for fixed u_x, ψ_L maps u values of points on A in a monotonic (linear) fashion with respect to L. This mapping is therefore strictly increasing fashion for $u_x > 0$, while points with $u_x = 0$ remain fixed. Thus, $\psi_L(A)$ will intersect B for sufficiently large L with $u_x > 0$.

The monotonicity of ψ_L in L, the continuity of ψ_L and the continuity of the curves A and B ensures that, as L increases, the first crossing must be tangential (generically, this will occur at a single point). Let us define L to be L^* at this critical value. The above properties also guarantee that at least two nontangential

intersections will exist for $L > L*$. The existence of solutions to equation (2.12) follow from the existence of these intersection points. □

2.3.7 Some properties of solutions

Proposition 2.9 *The steady state solutions of the scalar gap problem (2.1) have the following properties*

(i) Solutions are monotonically increasing.

(ii) Solutions have bounds $0 < u_x < w_{max}$, $0 < u(0) < \bar{u}_A$ *and* $U_B(w_{max}) < u(L) < 1$, *where* $w_{max} = \int_0^\alpha f(u)du$, $U_B(w_{max})$ *is defined such that* $w_{max} = \int_{U_B(w_{max})}^1 f(u)du$, *and* $\bar{u}_A$ *is defined such that* $\int_0^{\bar{u}_A} f(u)du = 0$.

(iii) For a given L, steady state solutions are nowhere equal. (i.e., they are ordered).

(iv) There exist an L^{**} *such that there are exactly two solutions for* $L > L^{**}$.

(v) There exists a solution $u(x)$ *such that* $u(0) = \alpha$ *for some* $L > L^*$. *Furthermore, this solution is stable.*

The first three properties follow directly from inspection of the phase portrait, so proof will not be given. Properties *(iv)* and *(v)* require only brief explanation.

The u values of all points on curve A with $u_x > 0$ are increased under ψ for $L > 0$ by the amount $u_x L$, thus all of these values of u on the shifted curve tend to infinity as $L \to \infty$. However, points (0,0) and (1,0) remain fixed and because the slopes of the unstable manifold of (0,0) and the stable manifold (1,0) are nonzero, property *(iv)* must follow.

To show that property *(v)* holds, we begin by plugging $u(0) = \alpha$ into the algebraic system (2.13) and rearranging the equations to get

$$(\frac{D}{L})^2(u(L) - \alpha)^2 = -2F(\alpha).$$

The right-hand side of this equation is a positive constant. As a function of $u(L)$, the left-hand side is a concave up parabola with a double zero at α. Therefore, a solution exists for all $D/L > 0$, but it is required that $\alpha < u(L) < 1$, because solutions must be monotonically increasing. However, the parabola gets arbitrarily narrow as L increases. Thus for sufficiently large L, a solution with $u(0) = \alpha$ and

$\alpha < u(L) < 1$ is guaranteed to exist. Generically, this is for $L > L^*$ and not $L = L^*$. The stability of the solution will be inferred from the next two sections. □

2.3.8 The appearance and disappearance of solutions

To acquire more information about the appearance and disappearance of solutions, we consider the bifurcation structure of system (2.12) in more detail. In doing so, we obtain a relationship that will help us to analytically determine the stability of solution branches.

Let $w = G_A(u) = \sqrt{-2F(u)}$ be the function describing the homoclinic orbit A for $w = u_x > 0$ on $u \in (0, \bar{u}_A)$ where $\int_0^{\bar{u}_A} f(u)du = 0$. $G_A(u)$ is strictly decreasing on $u \in (\alpha, \bar{u}_A)$, and thus can be inverted on this region, $u = G_A^{-1}(w) = U_A(w)$. Similarly, we can define $w = G_B(u) = \sqrt{2(F(1) - F(u))}$, and therefore $u = G_B^{-1}(w) = U_B(w)$, to describe the decreasing portion of the stable manifold of $(1, 0)$, curve B with $u \in (\alpha, 1)$. We can now express the map ψ_L as

$$\psi_L : [U_A(w), w] \mapsto [wL + U_A(w), w]$$

and look for solutions to

$$wL + U_A(w) = U_B(w)$$

where w is $u_x(0)$ on a solution of equation (2.12). Rearranging this equation, we obtain

$$H(w; L) = U_A(w) + wL - U_B(w) = 0. \tag{2.14}$$

Assume that we know a solution $u^*(x)$ of system (2.12) with $L = L_0$ where $u_x^*(0) = w_0$. Then

$$H(w_0; L_0) = U_A(w_0) + w_0 L_0 - U_B(w_0) = 0. \tag{2.15}$$

By expanding H in a Taylor series about $(w_0; L_0)$ and using the above equation, we get

$$H(w; L) = \qquad [U_A'(w_0) + L_0 - U_B'(w_0)](w - w_0) + w_0(L - L_0) +$$

$$[U_A''(w_0) - U_B''(w_0)](w - w_0)^2 + (w - w_0)(L - L_0) + H.O.T.$$
$$= 0.$$

Thus, bifurcations can (and do in this case) occur when

$$U_A'(w_0) + L_0 - U_B'(w_0) = 0. \tag{2.16}$$

Note that, $U_A'(w_0) < 0$ in order to have solutions to this equation, because L_0 and $-U_B'(w_0)$ are both positive. This is always the case for the branch of curve A that we have chosen to work with, however it is never the case on the $u \in (0, \alpha)$ branch of curve A, i.e., all bifurcations occur with $u(0) > \alpha$.

By using equations (2.15) and (2.16), we have two equations for the two unknowns w_0 and the value of L at the bifurcation point. Solving these equations for L_0, we get

$$L_0 = -U_A'(w_0) + U_B'(w_0) = -\frac{1}{w_0}[U_A(w_0) - U_B(w_0)] \tag{2.17}$$

To find the type of bifurcation algebraically, we let

$$L = L_0 + \epsilon L_1 + \epsilon^2 L_2 + \ldots$$

$$w = w_0 + \epsilon w_1 + \epsilon^2 w_2 + \ldots$$

where ϵ is a small positive parameter, and substitute into equation (2.14) and collect like terms. The $O(\epsilon)$ equation is

$$w_0 L_1 = 0,$$

which implies that $L_1 = 0$. The $O(\epsilon^2)$ terms give

$$w_0 L_2 + w_1^2[U_A''(w_0) - U_B''(w_0)] + L_1 w_1 = 0.$$

L_2 is arbitrary and we can choose it to give the direction of the perturbation away from the bifurcation point. If we choose $L_2 = +1$, then

$$w_1 = \pm\sqrt{\frac{-w_0}{U_A''(w_0) - U_B''(w_0)}},$$

which exists when $U_A''(w_0) - U_B''(w_0) < 0$. This implies that if there is a bifurcation at $L = L_0$, then two new solutions are born as L is increased. If we choose $L_2 = -1$, then

$$w_1 = \pm\sqrt{\frac{-w_0}{-U_A''(w_0) + U_B''(w_0)}},$$

which exists when $U_A''(w_0) - U_B''(w_0) > 0$. This implies that if there is a bifurcation at $L = L_0$, then two solutions coalesce at $L = L_0$ and vanish as L is increased. In the nongeneric case that $U_A''(w_0) - U_B''(w_0) = 0$, higher order terms must be considered to ascertain what happens.

The above gives a condition for the existence of more than two solutions: If $U_A''(w) - U_B''(w)$ change signs on $u \in (\alpha, \bar{u}_A)$, then more than two solutions can exist. In fact, the number of sign changes determines the number of possible tangent bifurcations and thus the number of solutions that can possibly coexist. If $U_A''(w) - U_B''(w)$ does not change sign, then there is a single bifurcation and a maximum of two solutions. This was the case for the cubic f as shown in Figures 2.12 and 2.13. Figure 2.16 shows the phase portrait (with mapping of curve A) for the case of $f = -u(u - 0.17)(u - 1.0)(u^2 - 1.1u + 0.3075)$ in which $U_A''(w) - U_B''(w)$ changes sign twice. As a result of these sign changes, three bifurcations occur: two saddle node bifurcations in which two solutions are born in each and one where the middle two solutions coalesce and vanish. This leads to a maximum of four steady state solutions.

Note that at the bifurcation point, where two solutions are born as L is increased,

$$H_w(w_0; L_0) = H_2(w_0) + L_0 = [U_A'(w_0) - U_B'(w_0)] + L_0 = 0,$$

and

$$H_{ww}(w_0; L_0) = H_2'(w_0) = U_A''(w_0) - U_B''(w_0) < 0.$$

Thus by continuity and ordering, the solution branch with $w < w_0$ immediately following the bifurcation point, and thus the "greater" solution (because $w = G_B(u)$ is monotonically decreasing in u in the pertinent region), will have

$$U_A'(w_0) - U_B'(w_0) + L_0 > 0.$$

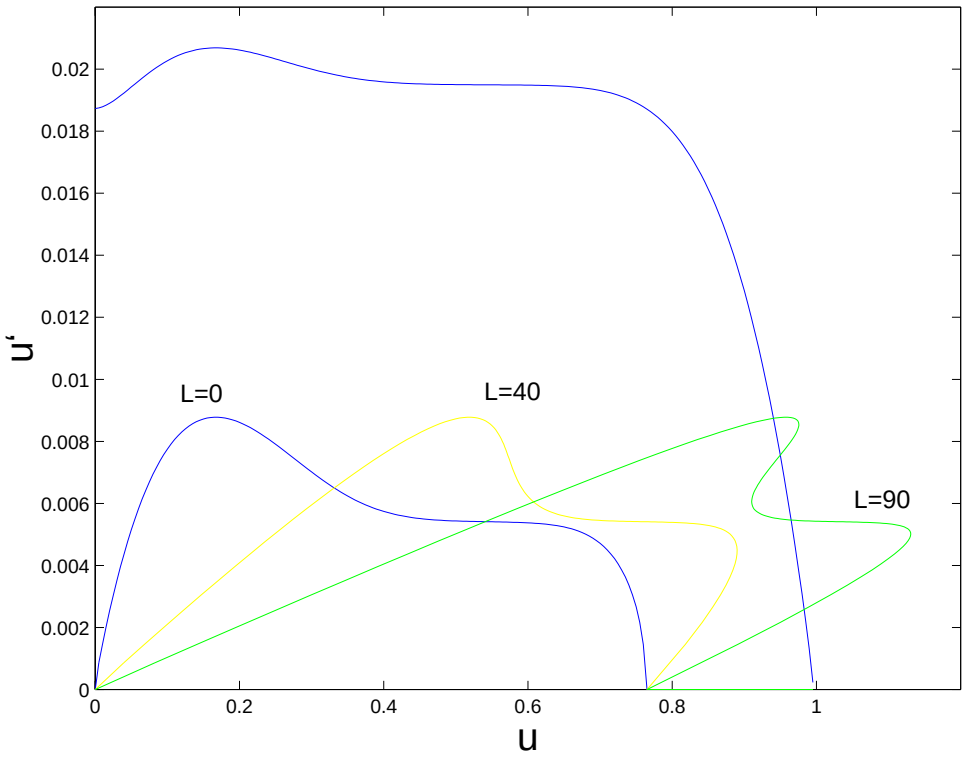

Figure 2.16. The u, u_x-phase portrait of $u_{xx} + f(u) = 0$ with images of the homoclinic orbit (curve A) under the map ψ_L. Here, a quintic reaction term is used $f = -u(u-0.17)(u-1.0)(u^2-1.1u+0.3075)$. At $L = 90$, it can be seen that there are four intersections of the mapped homoclinic orbit A and the stable manifold of $(1, 0)$ (curve B). These intersections correspond to four steady state solutions of the partial differential equation (2.1).

The solution branch with $w > w_0$ immediately following the bifurcation point, and thus the "smaller" solution, will have

$$U_A'(w_0) - U_B'(w_0) + L_0 < 0.$$

This condition will be used to show that the smaller solution is stable and the larger solution is unstable. The stability of one branch and the instability of the other is exactly what we expect given a saddle-node bifurcation. Note that one can justify this result graphically as well.

2.3.9 Stability of solutions

Stability can be determined by numerical simulations of the PDE (2.1) (i.e., observing dynamics for small perturbations away from steady states $u^*(x)$) or by linearizing around $u^*(x)$ and calculating the eigenvalues of the resulting Schroedinger-type equation. However, these results would only be applicable to the general case in an inferential way. Here, we will show stability for general f.

The following proposition implies that, any time two new solutions are born via a saddle-node bifurcation, the larger solution is unstable and the smaller is stable. We show this by attempting to construct time-independent super- and subsolutions that are solutions of system (2.1) everywhere except at $x = 0$. Therefore, they live on curve A for $x < 0$, they are straight lines on $0 < x < L$, they live on curve B for $x > L$, and have continuous second derivatives everywhere but $x = 0$ where a jump in the x-derivative will occur. Conditions for the existence of these super- and subsolutions give us our result.

Proposition 2.10 *Let $u(x)$ be a steady state solution of equation (2.1).*
(i) If $U_A'(u_x(0)) - U_B'(u_x(0)) + L < 0$, then there exists a time-independent supersolution $\bar{\phi}(x)$ and subsolution $\underline{\phi}(x)$ that are arbitrarily close to $u(x)$ with $\bar{\phi}(x) > u(x) > \underline{\phi}$. Therefore, $u(x)$ is a stable solution.
(ii) If $U_A'(u_x(0)) - U_B'(u_x(0)) + L > 0$, then there exists a time-independent supersolution $\bar{\phi}(x)$ and subsolution $\underline{\phi}(x)$ that are arbitrarily close to $u(x)$ with $\bar{\phi}(x) < u(x) < \underline{\phi}(x)$. Therefore, $u(x)$ is an unstable solution.

Assume that we want to construct a supersolution with $\bar{\phi}(x) < u(x)$. As we construct $\bar{\phi}$, it will be extremely useful to follow its trajectory in the phase plane shown in Figure 2.17. Let us attempt to build the supersolution starting from $x = \infty$ and then decreasing x to $x = -\infty$. From $x = L$ to ∞, take $\bar{\phi}$ to live on curve B with $\bar{\phi}'(L) = u'(L) + \epsilon$, where ϵ is arbitrarily small. Because curve B is monotonic with $U_B' < 0$ in the region of interest, it is required that $\epsilon > 0$ in order to have $\bar{\phi}(x) < u(x)$. For $0 < x < L$, take $\bar{\phi}$ to be a straight line such that $\bar{\phi}$ and $\bar{\phi}'$ are continuous at $x = L$. The equation for $\bar{\phi}(0)$ is then

$$\bar{\phi}(0) = -(u'(L) + \epsilon)L + U_B(u'(L) + \epsilon).$$

The remainder of $\bar{\phi}$ will be taken to live on curve A with $\bar{\phi}$ continuous. Thus, $\bar{\phi}$ is a solution everywhere except $x = 0$ where generically $\bar{\phi}'$ is not continuous (for $\epsilon \neq 0$). For $\bar{\phi}$ to be a supersolution, the jump condition $\bar{\phi}'(0^+) - \bar{\phi}'(0^-) < 0$ must be satisfied. Therefore, it is required that $\bar{\phi}(0) < U_A(u_x(L) + \epsilon)$ for points with $u \in (\alpha, \bar{u}_A)$ where $U_A' < 0$ (or $\bar{\phi}(0) > U_A(u_x(L) + \epsilon)$ for points with $u \in (\alpha, \bar{u}_A)$ where $U_A' > 0$). This gives the inequality

$$-(u'(L) + \epsilon)L + U_B(u'(L) + \epsilon) < U_A(u_x(L) + \epsilon).$$

Expanding the inequality about $\epsilon = 0$ and collecting like terms, we get

$$(U_A(u_x(L)) - U_B(u_x(L)) + u_x(L)L) + (U_A'(u_x(L)) - U_B'(u_x(L)) + L)\epsilon + \ldots > 0$$

Because $u(x)$ is a solution to system (2.7), we have that $U_A(u_x(L)) + u_x(L)L = U_B(u_x(0))$. Thus, since ϵ is positive and arbitrarily small, for $\bar{\phi}$ to exist with the given restrictions, it is required that

$$U_A'(u_x(L)) - U_B'(u_x(L)) + L > 0$$

The argument for the existence of sub- and supersolutions in other three cases are identical except for sign changes.

Because ϵ is arbitrarily small, the time-independent sub- and supersolutions are arbitrarily close to the steady state solutions $u(x)$. Therefore, based on the conditions for the existence of the sub- and supersolutions, the results presented in the previous section, and theorem 2.10, our stability result is obtained. □

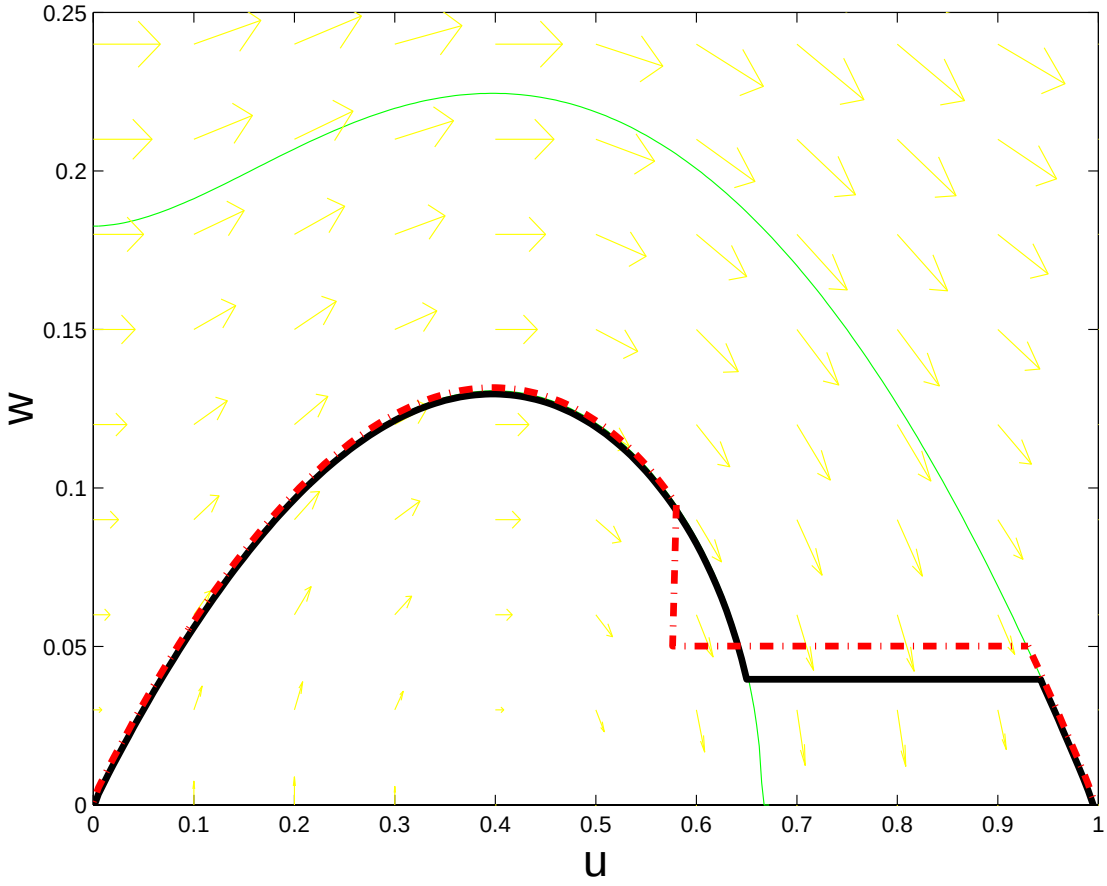

Figure 2.17. Phase plane for cubic f with $\alpha = 0.4$. The trajectory for a steady state solution u^* of (2.1) is plotted as a thick solid line. The trajectory for a time-independent supersolution $\bar{\phi}$ is plotted as a thick dot-dashed line. ($D = 1$,$L = 7.2$). Values of interest: $u^*(0) = 0.650$, $u^*(L) = 0.942$, $u_x^*(0) = u_x^*(L) = 0.041$. $\bar{\phi}(0) = 0.576$, $\bar{\phi}(L) = 0.930$, $\bar{\phi}_x(0+) = \bar{\phi}_x(L) = 0.051$, (i.e., $\epsilon = 0.1$), $\bar{\phi}_x(0-) = 0.0939$, $U_A(\bar{\phi}_x(0+)) \sim 0.64$.

2.3.10 Analogy to coupled cells

It was previously mentioned that the bifurcation parameter of interest is L/D when we are considering the existence of steady states. If $L \to 0$ with L/D constant, then we have the case of two identical excitable cables connected via an ohmic resistor. All results given here apply to this case, which may be a better model for the sucrose gap preparation than when L is taken to be large. This case in many respects is close to two excitable (bistable) cells coupled by a resistor of resistance $1/c_g$

$$\begin{cases} u_1' &= f(u_1) + c_g(u_2 - u_1), \\ u_2' &= f(u_2) + c_g(u_1 - u_2). \end{cases} \tag{2.18}$$

Indeed, Othmer [51] showed that under appropriate scaling, a finite cable with an inhomogeneity identical to the one considered here can be reduced to a pair of coupled cells.

The question that was considered for the full PDE system can also be considered for the case of the coupled cells: Assume the two cells are at rest ($u_1 = 0$,$u_2 = 0$) and cell 2 receives a sufficiently large perturbation for it to become excited. Is the signal transmitted to cell 2 (i.e., does cell 2 become excited as well) or is the signal blocked?

We will show that the bifurcation structure of steady states in system (2.18) has the exact same qualitative features as the full gap model. Also, ordering principles can be derived for system (2.18) in an almost identical way to those in section 2.2.3. Thus, the coupled cell problem (2.18) is analogous to the gap problem (2.1).

To see the similarity in bifurcation structure, the system is best studied in the u_2, u_1-phase plane. Figures 2.18–2.20 show the phase planes for various values c_g. The figures use a cubic f with $\alpha = 0.3$. Figure 2.18 show the phase plane for the uncoupled case $c_g = 0$. There are 9 steady states in all as seen by the intersections of the nullclines. The upper three, which have $u_2 = 1$, are of the most interest here. The steady state at $(u_1, u_2) = (0, 1)$ and $(1, 1)$ are stable nodes, which correspond to cell 2 being excited with cell 1 at rest and both cells being excited, respectively. The steady state at $(1, \alpha)$ is a saddle point that separates the basins of attraction of

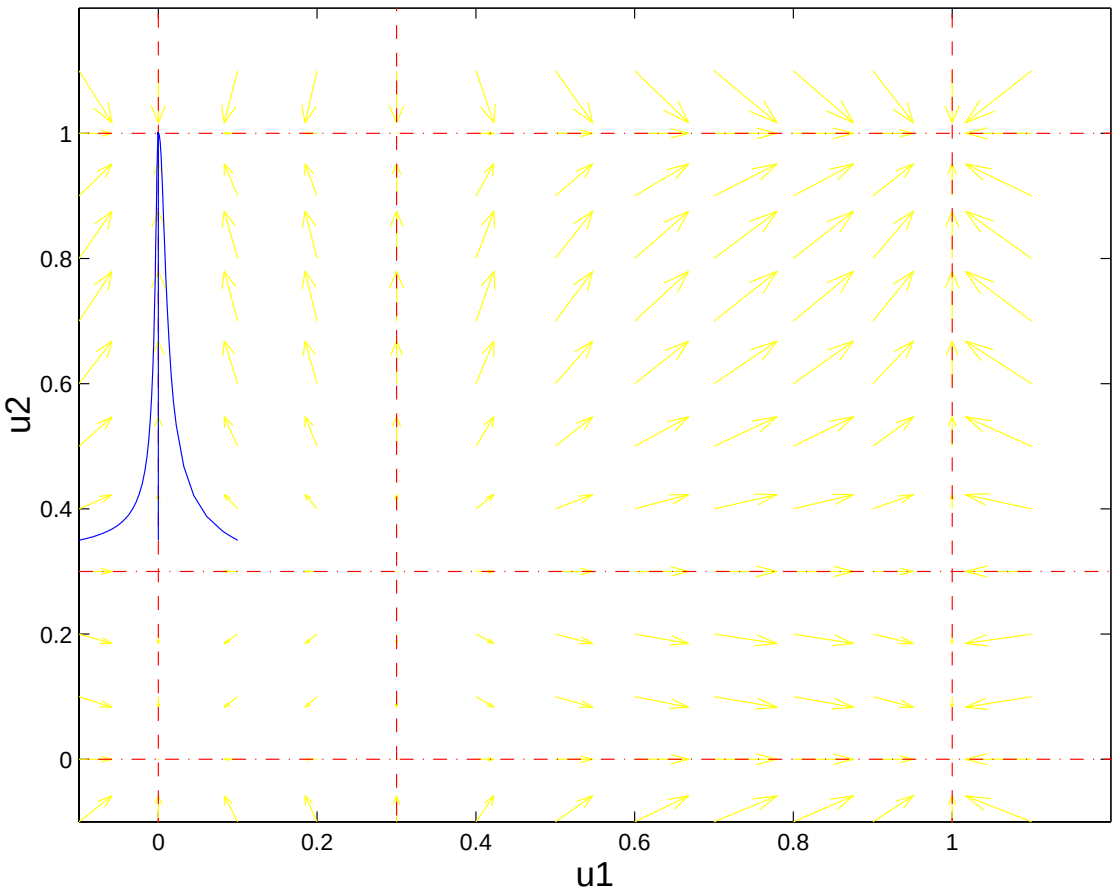

Figure 2.18. Phase plane of coupled cells for cubic f with $\alpha = 0.3$ and $c_g = 0$ (uncoupled). Dashed curves are portions of the u_1-nullcline and the dash-dotted curves are portions of the u_2-nullcline. A few trajectories are shown that begin at points corresponding to superthreshold perturbations of cell 2. The excitation signal is blocked, of course, because the cells are uncoupled and therefore cell 1 does not become excited.

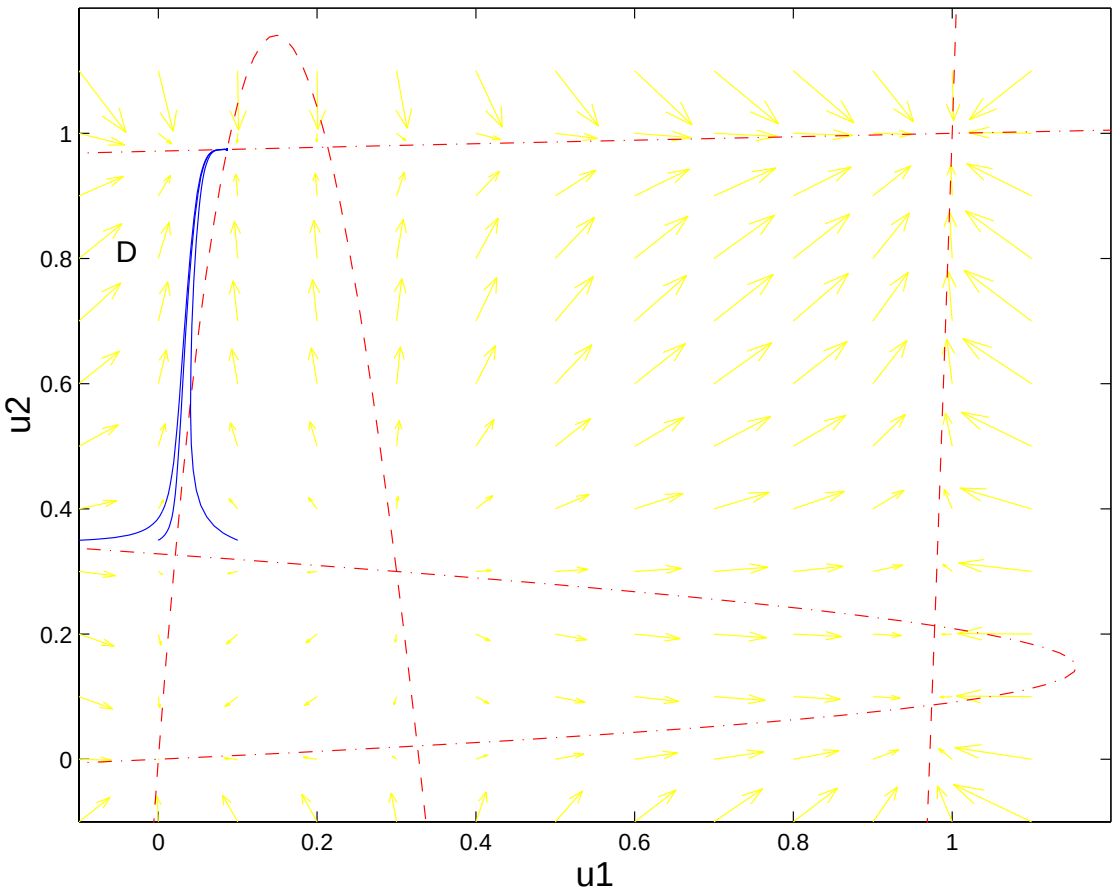

Figure 2.19. Phase plane of coupled cells for cubic f with $\alpha = 0.3$ and $c_g = 0.019$. Dashed curves are portions of the u_1-nullcline and the dash-dotted curves are portions of the u_2-nullcline. A few trajectories are shown that begin at points corresponding to superthreshold perturbations of cell 2. The excitation signal is blocked, because the coupling is not sufficiently strong and therefore cell 1 does not become excited.

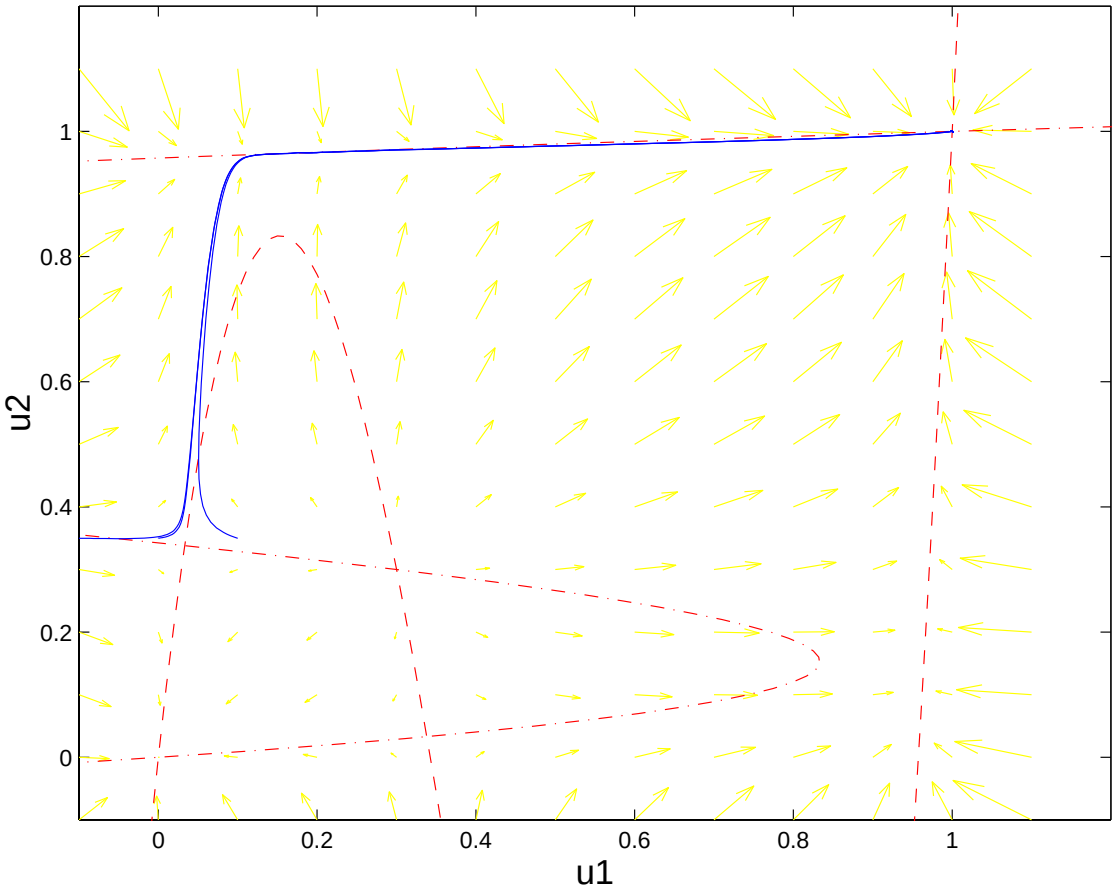

Figure 2.20. Phase plane of coupled cells for cubic f with $\alpha = 0.3$ and $c_g = 0.028$. Dashed curves are portions of the u_1-nullcline and the dash-dotted curves are portions of the u_2-nullcline. A few trajectories are shown that begin at points corresponding to superthreshold perturbations of cell 2. Here, the coupling strength is large enough so that the excitation of cell 2 leads to the excitation of cell 1.

the two stable nodes. If the cells are both at rest (i.e., at the stable node (0,0)) and a perturbation is given to cell 2 that raises u_2 above α, cell 2 will become excited and u_2 will increase to 1. Cell 1 will, of course, remain unchanged at $u_1 = 0$. Thus, the signal is blocked.

For small c_g, this behavior persists. Of note, however, is the appearance of the full structure of the nullclines and the fact that the node that was at $(0, 1)$ and the saddle point that was at $(\alpha, 1)$ are shifted towards one another. This is seen in Figure 2.19 where $c_g = 0.019$. Sufficiently large perturbations of cell 2 away from $(0, 0)$ fall into a positively invariant region D (limited by the immediately surrounding nullclines). The flow in this region funnels all trajectories into the only stable point in the region, the stable node that was shifted from $(0, 1)$. Thus, the signal is still blocked.

As c_g is increased further, however, the stable node that was at $(0, 1)$ and the saddle that was at $(\alpha, 1)$ for the uncoupled system collide and vanish via a saddle-node bifurcation. For the case shown in the figures, this bifurcation point is at $c_g = 0.0235$. Following the bifurcation, the basin of attraction of the old stable steady state is now absorbed by that of the steady state $(1, 1)$, and now perturbations that excite cell 2 lead to an excitation of cell 1 and the signal is successfully transmitted. This is seen in Figure 2.20 where $c_g = 0.028$.

Thus, we see the similarity between the coupled cell model and the gap problem. The saddle that was at $(\alpha, 1)$ in the uncoupled system is analogous to the unstable solution in the PDE and the stable node that was at $(0, 1)$ is analogous to the stable solution. Moreover, the transition between signal block and successfully signal transmission is associated with a saddle-node bifurcation.

In retrospect, we should not be surprised by the bifurcation structure in the gap problem, because of its similarity to the very easily studied coupled cell system. We will make use of this analogy between the gap problem and coupled cells in the next chapter in order to help us understand the dynamic mechanism underlying the phenomenon of wave reflection.

2.3.11 Summary

In section 2.3, we consider wavefront propagation in a spatially distributed scalar excitable medium that contains a local inhomogeneity. This inhomogeneity is a region of nonexcitability of length L in which information is transmitted only by diffusion. By quoting existing theorems, we link the ability of the local inhomogeneity to block wavefront propagation to the existence of solutions to the steady state equations (2.12). We then develop a geometric method that allows one to quickly and easily find when these steady state solutions exist. Furthermore, this method immediately shows several important features of solutions and the overall behavior of the problem.

One of these features is that there exists a critical gap length L^* such that no solutions exist for $L < L^*$, there is exactly one solution for $L = L^*$, and there are two (or more) solutions $L > L^*$. This suggests that the solutions arise via a saddle node bifurcation. Indeed, using upper and lower solution techniques, we prove that the larger of the two solutions is unstable, whereas the smaller solution is stable. The "distance" of the stable solution from the unstable solution gives an idea of the size of the basin of attraction of the stable solution (i.e., just how stable the stable solution is). The unstable solution can be interpreted as a threshold for jumping the gap.

Another benefit of the graphical representation is that it shows the important portions of f that determine whether or not block occurs. If the system is "highly excitable", there is a sizable portion of f that plays no role whatsoever in the dynamics of wavefront block.

In the following sections, we will show examples of how the geometric method can be extended to problems with gap dynamics other than strict diffusion.

2.4 Other Gap Dynamics

2.4.1 Variable diffusion coefficient

It should be noted that the true parameter involved in determining the existence of steady state solutions to system (2.1), and therefore wavefront block, is total resistance in the gap. Consider the case of a variable diffusion coefficient, $D(x)$, in

the gap $0 < x < L$ and the excitable portion as originally defined. The matching conditions change slightly to

$$\begin{aligned}
\lim_{x\to 0^-} u &= \lim_{x\to 0^+} u, \\
\lim_{x\to L^+} u &= \lim_{x\to L^-} u, \\
\lim_{x\to 0^-} u_x &= \lim_{x\to 0^+} D(0)u_x, \\
\lim_{x\to L^+} u_x &= \lim_{x\to L^-} D(L)u_x.
\end{aligned}$$

Integrating the equation for gap dynamics,

$$\begin{aligned}
(D(x)u_x)_x &= 0, \\
u_x(x) &= \frac{u_x(0)}{D(x)}, \\
u(x) = u_x(0)\int_0^x [D(y)]^{-1}dy &+ u(0).
\end{aligned}$$

This results in a map

$$\psi_L : [u(0), u_x(0)] \mapsto [v(L), v_x(L)] = [u_x(0)\int_0^L [D(x)]^{-1}dx + u(0), u_x(0)].$$

Thus we see that the total resistance $\int_0^L [D(x)]^{-1}dx$ determines the mapping of points on curve A through the gap to curve B.

This mapping implies that an asymmetric diffusion coefficient within the gap does not give rise to unidirectional block, i.e., it does not make it easier to block a wave traveling towards the gap in one direction compared to a wave traveling towards the gap in the other direction [32, 34, 42]. Unidirectional block can only occur when the two excitable regions of the cable have different diffusion coefficients. For a gap length of zero and only a change diffusion coefficients, this situation would be equivalent to problems considered by Pauwelussen [53] (changing diameter of a neuron), and Fife and Peletier [20] (changing mobility in space). It should be noted that if the gap has nonzero excitability and D varies through the gap, then one-way block can occur [20].

2.4.2 Leaky Gap and ischemic tissue

Similar analysis can be performed in the (perhaps more physical) case where gap dynamics include a leakage term, $-\gamma u$, in addition to diffusion:

$$u_t = Du_{xx} - \gamma u, \quad x \in (0, L).$$

Because only the dynamics in the gap are altered, only the map ψ_L is changed. The new map is:

$$\begin{aligned}\tilde{\psi}_L : [u(0), u_x(0)] \mapsto \quad & [\tfrac{u_x(0)}{\sqrt{D\gamma}} \sinh \sqrt{\tfrac{\gamma}{D}} L + u(0) \cosh \sqrt{\tfrac{\gamma}{D}} L, \\ & u_x(0) \cosh \sqrt{\tfrac{\gamma}{D}} L + Du(0) \sqrt{\tfrac{\gamma}{D}} \sinh \sqrt{\tfrac{\gamma}{D}} L].\end{aligned}$$

It is easy to show that as $\gamma \longrightarrow 0$, $\tilde{\psi}_L \longrightarrow \psi_L$. However, for a sizeable leakage term, results look different, as shown in Figures 2.21–2.25. The addition of this leakage term results in a lower critical gap length L^* as expected. It also allows for the possibility for nonmonotonic solution (which are always unstable according to Sturm-Liouville theory). Furthermore, for γ not too small, almost the entire function f is represented along solutions (i.e., very little of f is unimportant in determining block unlike the case with $\gamma = 0$). All of these differences are products of the new map having only one fixed point (0,0) (rather than two) and lifting the rest of the homoclinic orbit including the point $(\alpha, 0)$ towards the stable manifold of (1,0).

Despite the difference in the map and solutions, the important aspects of the topology of the system remain the same as those for the strictly diffusive gap. Hence, the super- and subsolutions needed to determine stability of solutions can be constructed in the same manner as before, and they lead to results that are very similar to the strictly diffusive case (see Figure 2.23).

The above may be more realistic for the AV node in which the resting potential is not too different from atrial and bundle of His tissue, however an additional factor may be important to include in the case of an ischemic region. One of the major changes that occurs when a tissue becomes ischemic is that the membrane

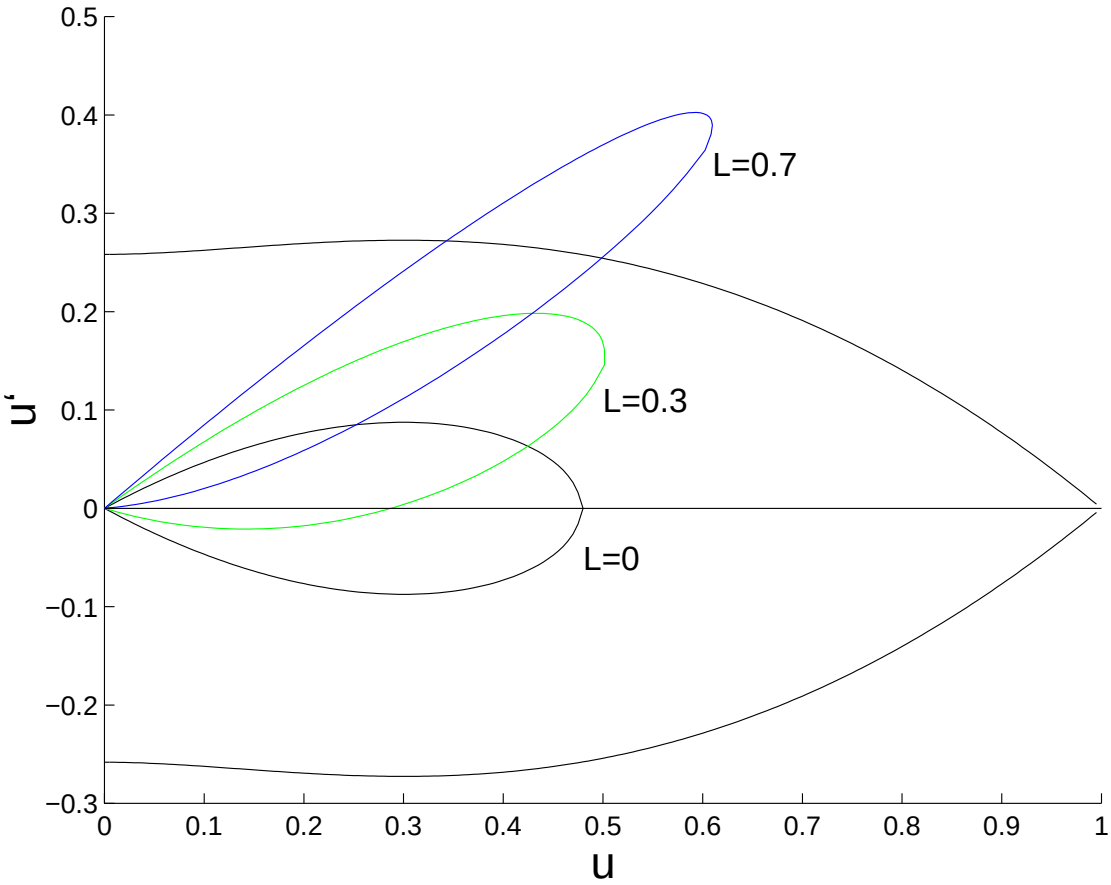

Figure 2.21. The u, u_x-phase portrait of $u_{xx} + f(u) = 0$ with images of the homoclinic orbit (curve A) under the map $\tilde{\psi}_L$ for leaky gap. The first intersection is at $L^* = 0.426$.

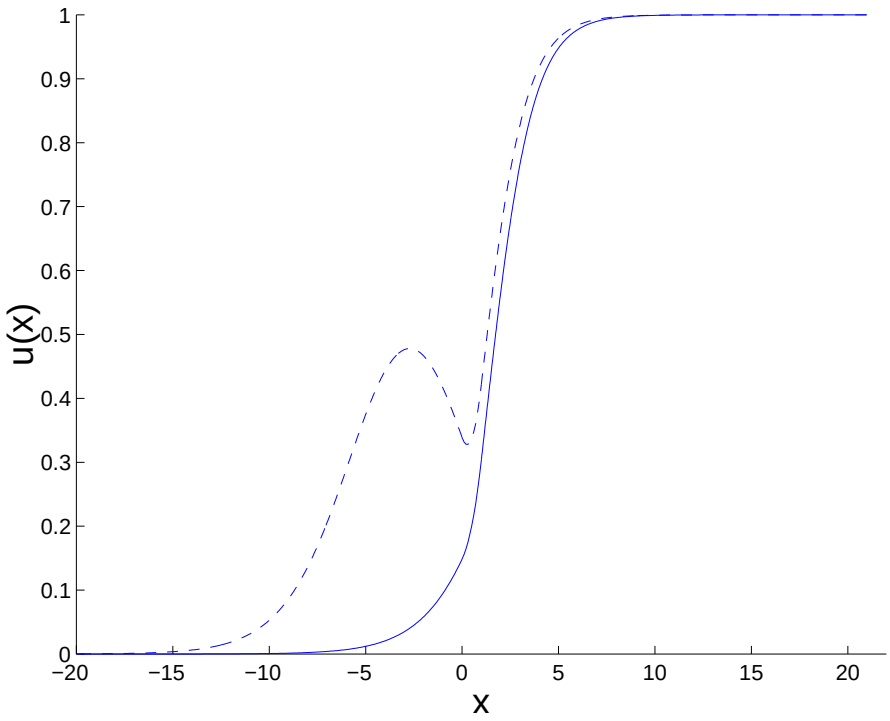

Figure 2.22. The steady states for leaky gap at $L = 1.0$. The solid line represent the stable solution and the dashed line represent the unstable solution. The parameters are $\alpha = 0.3$, $D = 1$, $\gamma = 1.0$.

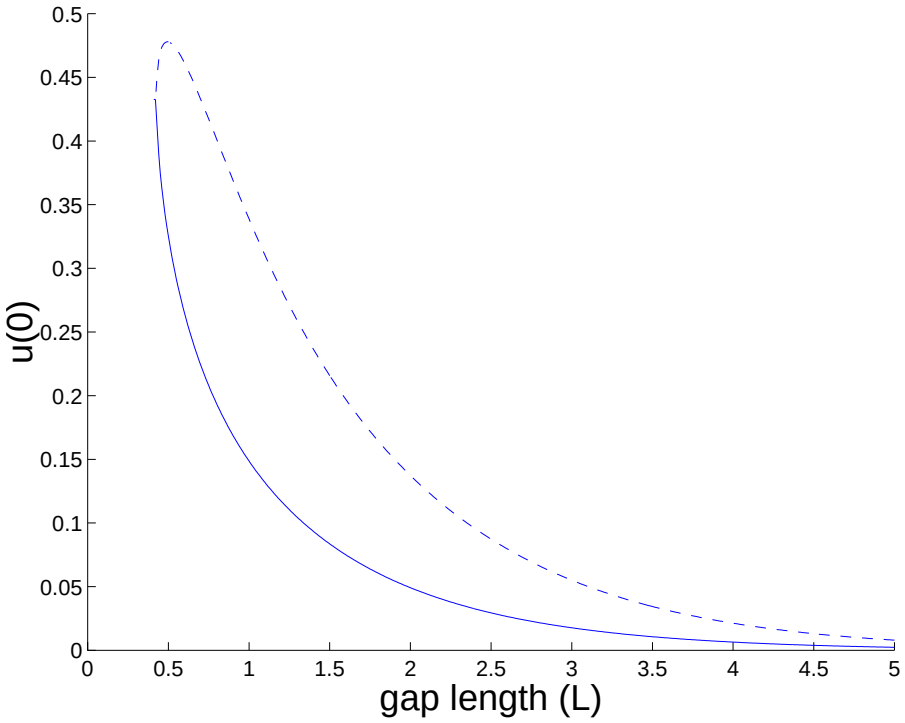

Figure 2.23. Bifurcation diagram for leaky gap: $u(0)$ of the steady state vs. gap length (L). The solid line represent stable solutions and the dashed line represent unstable solutions. The critical gap length is $L^* = 0.426$. The parameters are $\alpha = 0.3$, $D = 1$, $\gamma = 1.0$.

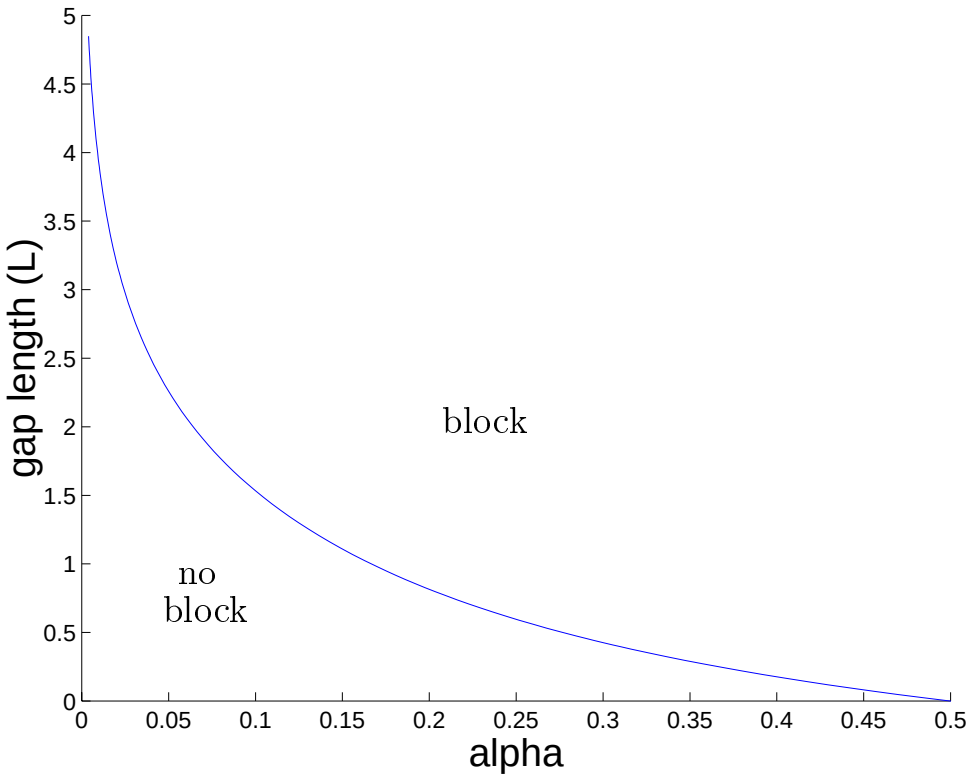

Figure 2.24. Critical gap length (L^*) vs. α for leaky gap. (Locus of the fold). This curve was calculated using AUTO [16].

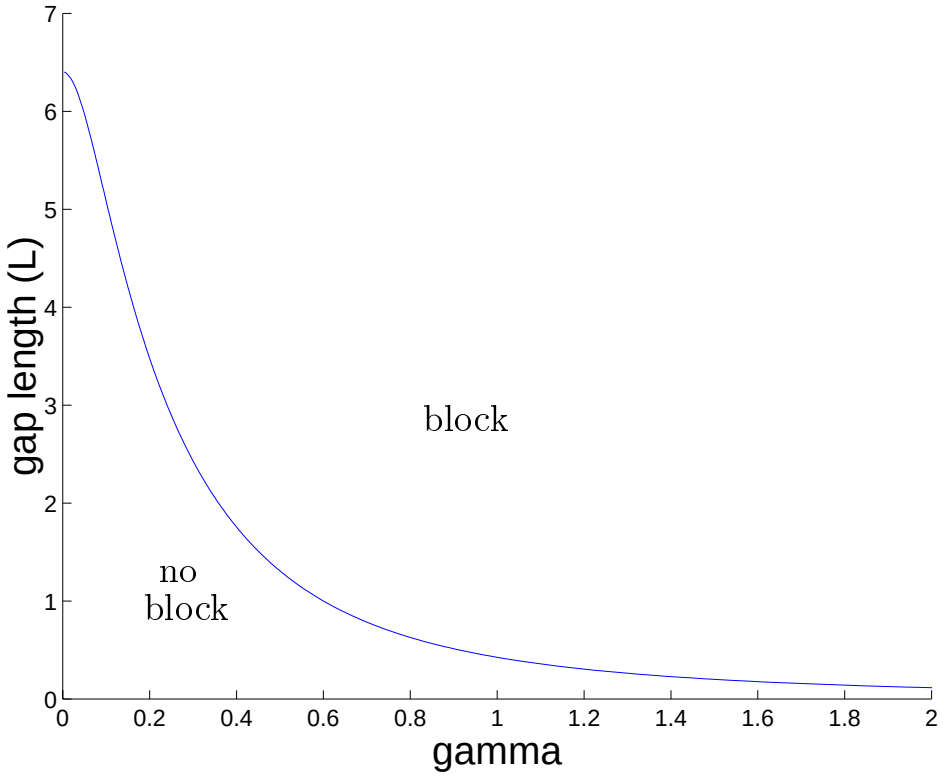

Figure 2.25. Critical gap length (L^*) vs. γ for leaky gap. (Locus of the fold). This curve was calculated using AUTO [16].

potential depolarizes (increases with respect to surrounding healthy tissue), thus the gap dynamics become

$$u_t = Du_{xx} - \gamma(u - u_r), \quad x \in (0, L).$$

and the map is adjusted to have a shift in the phase plane

$$\begin{aligned}\tilde{\psi}_L : [u(0), u_x(0)] \mapsto \quad & [u_r(1 - \cosh\sqrt{\tfrac{\gamma}{D}}L) + \tfrac{u_x(0)}{\sqrt{D\gamma}}\sinh\sqrt{\tfrac{\gamma}{D}}L + u(0)\cosh\sqrt{\tfrac{\gamma}{D}}L, \\ & -u_r\sqrt{\gamma D}\sinh\sqrt{\tfrac{\gamma}{D}}L u_x(0)\cosh\sqrt{\tfrac{\gamma}{D}}L + u(0)\sqrt{\gamma D}\sinh\sqrt{\tfrac{\gamma}{D}}L].\end{aligned}$$

Because the adjustment terms in the map are always negative, the shift of $\tilde{\psi}_L(A)$ is down and away from curve B, and therefore delays the critical gap length at which block occurs when compared to the leaky gap result. This may not be surprising, because the depolarized region acts as an extra source that will aid in transmission of signals across the gap.

2.4.3 Gap with low excitation

In this section, gap dynamics of reduced excitability will be considered. The main results presented are essentially due to Fife and Peletier [20] in that the super- and subsolutions constructed to prove the results are the same as theirs. We will modify their main theorem and its proof to use terminology consistent with the rest of this thesis and rework resulting approximations of (bounds on) the critical gap length L^* enabling a few new observations. In particular, a smaller lower bound on L^* is obtained. This bound has explicit dependence on $s(x)$ and does not rely on a specific form of $s(x)$. Also, an interpretation of the problem is given in terms of the phase plane for the case when s in the gap is constant.

Let us study the equation (2.1) with a local inhomogeneity described by

$$s(x) = \begin{cases} s_g(x), & 0 \le x < L, \\ 1, & \text{otherwise.} \end{cases} \tag{2.19}$$

It is mentioned above that we are considering reduced excitability in the gap. One could take this to imply that $s_g(x) < 1$, however we will see that it actually is the

average level of excitability in the gap that will appear in our bound on L^*, thus this is not a necessary restriction.

Proposition 2.11 *Let M be the maximum of f on $u \in (\alpha, 1)$ and $\bar{s}$ be the average excitability in the gap $\frac{1}{L}\int_0^L s_g(x)dx$.*

If

$$\bar{s} \leq \frac{-F(\alpha)}{2M(1-\alpha)},$$

and

$$L \geq \frac{\sqrt{-2F(\alpha)}}{2\bar{s}M}\left(1 - \sqrt{\frac{1-2(1-\alpha)}{-F(\alpha)\bar{s}M}}\right). \tag{2.20}$$

then equation (2.1) with inhomogeneity (2.19) has a stable steady state solution.

If the reaction term in the gap $s_g = 0$, then this bound reduces to

$$L > \frac{(1-\alpha)}{\sqrt{-2F(\alpha)}}. \tag{2.21}$$

To prove this, we attempt to construct a time-independent subsolution $\underline{\phi}$ and a time-independent supersolution $\bar{\phi}$ for equation (2.1) with condition (2.19) such that $\underline{\phi} > \bar{\phi}$. When these exist, according to theorem 2.11, we are guaranteed the existence of a stable steady state solution of (2.1).

The supersolution, $\bar{\phi}$, consists of $u = 0$ for $x \leq L$ and the solution the lives on the stable manifold of (1,0) (curve B) starting from $u = 0$ at $x = L$ and going to $u = 1$ as $x \to \infty$. Note that $\bar{\phi}$ is a solution everywhere except at $x = L$ where $\bar{\phi}'(0^+) - \bar{\phi}'(0^-) > 0$, therefore the supersolution, $\bar{\phi}$, always exist.

Set $L = \bar{L}$, where $\bar{L}$ is the minimum value of L for which we can construct a particular subsolution, $\underline{\phi}$. This subsolution, $\underline{\phi}$, consists of 3 regions. On $x \in (-\infty, 0]$, $\underline{\phi}$ lives on the homoclinic orbit A with $\underline{\phi}(0) = \alpha$ and $\underline{\phi}'(0) = \sqrt{-2F(\alpha)}$. On $x \geq \bar{L}$, $\underline{\phi} = 1$. The portion of $\underline{\phi}$ in $x \in (0, \bar{L})$, which will be called v, is given by the initial value problem

$$\begin{aligned} &v'' + s_g(x)M = 0, \\ &v(0) = \alpha, v'(0) = \sqrt{-2F(\alpha)}. \end{aligned} \tag{2.22}$$

As a subsolution, $\underline{\phi}$ is required to be continuous, so we must set $v(\bar{L}) = 1$. Thus, $\underline{\phi}'' + s(x)f(\underline{\phi}) \leq 0$ and $\underline{\phi}'(0^+) - \underline{\phi}'(0^-) < 0$ (i.e., if it exists, then $\underline{\phi}$ is indeed a subsolution).

We now find conditions for the existence of $\underline{\phi}$. From equation (2.22), $v'' < 0$. This implies that a requirement for the existence of $\underline{\phi}$ is that $v'(0)\bar{L} > (1 - \alpha)$, which is exactly the inequality (2.20). Note that this bound does not depend on details of the inhomogeneity. In fact, this is the bound that for the solely diffusive case, $s_g = 0$ given in inequality (2.21).

Integrating equation (2.22) for $x \leq \bar{L}$, we obtain

$$v'(x) - v'(0) = -M \int_0^x s_g(z)dz \geq -M \int_0^{\bar{L}} s_g(z)dz = -M\bar{s}\bar{L}.$$

Integrating again and evaluating at $x = \bar{L}$, we find that

$$v(\bar{L}) - v(0) = 1 - \alpha \geq (-M\bar{s}\bar{L} + v'(0))\bar{L}.$$

Rearranging and using the quadratic formula, we find that

$$\bar{L} \geq \frac{v'(0) - \sqrt{v'(0)^2 - 4M\bar{s}(1-\alpha)}}{2\bar{s}M}.$$

(i.e., the larger "root" is of no consequence). Rearranging this inequality, we arrive at inequality (2.20). Note that this bound relies on the average excitability in the gap and not on the explicit form of $s(x)$. The condition for the existence of such a bound is given by the discriminant, which is equivalent to the condition stated in the hypothesis of the proposition.

Also, although we have already validated inequality (2.21), it is comforting to see that (2.20) reduces to (2.21) as the average level of excitability in the gap $s_g(x)$ goes to 0.

Finally, note that if $L > \bar{L}$, then the same $\underline{\phi}$ exists. □

When $s_g(x)$ is a constant the bound on L can be improved to

$$L \geq \frac{\sqrt{-2F(\alpha)}}{\bar{s}M}\left(1 - \sqrt{\frac{1-2(1-\alpha)}{-2F(\alpha)\bar{s}M}}\right), \tag{2.23}$$

which exists when

$$s_g \leq \frac{-F(\alpha)}{M(1-\alpha)/2}.$$

This bound on s_g is reminiscent of a similar bound in a model where there is an abrupt decrease in excitability [20, 53], especially if one thinks of $M(1-\alpha)/2$ as an approximation of $\int_\alpha^1 f(u)du$.

Also, when $s_g(x)$ is a constant, we can apply techniques similar to those used in the purely diffusive case. We can generate a map under the flow of the gap dynamics, use this to map points on the homoclinic orbit determined by the outer equations, and look for intersections of this mapped curve with the stable manifold of (1,0). The only difference is that the map can not be written explicitly and must be generated numerically. Examples of the mapping is shown in Figure 2.26 where L is varied and Figure 2.27 where s_g is changed. Also, the geometric technique presented here can be extended to apply to piecewise constant changes in $s(x)$. In this case, steady state solution could be found by simply applying a series of maps to curve A before looking for intersections with curve B.

2.5 Discussion

We believe the analysis and results that we present here helps to elucidate the problem of determining which properties regulate the ability of a wave of excitation to be transmitted across gaps of inexcitability or low excitability. However, because only the scalar system is considered, the direct applicability of this work to general excitable media needs further consideration. When the time scale of recovery is much larger than the characteristic time for diffusion and excitation, the analysis here will predict the critical gap length well. On the other hand, in some physical situations, recovery dynamics are not slow enough to ignore and can play a large role in determining whether or not a wave is blocked by a gap. To make matters worse, excitation is not always described by a single variable in many systems.

Most simple caricature models of the electrical activity in cardiac tissue do not have these problems. Generally, they have a single fast variable that is responsible for the autocatalytic process in excitation and fairly slow recovery variables.

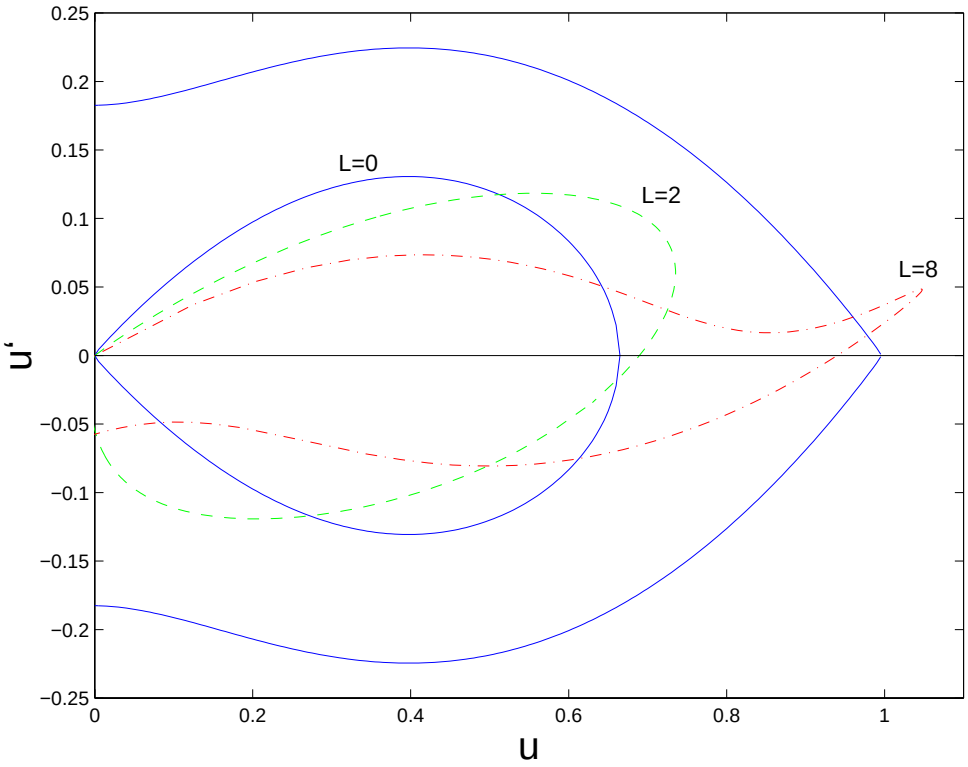

Figure 2.26. The u, u_x-phase portrait of $u_{xx} + f(u) = 0$ with images of the homoclinic orbit under the map flow of $u_{xx} + s_g f(u) = 0$. $\alpha = 0.4$, $s_g = 0.3$.

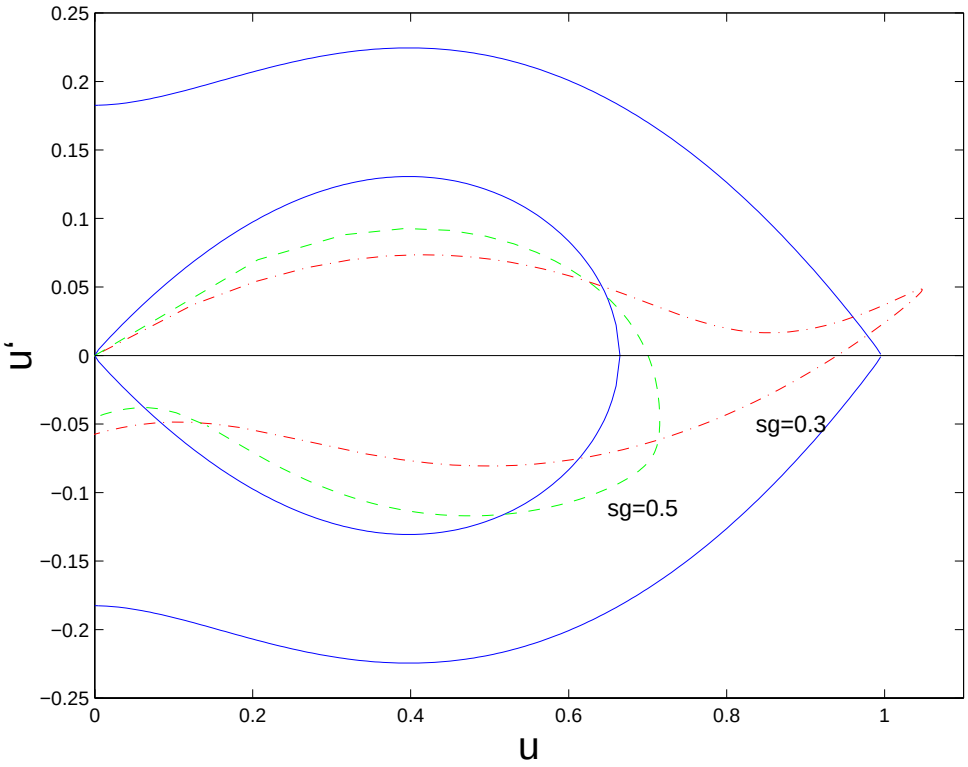

Figure 2.27. The u, u_x-phase portrait of $u_{xx} + f(u) = 0$ with images of the homoclinic orbit under the map flow of $u_{xx} + s_g f(u) = 0$. $\alpha = 0.4$, $L = 8.0$.

Therefore, if we implement these models in the gap problem, we can set the recovery variables to constants, apply our geometric method, and confidently approximate the critical gap length. Unfortunately, detailed models of cardiac tissue have both several excitability variables and some fairly fast recovery variables. It is not easy to get good quantitative approximations of the critical gap length from a physiological standpoint. It may be possible that this can be overcome by deriving "effective" one variable excitation terms for these detailed model. We have had some preliminary success in accomplishing this for a specific case (the Noble model [49]), but much more work needs to be done before a general method for this type of reduction can be attained.

CHAPTER 3

REFLECTION

3.1 Including Recovery

The previous chapter dealt with propagation failure in excitable media having a distinct region with weak or no excitability. It was assumed that recovery was slow enough so that it could be ignored. The benefit of ignoring recovery was that the resulting equation was a scalar parabolic partial differential equation, and ordering principles for these types of equations allowed us to obtain analytical results concerning conditions for propagation failure. However, propagation failure was one of the few behaviors that can be studied with this model.

When recovery is included, one problem of interest is how recovery dynamics modulate the critical gap length that marks the transition from successful transmission of the signal through the gap to transmission block. Figure 3.1 shows the time it takes for a signal to be transmitted through the gap as a function of gap length for the scalar gap problem. As the gap length is increased towards the critical gap length, the transmission time goes to infinity. (This reflects the presence of the zero eigenvalue associated with the saddle-node bifurcation). When recovery is included, the medium on the proximal side of the gap is only excited for a finite amount of time and therefore can only source current to medium on the distal side for that finite amount of time. Thus, it is obvious that the block must occur at smaller gap lengths in a model that contains recovery dynamics than the critical gap length in a comparable scalar model, and in order to get a complete picture of wave block, one must study the relationship between recovery dynamics on the proximal side of the gap, threshold dynamics on the distal side of the gap, properties of the gap and the critical gap length.

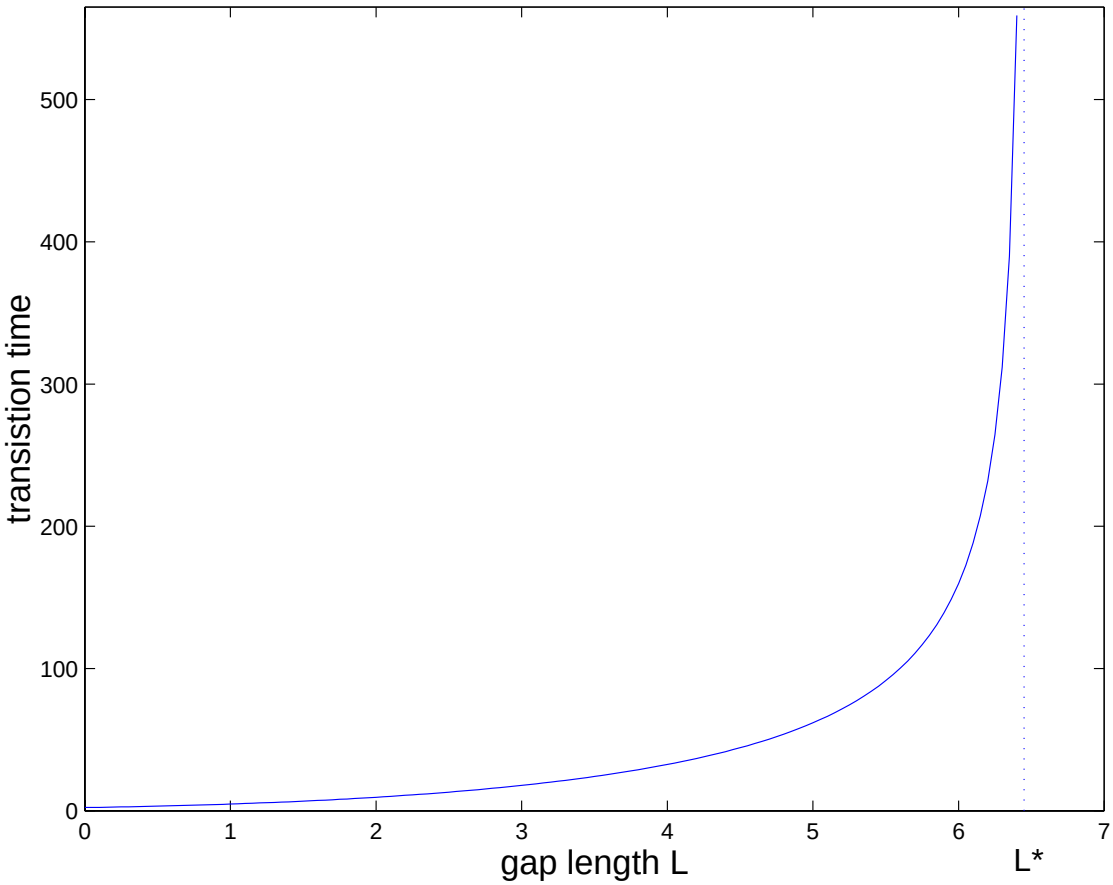

Figure 3.1. The time required for the wavefront to cross the gap as a function of the length of the gap (L) for equation (2.1) with f cubic and $\alpha = 0.3$. As L approaches the critical gap length $L* \sim 6.45$, the transmission time goes to ∞.

When recovery is included in the model, more interesting behavior can occur than simply propagation failure or successful transmission. Because cardiac tissue usually receives periodic input stemming from the sino-atrial node, the response to periodic stimulation is of particular interest in cardiac electrophysiology. Different periods and amplitudes of stimulation uncover the dependency of excitation threshold and excitation duration on recovery times and give rise to various different excitation patterns [43, 67, 46, 11]. Preliminary studies show that the gap model exhibits patterns of activity known as Wenckebach rhythms [47, 36]. Wenckebach rhythms are also seen clinically and in sucrose gap experiments [7, 29], *in vivo* and *in vitro* AV nodal preparations [6], as well as ventricular tissue [14] and Purkinje fiber [64]. Furthermore, Guevara saw these same patterns in a detailed model of Purkinje with a region of reduced excitability [24]. This increases confidence that the gap model is a viable simple analog for the AV node as well as damaged tissue.

Another behavior that is important in cardiac electrophysiology is a phenomenon known as reflection or echo waves [39]. Reflection is characterized by a wave that is propagating in one direction giving rise to another wave that travels back in the direction from which the original wave came. This behavior has been observed in sucrose gap experiments [7, 29] and in experiments where the gap contains an ischemic like medium [59]. These experimental results have lead to the belief that reflection can play a key role in the initiation of the fatal cardiac arrhythmias ventricular tachycardia and fibrillation. The exact mechanism, however, is not at all clear. Reflection has also been described in models of neurons with inhomogeneities such as changes in axonal diameter, temperature and channel density [18, 70, 22] or a region of injury [27]; however only partial reflection has been seen in actual experimental neural preparations [56].

In this chapter, we describe the behavior associated with reflection in the gap model and attempt to obtain insight into the physical and dynamical mechanisms underlying this behavior. As mentioned above, it is the inclusion of recovery dynamics that gives rise to behaviors such as reflection. Unfortunately, when recovery dynamics are included, the model is no longer a scalar equation and

ordering principles no longer hold. This makes the more interesting behavior of the system more difficult to study directly. For this reason, our insight into the underlying mechanisms will hinge on simplifications of the full system.

3.2 Reflection in the Gap Model

3.2.1 Numerical simulations

The following describes results of numerical simulations of the gap problem using Morris-Lecar dynamics [48]. (The next section will describe these dynamics in detail). The simulations begin with a wave of excitation traveling towards the gap and show the different behaviors that result as the gap length, L, is varied.

At small gap lengths, the wave propagates towards the gap and stalls as it reaches it. This stall is brief, because the wave quickly sources enough current through the purely diffusive region of the medium to excite the portion of the medium on the distal side of the gap. The wave is thus reestablished and continues to propagate into the remainder of the medium. Figure 3.2 shows an example of this for $L = 1.5$. It is interesting to note that excitation on the distal portion of the medium starts at a point that is not immediately next to the gap. Figure 3.3 depicts a situation in which the gap length is large enough to block the wave, $L = 1.7$. In this case, when the wave hits the gap, it cannot source enough current through the gap to excite the medium on the distal side before the excitation ends on the proximal side. So far, this behavior is similar to the behavior described in the previous chapter. However, when we look at the behavior for intermediate gap lengths, we see much more interesting behavior.

At a gap length of $L = 1.6$, the wave successfully bridges the gap, however the delay between hitting the gap and exciting the distal side is long. In fact, it is long enough so that when the distal side becomes excited, the proximal side is recovered. This results in not only the wave propagating down the distal side of the medium, but also the distal excitation sources current back through the gap and is able to re-excite the recovered proximal side. This is seen in Figure 3.4. The result is a "reflected" wave that travels through the medium in a retrograde fashion. This is exactly the behavior that is exhibited in the sucrose gap experiments.

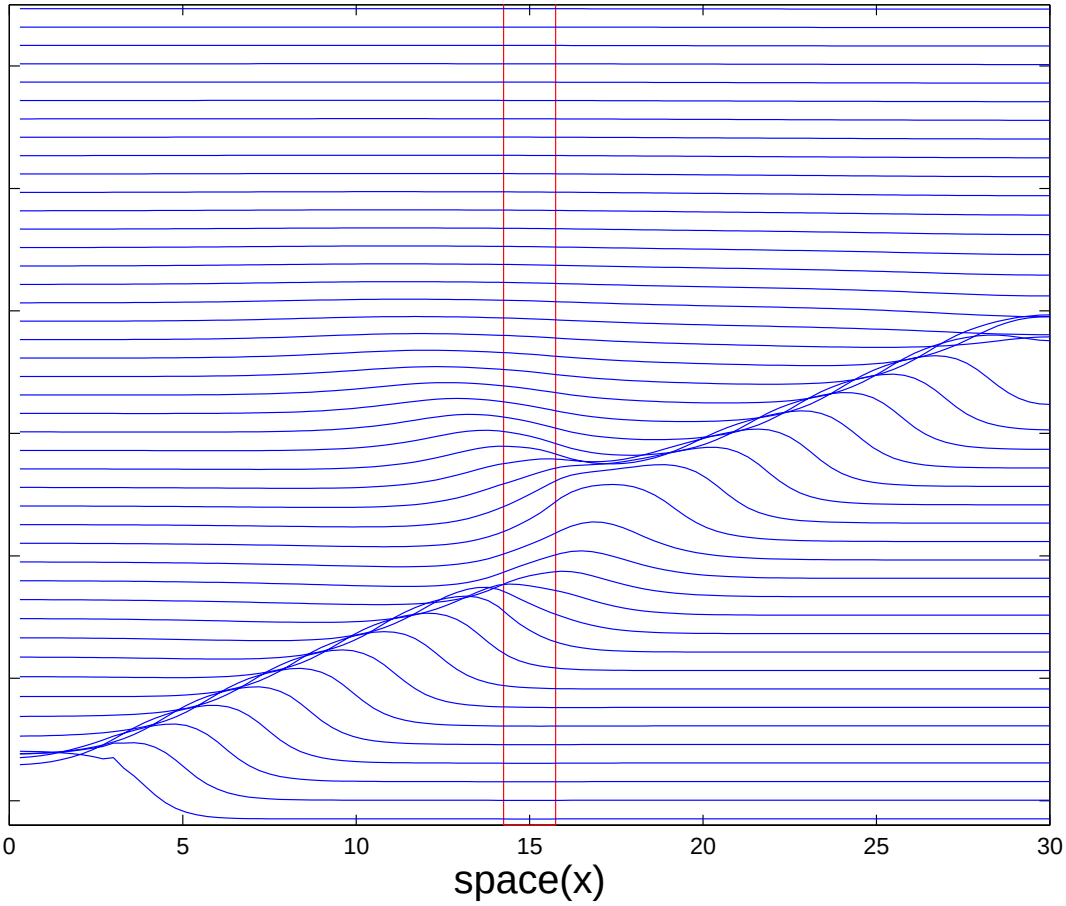

Figure 3.2. Numerical simulation of the gap problem (2.1) using ML excitation dynamics with a gap length $L = 1.5$. At this gap length, the wave successfully crosses the diffusive gap - 1:1 pattern. For this figure and the next five figures, u vs. space (x) is plotted. Each curve is the solution at a fixed time (every 1 ms) and as time progresses the curves are lifted slightly.

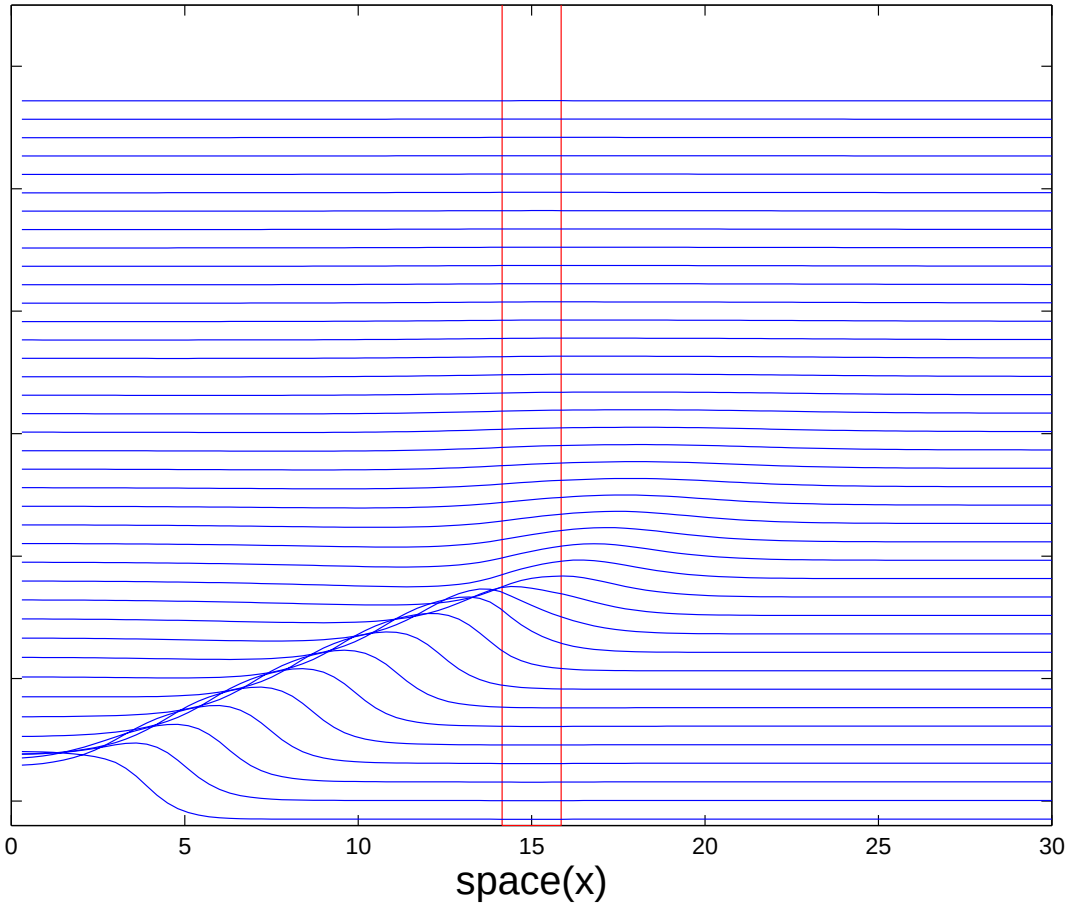

Figure 3.3. Numerical simulation of the gap problem (2.1) using ML excitation dynamics with a gap length $L = 1.7$. At this gap length, the gap blocks the wave - 1:0 pattern. This simulation was performed using the implicit-explicit method of Hines [26] with a time step of $\Delta t = 0.01$ and a space step of $\Delta x = 0.05$.

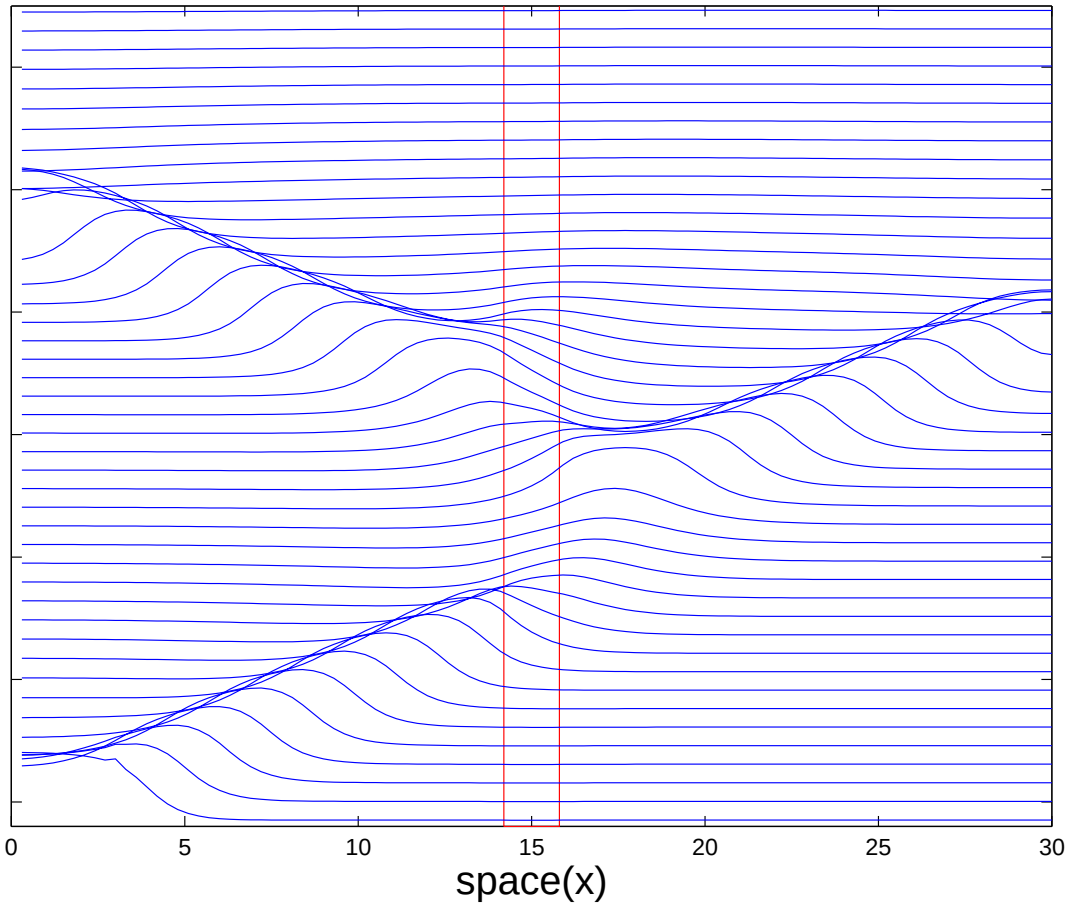

Figure 3.4. Numerical simulation of the gap problem (2.1) using ML excitation dynamics with a gap length $L = 1.6$. At this gap length, the wave successfully crosses the diffusive gap and then produces a reflected wave - 2:1 pattern. This simulation was performed using the implicit-explicit method of Hines [26] with $\Delta t = 0.01$ and $\Delta x = 0.05$.

If we probe the fine detail of parameter L space, we see even more exotic behavior. At $L = 1.52$, a reflected wave occurs, but the reflected wave itself actually elicits a reflection of its own. At $L = 1.544$, the reflection of the reflection gives rise to another reflection, and at $L = 1.543$, yet another reflection occurs on top of these. Figures 3.5, 3.6, and 3.7 show these behaviors.

As L space is probed even deeper, many more reflected waves occur, although the behavior occurs over a very small region of parameter space.

Let us define an N:M reflection pattern such that N is the number of waves occurring on the proximal side of the gap (including the original incoming wave) and M is the number of waves occurring on the distal side of the gap. The sequence of behavior that the above simulations suggests can then be expressed as

$$1:1,\ 2:2,\ 3:3,\ \ldots,\ N:N,\ \ldots,\ldots,\ N+1:N,\ \ldots,\ 3:2,\ 2:1,\ 1:0 \quad (3.1)$$

as the gap length L is increased. Ermentrout and Rinzel [18] observed this same sequence of reflection in a cable model with an abrupt change in cable diameter.

We will attempt to uncover the dynamical mechanism underlying this sequence, but first we give a detailed description of the ML model that will lead to a "physical" explanation of reflection in the model.

3.2.2 The Morris-Lecar (ML) model

The ML model was originally designed as an ionic (Hodgkin-Huxley-like) model for "slow potential" activity in the barnacle muscle [48], but now is generally used as a simple model of excitable media that exhibits true threshold behavior. The property of having a true threshold is known as type I excitability [57] and it will be shown here that it facilitates the appearance of reflected waves.

The ML equations are

$$u_t = f(u,w) = I - g_{Ca} m_\infty(u)(u - E_{Ca}) - g_K w(u - E_K) - g_l(u - E_l),$$

$$w_t = g(u,w) = \frac{1}{\tau_w(u)}(w_\infty(u) - w),$$

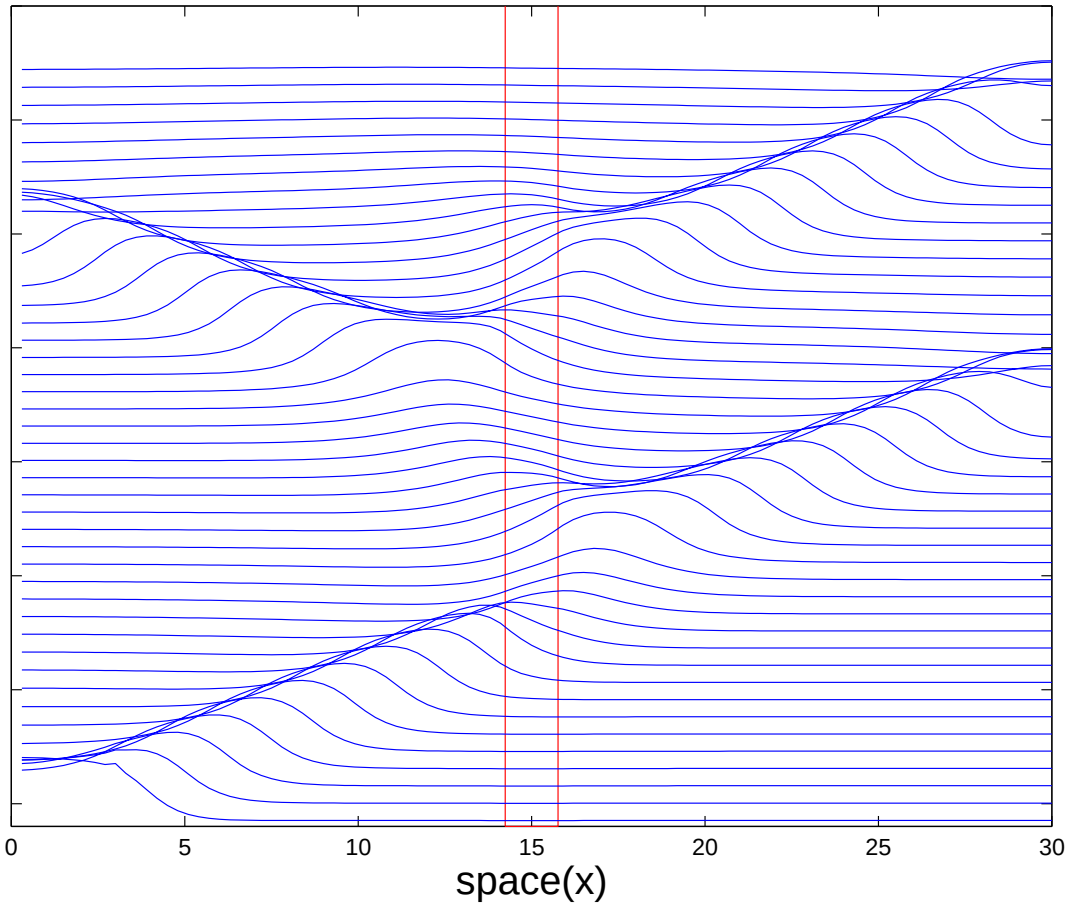

Figure 3.5. Numerical simulation of the gap problem (2.1) using ML excitation dynamics with a gap length $L = 1.52$. At this gap length, the wave successfully crosses the diffusive gap and then leads to two reflected waves - 2:2 pattern. This simulation was performed using the implicit-explicit method of Hines [26] with $\Delta t = 0.01$ and $\Delta x = 0.01$.

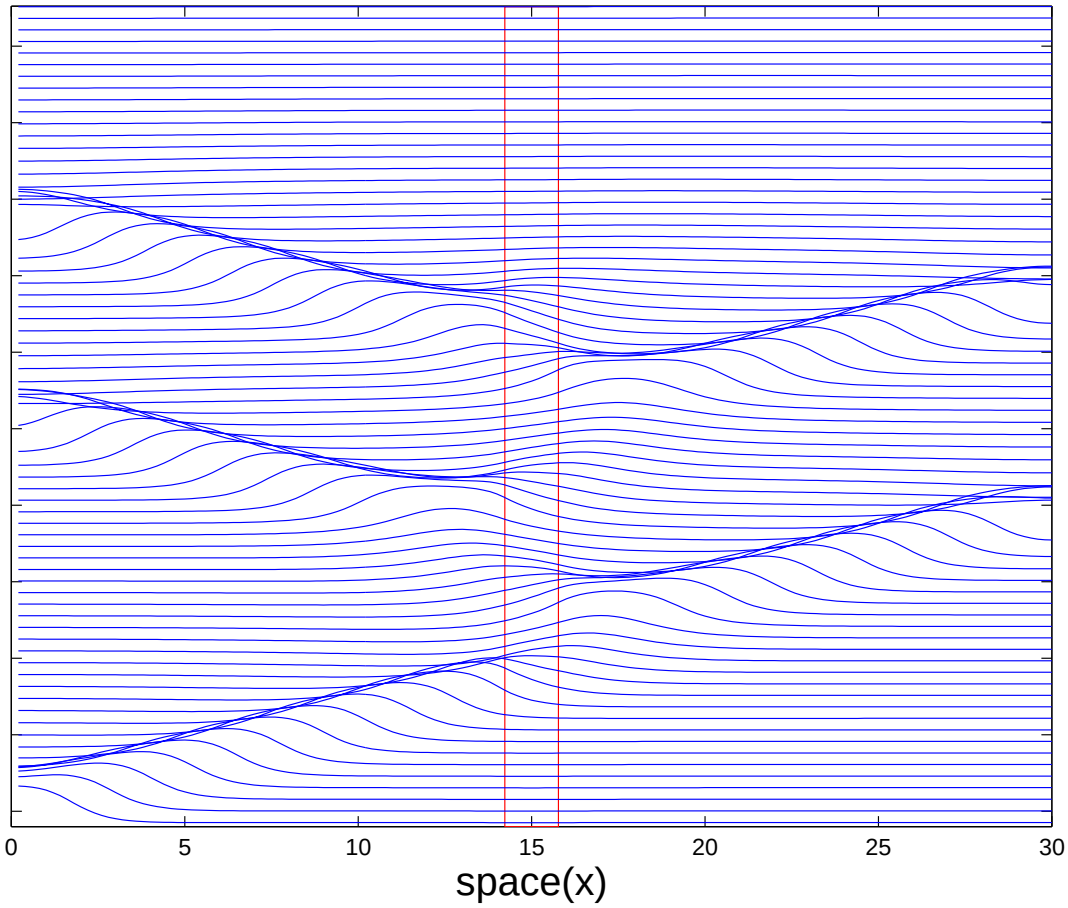

Figure 3.6. Numerical simulation of the gap problem (2.1) using ML excitation dynamics with a gap length $L = 1.544$. At this gap length, the wave successfully crosses the diffusive gap and then leads to a series of three reflected waves - 3:2 pattern. This simulation was performed using the implicit-explicit method of Hines [26] with a time step of $\Delta t = 0.01$ and a space step of $\Delta x = 0.001$.

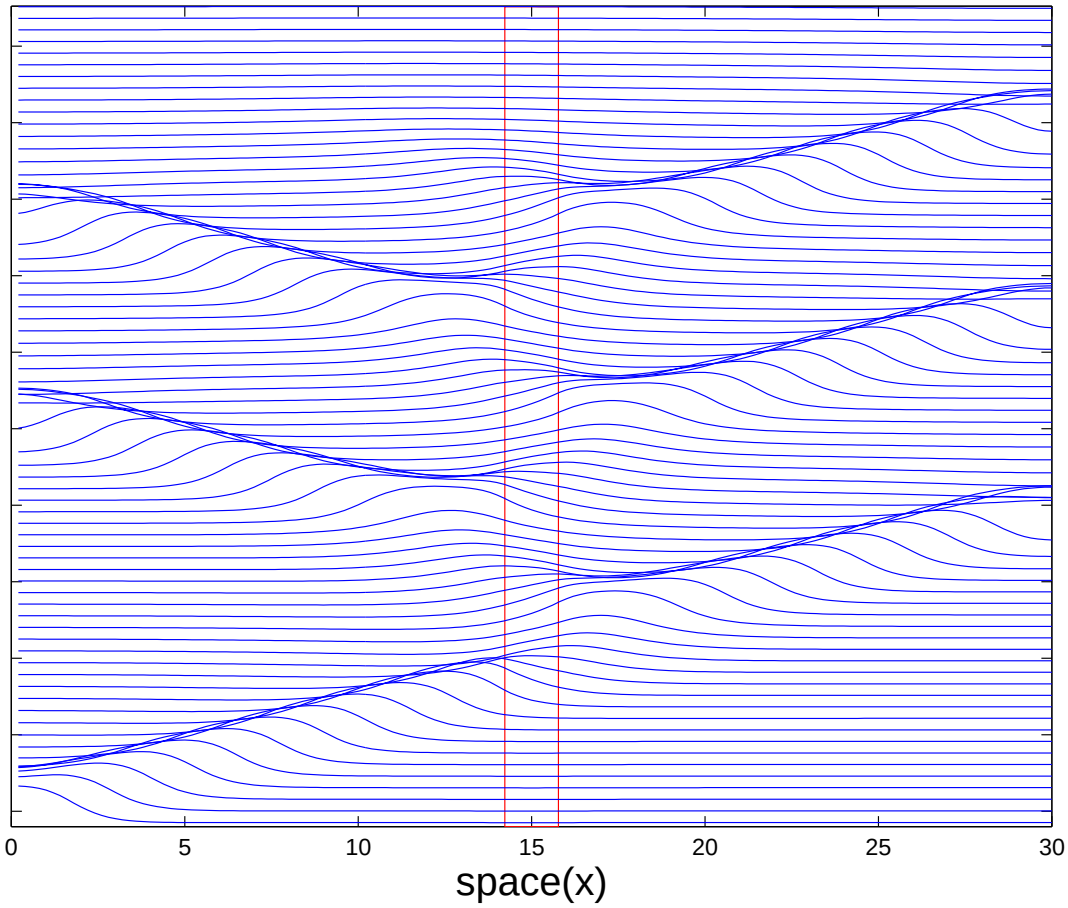

Figure 3.7. Numerical simulation of the gap problem (2.1) using ML excitation dynamics with a gap length $L = 1.543$. At this gap length, the wave successfully crosses the diffusive gap and then leads to a series of four reflected waves - 3:3 pattern. This simulation was performed using the implicit-explicit method of Hines [26] with a time step of $\Delta t = 0.01$ and a space step of $\Delta x = 0.001$.

where

$$m_\infty(u) = 0.5(1 + tanh(\tfrac{u-v_1}{v_2})),$$
$$w_\infty(u) = 0.5(1 + tanh(\tfrac{u-v_3}{v_4})),$$
$$\tau_w(u) = a \cosh^{-1}(\tfrac{u-v_3}{2v_4}).$$

Here, we take the parameters to be as follows: $a = 3.0$, $g_l = 0.5$, $g_K = 2.0$, $g_{Ca} = 1.0$, $v_1 = -0.01$, $v_2 = 0.15$, $v_3 = 0.1$, $v_4 = 0.145$, $E_{Ca} = 1.0$, $E_K = -0.7$, $E_l = -0.5$ and $I = 0.08$.

The system using these parameters exhibits a true all-or-none threshold (type I excitability). The reason for this is easily seen in the phase plane in Figure 3.8. The intersections of the nullclines show that there are three steady states of the system. From left to right (in order of increasing u), the steady states are a stable node, a saddle point and an unstable focus. The existence of the saddle point is responsible for the all-or-none behavior, because its stable manifold acts as a local separatrix dividing initial conditions that are subthreshold and those that are superthreshold. When a perturbation brings the system to a point to the left of the stable manifold, the system simply returns to the rest state. If a perturbation brings the system to a point to the right of the saddle point, u increases in an autocatalytic fashion and the flow must circumnavigate the unstable focus before the system is able to return to the rest state.

When the saddle point does not exist, the behavior is fundamentally different (as is the case for the usual FitzHugh-Nagumo equations). In this case, there exists a region in phase space that separates subthreshold and superthreshold behavior, but within this region, a family of graded responses exists. This makes the distinction between subthreshold and superthreshold responses arbitrary. Thus, we say that there exist a "quasithreshold" and that the system demonstrates type II excitability.

Note that the true threshold, unlike the quasithreshold, allows for infinite delays prior to a large excitation and therefore it is much easier in general to get long delays in type I excitable systems as opposed to type II excitable systems. This ability to produce long delays before excitation seems to promote the appearance of reflections in the gap model. This is the reason why the ML model was used in the above simulations.

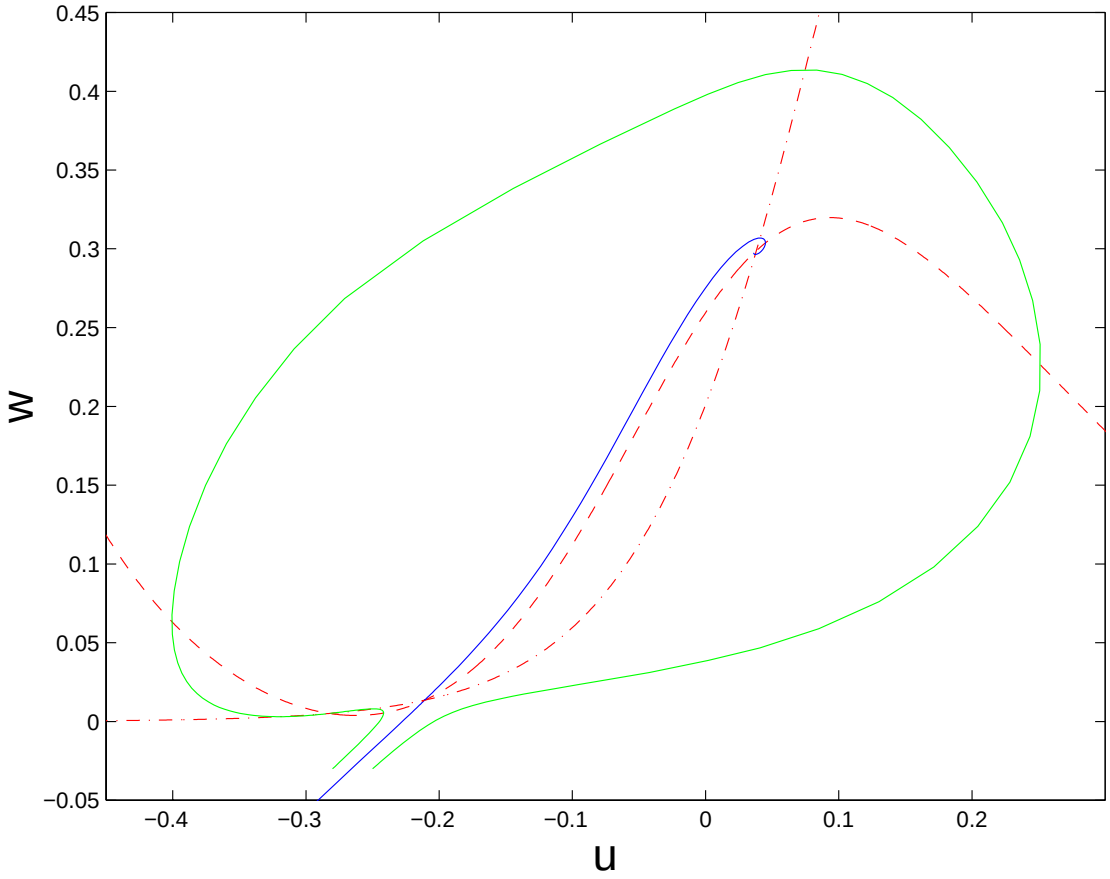

Figure 3.8. The phase plane of Morris-Lecar, parameters as in text. u-nullcline is the dashed curve and the w-nullcline is the dot-dashed curve. The stable manifold of the saddle point and the trajectories of a subthreshold and superthreshold response are also shown.

3.2.3 Physical mechanism of reflection

By inspecting the excitability variable as a function of time at a point on the proximal side of the gap and a point on the distal side of the gap, we can see the "physical" mechanism allowing reflection to occur. This mechanism is the ability of the local dynamics to produce a long delay by remaining close to threshold for an extended period of time before becoming excited. This consists of both u remaining at a threshold level and only small changes in the recovery variable w, so that the medium remains excitable.

Figure 3.9 shows an example of this behavior with L adjusted to produce a single reflection ($L = 1.6$). Following excitation on the proximal side of the gap, u on the distal side of the gap increases fairly slowly towards threshold. As the distal side reaches a level just above threshold and is ready to take off, u on the proximal side becomes unexcited. The value of u on the proximal side actually falls below the resting value before beginning to rise again. This causes a further delay before the autocatalytic excitation process can occur on the distal side. After hovering just above threshold, the distal side finally becomes excited. By this time, the proximal side is almost fully recovered and thus the distal side is able to reexcite the proximal side.

3.3 Coupled Cells and Reflection

We would like to get insight into the dynamical mechanism underlying the behavior described above, however it is difficult to work on the full partial differential equation model. Thus, we attempt to reduce the system while still keeping key features that seems to underlie the physical mechanism of reflection, i.e., the true threshold behavior. Because we saw that a model of two cells coupled by an resistor mimicked the behavior of the PDE model, the coupled cell model seems like a good place to begin.

3.3.1 Previous work

As mentioned previously, Ermentrout and Rinzel [18] saw the same reflection sequence in a cable model with an abrupt increase in cable diameter that we describe

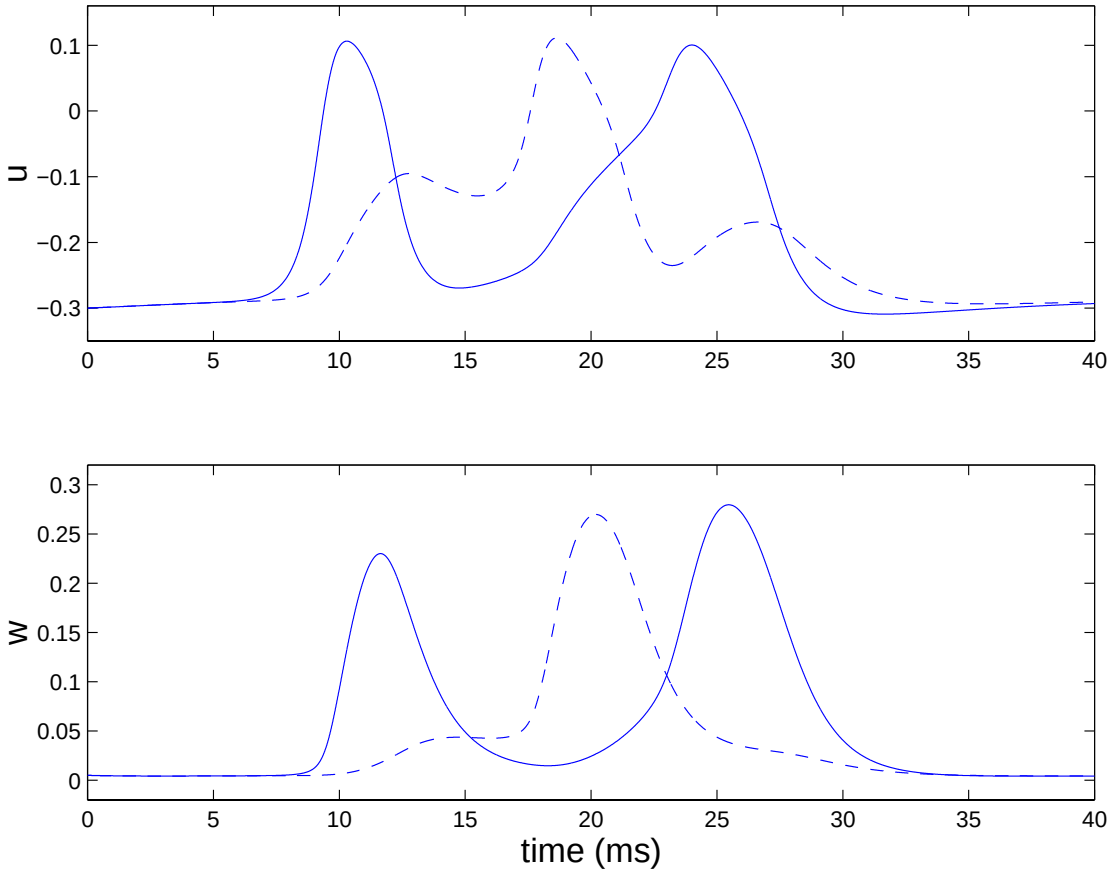

Figure 3.9. "Physical" reflection mechanism. The u values and the w values at points on the proximal side (solid line) and distal side (dashed line) of the gap. The gap length is $L = 1.6$ as in Figure 3.4 where one reflected wave occurs.

for the gap model. In their work, they consider coupled cells of different sizes as an analog to the PDE model. By studying this simpler model, they are able to suggest a link between reflection and the existence of an unstable periodic orbit.

Reflection in coupled excitable cells has been of interest for some time (although Ermentrout and Rinzel were unaware of this). Krinskii et al. [40] observed transient multiple reflections similar to those described here in a FitzHugh-Nagumo-like model and attempted to construct a periodic orbit in a reduction of phase space. Nordhaus [50] actually proved the existence of an unstable periodic orbit in a system of coupled piecewise linear FitzHugh-Nagumo cells. His proof was for the singular limit (very slow recovery dynamics) and for small coupling. The cells also had to be at the threshold of becoming self-oscillatory. This final condition enabled him to link this unstable periodic orbit with the anti-phase solution of two coupled oscillators. Also, Nordhaus [50] and Tyson [63] showed the existence of stable reflection oscillations in numerical simulations of a coupled piecewise linear FitzHugh-Nagumo model and a model of the Belousov-Zhabotinsky (BZ) reaction, respectively. (We should note the stable oscillations in coupled cell models studied by Smale [61] and Alexander [2] seem to stem from a mechanism similar to diffusion driven instability, which relies on the coupling via more than a single variable. This is fundamentally different than the process considered here).

The analysis and the initial conclusions that follow are quite similar to the work of Ermentrout and Rinzel [18]. However, we derive different "reduced" dynamics to use in a coupled cell model. This allows a clearer explanation of the results and extends them over a wider parameter range. Also, our modifications allow us to easily set the results in a broad dynamical context and link them to the behavior described above. In doing so, we are able to suggest how stable oscillations may arise.

3.3.2 A reduced model of coupled cells

As stated above, we would like to find a simple system that keeps the key features appearing to underlie the physical mechanism of reflection. Because we saw that the coupled cell model described in the previous chapter displayed very similar

behavior to the full PDE model, we will consider the coupled cell model once more.

Equations for coupled cells are

$$\begin{cases} u_i' = f(u_i, w_i) + c_g(u_i - u_j), \\ w_i' = g(u_i, w_i), \end{cases} \tag{3.2}$$

where $i, j = 1, 2$ with $j \neq i$. Cell i and cell j are coupled through an ohmic resistor (a limiting case of the gap model). The parameter c_g is the coupling strength between the cells (analogous to D/L in the gap model). Indeed, as c_g is varied, the equations describing coupled ML cells exhibit an identical reflection sequence (3.1) as the PDE system.

The 4 variable system of ordinary differential equations (3.2) describing coupled ML cells is much easier to study than the PDE model, but it is still fairly difficult to analyze without making further simplifications. We will now describe a simpler coupled cell model that also exhibits reflection dynamics and is even easier to study than system (3.2). In fact, the dynamics of this simplified system will be shown to reduce to a one-dimensional map (a finite difference equation) in the following subsections.

The model consists of excitable cells that are each described by a single variable obeying the differential equation

$$u' = f(u), \tag{3.3}$$

where f is similar to the cubic-like function described in Chapter 2. Here, assume that f has zeros at $u = 0$, α and 1 and that these are the only zeros in $[v_{min}, 1]$ for $v_{min} < 0$. Furthermore, $\alpha < 0.5$ and $f'(0) < 0$, $f'(\alpha) > 0$ and $f'(1) < 0$. Thus, there is a stable rest state at $u = 0$, and if u is perturbed so that u is still less than α, then the system will decrease back to the rest state. If the perturbation knocks u above the threshold point at α, then excitation will occur and u will increase towards the stable excited state at 1. We truncate this system to include only $v_{min} < u < v_{max}$ where v_{max} is close to, but less, than 1. At $u = v_{max}$, u_t

is still positive, however at this point, we take u to relax to v_{min} infinitely fast. Therefore, the system will respond to subthreshold perturbations as before, but for superthreshold perturbations, u will increase to v_{max}, "rapidly" relax to v_{min}, and then recover from $u = v_{min}$ towards $u = 0$.

We call this reduced model the "integrate-and-relax" model for excitable cells. Figure 3.10 shows typical superthreshold and subthreshold responses of the model. The benefit of the model is that it keeps the threshold behavior that appears to play a major role in the mechanism of reflection and keeps a physical coupling term (unlike [18]), yet two coupled cells are described by a system of two first-order ordinary differential equations

$$\begin{cases} u_1' &= f(u_1) + c_g(u_2 - u_1), \\ u_2' &= f(u_2) + c_g(u_1 - u_2). \end{cases} \tag{3.4}$$

This system can be understood by considering flow in the u_1, u_2-phase plane.

3.3.3 the u_1, u_2-phase plane

Figures 3.11 and 3.12 show examples of the phase plane of the reduced coupled cell model (3.4). Notice that this model is simply a truncated version of the one discussed in section 2.2.10, Figure 2.20. Here, trajectories hitting $u_1 = v_{max}$ at an arbitrary value of u_2 get immediately reinjected into the phase plane at $u_1 = v_{min}$ and the same value of u_2. Similar dynamics are prescribed for trajectories hitting $u_2 = v_{max}$. Thus, the system is described by continuous (C^0) flow on a torus. The line $u_1 = v_{max}$ will be called the u_1-excited edge of the phase plane and the $u_1 = v_{min}$ to be the u_1-recovery edge of the phase plane. Similar definitions will be taken for the u_2-excited and u_2-recovery edges.

There are several important curves drawn on the phase plane. The thin dashed curve is the portion of the u_1-nullcline in the restricted domain and the thin dash-dotted curve is the same for the u_2-nullcline. For the choice of c_g and f in both Figures 3.11 and 3.12, there are four steady states. There is stable rest point at $(0, 0)$ and an unstable node at (α, α). Also, there are two saddle points at $(\alpha^+, 0^+)$ and $(0^+, \alpha^+)$ where 0^+ is slightly larger than 0 and α^+ is slightly larger than α. If

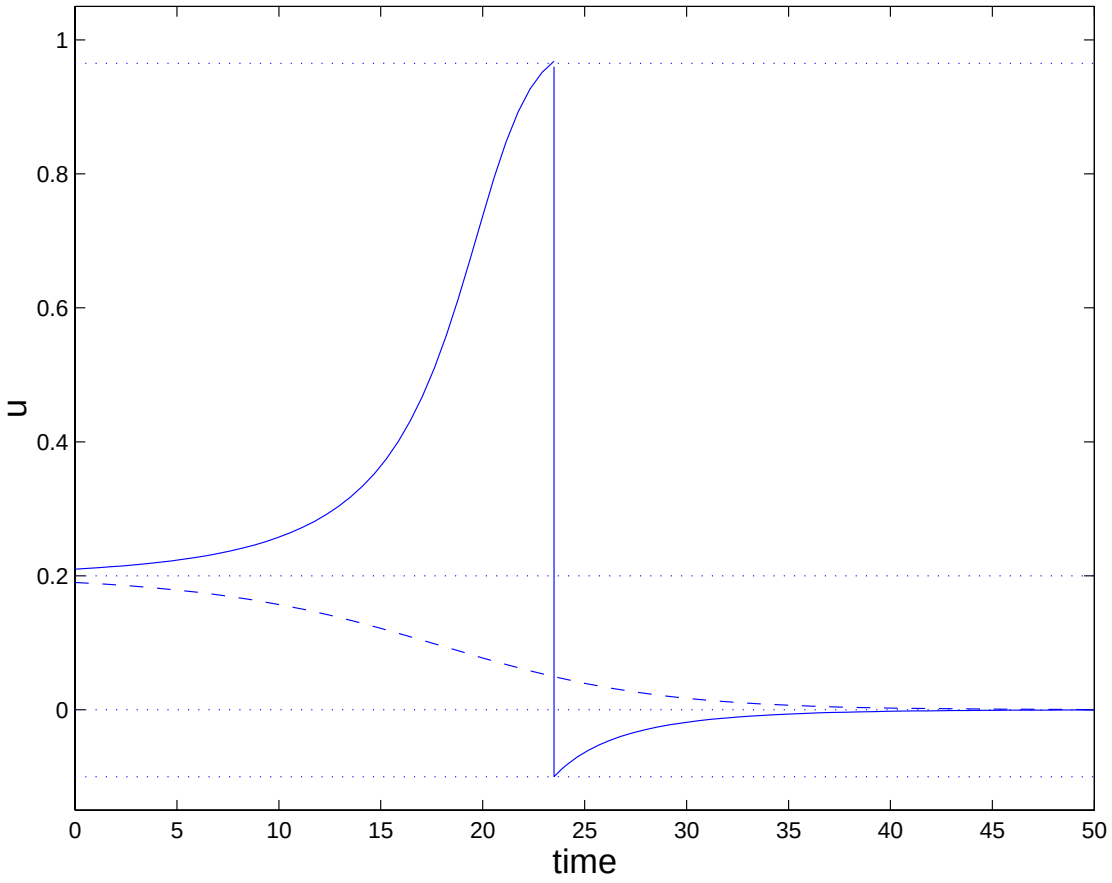

Figure 3.10. Superthreshold (solid curve) and subthreshold (dashed curve) responses of the "integrate-and-relax" model. The horizontal dotted lines correspond to $v_{min} = -0.1$, $u = 0$ (rest point), $u = \alpha$ (threshold) and $v_{max} = -0.95$.

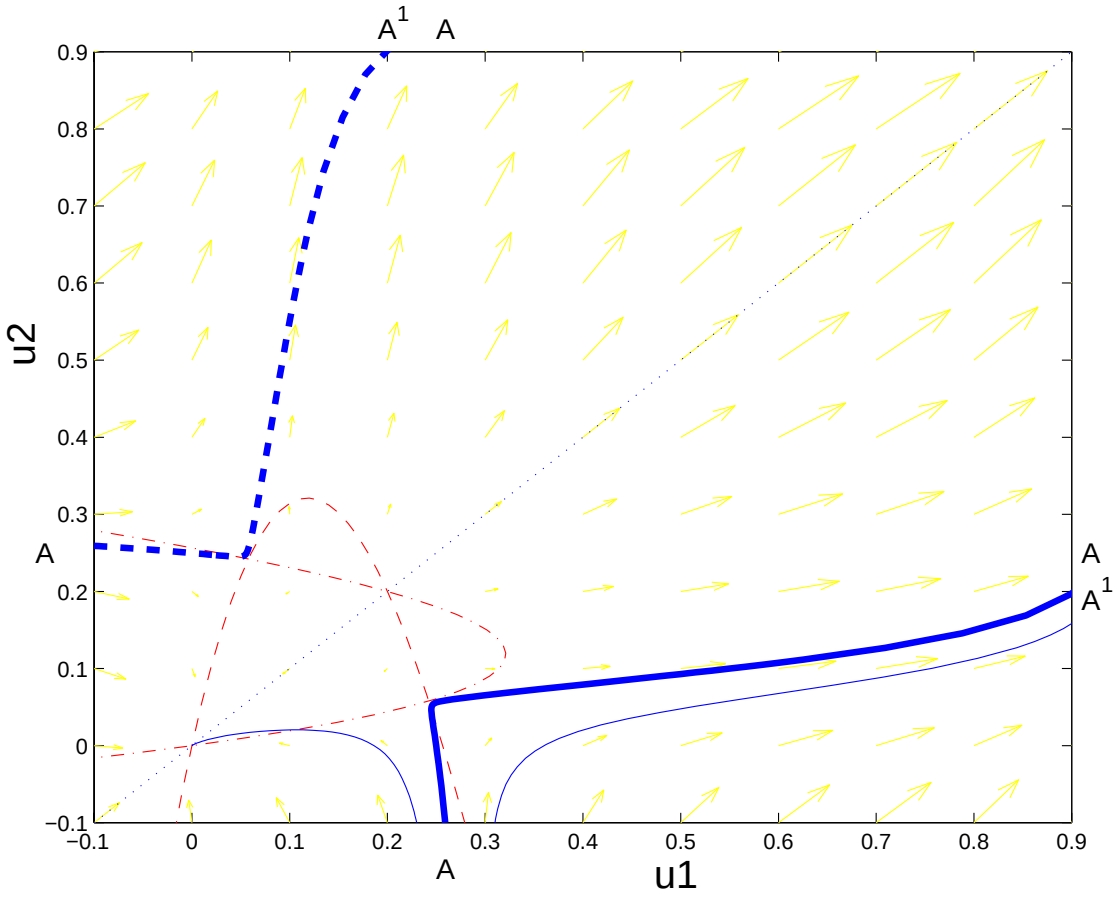

Figure 3.11. Phase plane of two coupled "integrate-and-relax" cell (system (3.4)) with cubic f with $\alpha = 0.2$ and $c_g = 0.042$. The dashed curve is the u_1-nullcline and the dash-dotted curve is the u_2-nullcline. The thick solid and thick dashed lines are the unstable and stable manifolds of the saddle points (the fixed points off the diagonal). The thin solid lines represent trajectories under the flow. $A = 0.259$, $A^1 = 0.197$.

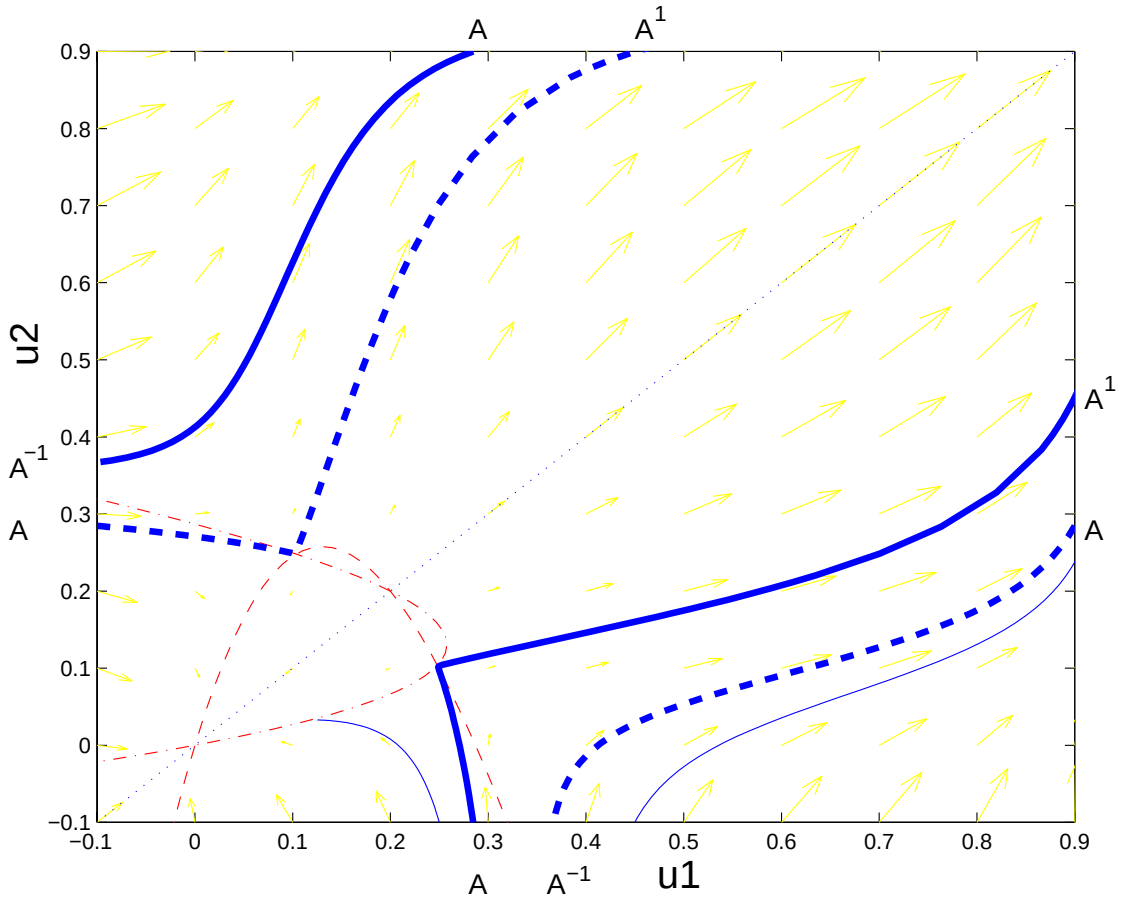

Figure 3.12. Phase plane of two coupled "integrate-and-relax" cell (system (3.4)) with cubic f with $\alpha = 0.2$ and $c_g = 0.062$. The dashed curve is the u_1-nullcline and the dash-dotted curve is the u_2-nullcline. The thick solid and thick dashed lines are the unstable and stable manifolds of the saddle points (the fixed points off the diagonal). The thin solid lines represent trajectories under the flow. $A = 0.285$, $A^{-1} = 0.368$, $A^1 = 0.468$.

the domain were unrestricted, there would also be a stable excited point at $(1,1)$. Notice that because the cells are identical, the phase plane is symmetric about the line $u_1 = u_2$, which is drawn as a dotted line. Flow on this line reduces to the case of two single cells with a stable resting state at $(0,0)$ and a threshold at (α,α), because in this case the coupling terms $\pm c_g(u_2 - u_1) = 0$. Perhaps the most important curves drawn in Figures 3.11 and 3.12 are the portions of the unstable and stable manifolds of the saddle points. These are drawn as thick solid lines for the saddle point at $(\alpha^+, 0^+)$ and as thick dashed lines for $(0^+, \alpha^+)$.

Associated with the unstable and stable manifolds of the saddle points, there are values that will be called A, A^{-1}, and A^1. The relative magnitudes of these values will be essential in determining the type of behavior that the system exhibits. Let us define A to be the value of u_1 at which the stable manifold of $(\alpha^+, 0^+)$ emerges from the u_2-recovery edge of the phase plane and A^1 to be the value of u_2 at which the unstable manifold of $(\alpha^+, 0^+)$ hits the u_1-excited edge of the phase plane. We can think of (v_{max}, A^1) as the image of (A, v_{min}) under the flow. Likewise, we will define A^{-1} by letting (v_{min}, A^{-1}) be the preimage of (A, v_{max}) under the flow. Because the flow is symmetrical, A, A^1 and A^{-1} can be equally defined by exchanging the positions of u_1 and u_2.

Now, let us study the dynamics of system (3.4). Specifically, we will examine the response of the system for initial conditions on the u_2-recovery edge (i.e., points (u_1, v_{min})). Different qualitative dynamics can occur for different ordering of A, A^{-1} and A^1.

First, let us consider the case of $A^1 < A$. This is always the case for low coupling (as inferred by the $c_g = 0$ case). An example of this case is shown in Figure 3.11. (In this case, A^{-1} is the unstable node at (α,α)). Notice that the value A acts as a threshold. If u_1 is taken to be less than A, flow dictates that trajectories immediately get absorbed by the resting state (0,0) and neither cell becomes excited. This would correspond to a 0:0 pattern. If u_1 is taken to be greater than A, then the flow increases u_1 and eventually the trajectory hits the u_1-excited edge of the phase plane (at $u_1 = v_{max}$). Because $A^1 < A$, when the flow

is reinjected on the u_1-recovery edge, u_2 is always less than A and trajectories gets absorbed by the resting state without cell 2 becoming excited. This corresponds to a 1:0 pattern. These are the only two possible results for low coupling ($A^1 < A$).

As c_g is increased, A^1 moves toward A. At a critical parameter value c_g^*, $A = A^1 = A^{-1}$, and for $c_g > c_g^*$, both $A < A^1$ and $A < A^{-1}$. At $c_g = c_g^*$, the unstable manifold of each saddle point becomes the stable manifold of the other saddle point and there is a heteroclinic connection. Hence, as c_g is increased past c_g^*, the system undergoes a heteroclinic (or saddle-loop) bifurcation. This suggests that a periodic orbit is born. We will return to this issue soon.

For cases when $A < A^1$ ($c_g > c_g^*$) , the value A again acts as a threshold. If u_1 is taken to be less than A, a 0:0 excitation pattern occurs (see Figure 3.12). If u_1 is taken to be greater than A, then as before the flow increases u_1 to v_{max}. However, what follows depends on the exact starting point. If u_1 is taken to be greater than A^{-1}, the resulting trajectory hits the u_1-excited edge at a value of u_2 that is less than A, and therefore when it is reinjected on the u_1-recovery edge, u_2 is less than A and the trajectory gets absorbed by the resting state without cell 2 becoming excited. This corresponds to a 1:0 pattern (see Figure 3.12). When initial conditions (u_1, v_{min}) are such that $A < u_1 < A^{-1}$, more interesting dynamics occur. These dynamics will be described by the return one-dimensional map that is derived below.

3.3.4 The one-dimensional map

Consider the flow in the phase plane discussed above. Let the function $q(u_1)$ be defined as follows. If $u_1 < A$, $q(u_1) = 0$. If $A \leq u_1 \leq v_{max}$, then let $q(u_1)$ be equal to the value of u_2 at the point on the u_1-excited edge of the phase plane that is the image of (u_1, v_{min}) under the flow. Thus, $q : u_1 \to u_2$ is a map that describes how the flow of equation (3.4) takes points (u_1, v_{min}) on the u_2-recovery edge to points (v_{max}, u_2) on the u_1-excited edge of the phase plane.

Note that because the flow is symmetric around the line $u_2 = u_1$, an identical map is generated by flow above $u_2 = u_1$. Therefore, the entire dynamics of the flow are exactly described by the one-dimensional return map

$$x_{i+1} = \begin{cases} q(x_i), & A \leq x_i \leq v_{max}, \\ 0, & \text{otherwise.} \end{cases} \tag{3.5}$$

The variable x_i for odd i corresponds to the value of u_2 when cell 1 becomes excited (i.e., when flow in the reduced coupled cell model hits the u_1-excited edge of the phase plane) and x_i for even i corresponds the value of u_1 when cell 2 becomes excited (i.e., when flow in the reduced coupled cell model hits the u_2-excited edge of the phase plane). By iterating this map, we can observe the excitation dynamics of the ODE system (3.4).

3.3.5 The existence of a periodic orbit

The following describes two important properties of the map for $A < A^1$ and $A < A^{-1}$ from which the existence of a periodic orbit in system (3.4) can be deduced.

The important portion of the map is, of course, $x \in (A, v_{max})$. Because the map is generated by a flow of a system of ODEs, it is continuous on $x \in (A, v_{max})$. The smoothness is determined by that of the flow. Also, notice that, in a sense, the flow flips the ordering of points as it takes points from one recovery edge to the other. This implies that the map is monotonically decreasing on $x \in (A, v_{max})$.

By construction, two points on the map are (A, A^1) and (A^{-1}, A). Thus, when $A < A^1$ and $A < A^{-1}$ (i.e., for $c_g \geq c_g^*$ so that A is not greater to A^1), the map is guaranteed to have a fixed point, x^*, by the intermediate value theorem. Furthermore, because the map is strictly decreasing, this fixed point is unique.

The existence of the fixed point on the map implies that there exists a periodic orbit in the coupled cell system (3.4) for sufficiently large coupling ($c_g \geq c_g^*$). We will now show that the reflection patterns that we have described are associated with the existence of this periodic orbit.

3.3.6 The dynamical mechanism for reflection

Let us consider the case in Figure 3.12 where $A^1 > A^{-1} > A$. The map corresponding to the flow in Figure 3.12 is depicted in Figure 3.13. The slope of map at the fixed point, x^*, is less than negative one, and thus the fixed point is unstable and repels iterates.

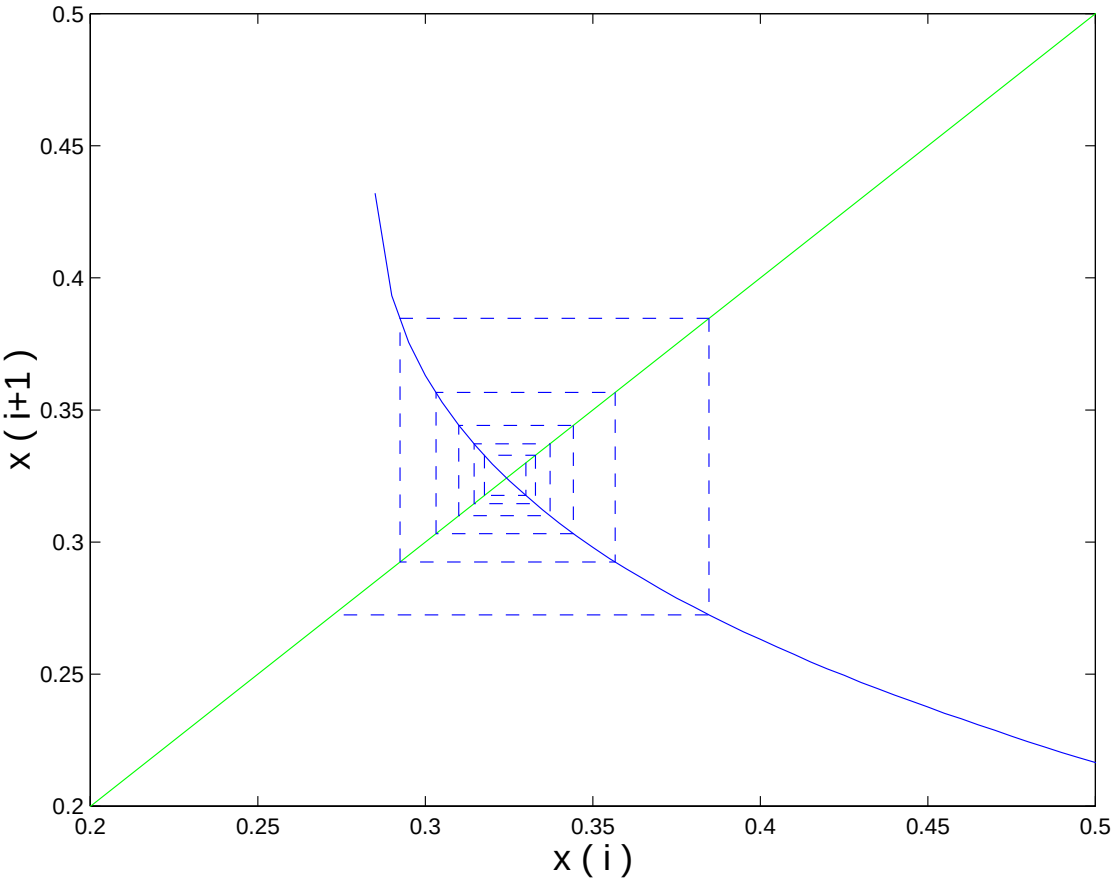

Figure 3.13. A portion of one-dimensional return map for the flow in Figure 3.12. the cobwebbing shows an example of an iteration of the map. The initial condition $x_0 = 0.33$ leads to 11 iterates before $x = 0$. This correspond to a 6:5 reflection pattern in the coupled cell model.

By choosing different initial conditions and iterating the map, we are able to observe behavior that corresponds to the various reflection patterns that were observed in the ODE and PDE models. Remember that every nonzero iterate corresponds to one of the cells being excited.

If we choose the initial condition to be larger than A^{-1}, then we are only able to iterate once before $x_i = 0$ (i.e., before the iterations fall off the nonzero branch of the map). This corresponds to a 1:0 pattern in the ODE. If we choose an initial condition close to, but greater than A, then we are able to iterate twice, corresponding to a 1:1 pattern. As the initial condition approaches the unstable fixed point at $x = x^*$, the number of iterates prior to $x = 0$ goes to infinity. Furthermore, initial conditions with $x_0 < x^*$ lead to an even number of iterations prior to $x = 0$ and initial conditions with $x_0 > x^*$ lead to an odd number of iterations prior to $x = 0$. In general, if N is the total number of iterations of the map prior to the value of x_i becoming 0, then the reflection pattern is $N/2{:}N/2$ for N even or $(N-1)/2+1{:}(N-1)/2$ for N odd.

Thus, as the initial condition is increased from $x_0 = v_{min}$ to $x_0 = v_{max}$, the number of iterates goes through the sequence 0, 2, 4, 6, 8, ... accumulating to infinity when $x = x^*$ and then decreasing from infinity as when move past $x = x^*$, ..., 7, 5, 3, 1. This corresponds to the exact same sequence as the reflection sequence observed in both the ODE and PDE ML simulations. The initial value space can easily be divided into regions that give the number of iterates, and therefore different reflection patterns, by finding the preimages of A (iterate backwards with $x_0 = A$). In doing so, we see that the higher the number of iterates, the smaller the region of initial condition space. This agrees with the observation in the PDE and ODE ML models that higher number of reflections are associated with smaller regions of parameter L space and parameter c_g space, respectively.

As c_g is increased, the map shifts to the right (and upwards), and the fixed point and "pattern space" shift along with in. Therefore, when the initial conditions are fixed, the same reflection sequence will be observed as c_g is increased. Also of note is that changing initial conditions in the ML coupled cell system results in the same

reflection sequence as well. However, note that we can do not have real control over the initial conditions of the PDE, because the wave generated on the proximal side of the gap quickly approaches a shape similar to the unique stable traveling wave that the homogeneous system exhibit. We are thus restricted to changing parameters of gap dynamics in order to observe the reflection sequence.

The conclusion is that as c_g or L changes, the system is effectively marching through initial condition space and visiting the various possible transient behaviors associated with being close to an unstable periodic orbit. No bifurcation is involved in the changes in behavior. This includes the initial appearance of reflection. The heteroclinic bifurcation that gives rise to the periodic orbit generically occurs prior to the point when reflections are observed.

To complete the picture, let us consider what happens when c_g becomes very large. As c_g increases, there is a pitchfork bifurcation in which the two saddle points coalesce with the unstable node leaving only a saddle point at (α, α). (This happens when $c_g = f'(\alpha)/2$). In this case, $A^1 = v_{max}$ which is always greater than A^{-1} for the restricted domain. Thus, despite the decreased number of steady states, the behavior described above persists.

However, notice that as c_g increases further $u_1 = u_2$ becomes rapidly attracting. This causes A^{-1} to increase to $v_{max} = A$ at, say, $c_g = c_g^{**}$. As a result, the periodic orbit vanishes via another heteroclinic bifurcation. Thus, the periodic orbit exists for only a finite interval of coupling strength, i.e., $0 < c_g^* < c_g < c_g^{**}$.

3.4 Links to Other Behavior

The link between an unstable periodic orbit and reflection patterns was nicely described by Ermentrout and Rinzel [18]. They saw reflections in a PDE model with ML dynamics in response to an abrupt change in cable diameter. They explained this behavior by considering the dynamics of two coupled phase model cells [17] that describes flow on a torus. They took the cells to be of different sizes to mimic the change in cable diameter, and in the well-coupled limit where only two steady states exist, they constructed a negatively invariant annulus and used the

Poincare-Bendixson theorem to prove the existence of an unstable periodic orbit. They then suggested that as the diameter of one of the cells is varied, all the different reflection patterns can be seen with fixed initial conditions.

However, changing the size of one cell in a coupled cell model makes the system asymmetric and the complexity of the coupling in the two cell phase model makes it difficult to see how the nullclines are changing in response to changes in parameters. Here, our choice of both "reduced" cell dynamics and bifurcation parameter allows for a clearer, more complete, phase plane analysis, as well as the reduction of flow to a one-dimensional return map. As shown above, this enables us to ease the restriction of the well-coupled limit imposed by Ermentrout and Rinzel. It also enables a clear demonstration of the connection to other possible behavior such as stable reflection oscillations and the connection to coupled oscillators.

3.4.1 Coupled oscillators

The fact that an unstable periodic orbit underlies reflection may seem somewhat surprising. However, it makes prefect sense when we note that oscillators coupled via ohmic resistors are known to usually have stable in-phase oscillations and unstable antiphase oscillations [5]. For a special case, Nordhaus [50] showed that the unstable periodic orbit associated with reflection in coupled excitable cells is a continuation of the unstable antiphase oscillation for coupled relaxation oscillators. This is very easily seen in our simple coupled cell model.

Consider system (3.4) with a reaction term $f(u) - I$ where f is as previously described and I is a new parameter. Note that when I is sufficiently large, f loses the two zeros that were at 0 and α for $I = 0$. This renders each cell self-oscillatory. Let us choose parameters to be those described for Figure 3.12 and begin to increase I from zero. As I increases, a pitchfork bifurcation occurs leaving only the two steady states along the identity line (see Figure 3.14), however the unstable orbit persists along with the reflection patterns.

Increasing I further, the remaining two fixed points collide and vanish via a saddle-node bifurcation. There are two important observations to make here. One is that prior to the saddle-node bifurcation the two steady states lived on

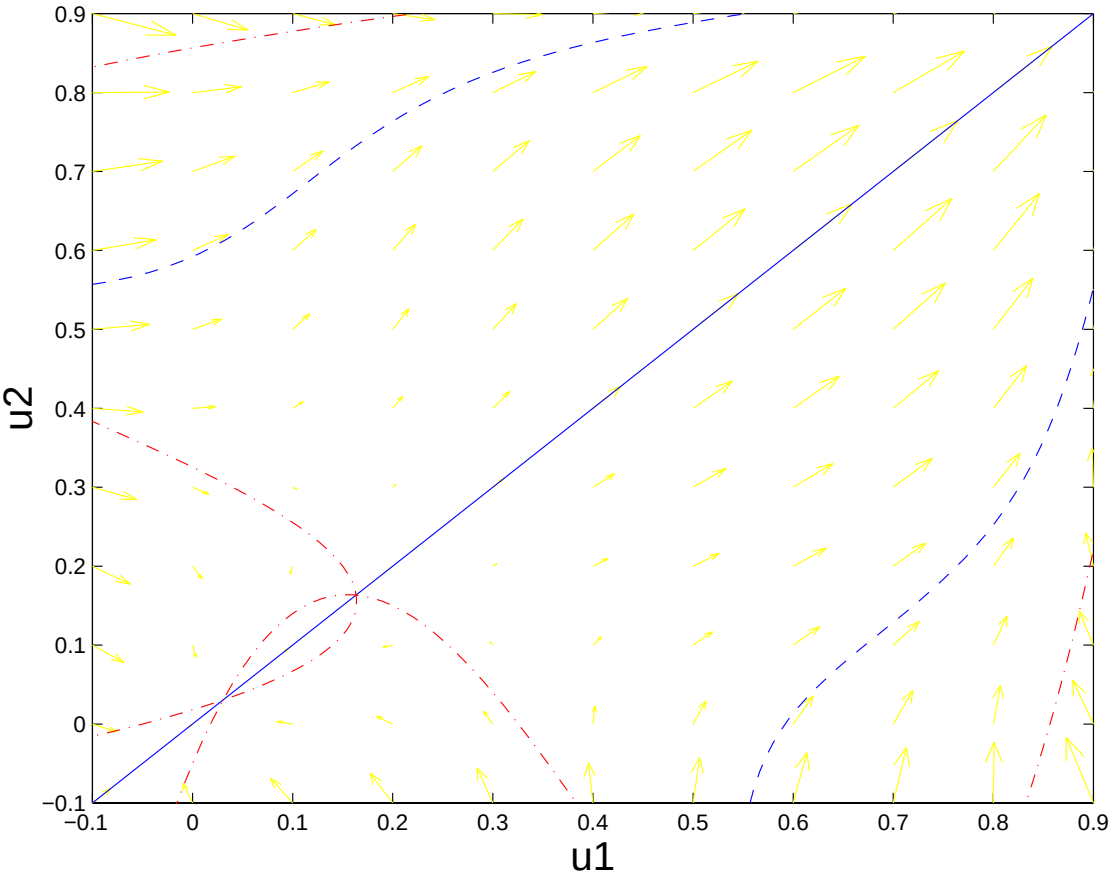

Figure 3.14. Phase plane of two coupled "integrate-and-relax" cell (system (3.4)) with cubic $f + I$ with $\alpha = 0.2$. The dash-dotted curve are the nullclines. The dashed line is the unstable orbit and the solid line is the heteroclinic connection of the stable node at (0,0) and the saddle-point at (α, α). $c_g = 0.1$, $v_{min} = -0.1$, $v_{max} = 0.9$, $I = 0.05$.

an attracting heteroclinic loop. Thus, as they vanish, a stable periodic orbit is born. This is the in-phase oscillation of coupled oscillators. The other observation is that the bifurcation is local and therefore does not affect trajectories away for the orbit undergoing the bifurcation. Thus, we see that the unstable orbit underlying reflections is the continuation of an antiphase oscillation of coupled oscillators (see Figure 3.15). We have shown that under the appropriate conditions cells do not need to be close to self-oscillatory in order for this orbit to persist.

3.4.2 Stable reflection oscillations

The possibility of stable reflection oscillations is an extremely interesting issue. Tyson [63] observed stable reflection oscillations in numerical simulations of a model of BZ reaction. He hypothesized that these stable oscillations might be the result of a saddle-node type bifurcation in which a stable and an unstable periodic orbit were born. Although this may be a plausible scenario in more complex models, it cannot happen in our simple model. This is seen by the fact that the maps describing the dynamics in the simple model are monotonically decreasing, which excludes the possibility of saddle-node bifurcations. However, there are two other possibilities by which stable oscillations can arise. One is that a periodic orbit born out of the heteroclinic bifurcation (discussed earlier) could appear as a stable oscillation. This is this case when $A^{-1} < A^1$ immediately following the bifurcation, which makes the return map a contraction map. Another possibility is that if an unstable orbit is born via the heteroclinic bifurcation, a subcritical period doubling bifurcation could take place as c_g is changed. This would give rise to an unstable period-two orbit and a stable period-one orbit.

Both of these scenarios can be seen in our simple model by adjusting parameters. Figure 3.16 shows an example of a map for c_g just above c_g^*. Below c_g^* ($A^1 < A$), the entire nonzero portion of the map lies the right of the identity line. As c_g increases, the map shifts to the left leading to the appearance of a fixed point. When the fixed point appears, the slope is greater than -1 (and less than 0 of course), thus the period-1 orbit is stable as soon as it is born. Figure 3.17 shows an example of

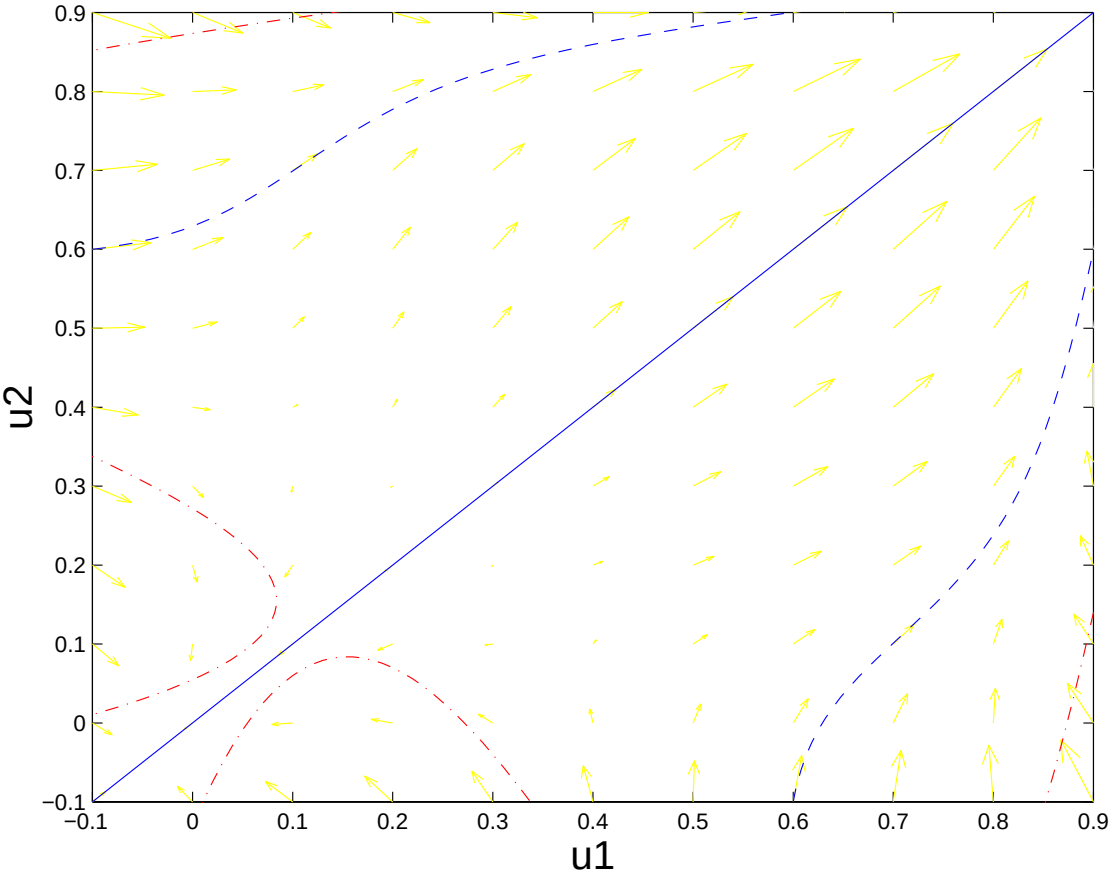

Figure 3.15. Phase plane of two coupled "integrate-and-relax" cell (system (3.4)) with cubic $f + I$ with $\alpha = 0.2$. The dash-dotted curve are the nullclines. The dashed line is the unstable orbit and the solid line is the stable orbit. $c_g = 0.1$, $v_{min} = -0.1$, $v_{max} = 0.9$, $I = 0.13$.

a map just past a period doubling bifurcation where an unstable period-two orbit (the dashed box) has grown out of the fixed point, which is now stable. If initial conditions are chosen to be within the period-2 orbit, the system will evolve to stable period-1 oscillations.

The possibility of stable reflection oscillations is especially interesting in the context of cardiac electrophysiology. It is hypothesized that there are two main pathways through the AV node and the current dogma is that most AV nodal tachycardias result from reentrant circulation of an electrical impulse down one pathway and up the other [1]. However, there is no direct evidence for reentry underlying these arrhythmias or even for the existence of dual pathways. The analogy of the gap model between the AV node, along with the results provided here, suggests that the existence of stable oscillations of reflection could be an viable alternative mechanism of AV nodal tachycardia.

3.5 Reflection and the Induction of Spiral Waves

Cardiac arrhythmias such as ventricular and atrial tachycardia and ventricular fibrillation are almost always due to self-perpetuating circulating wavefronts of electrical activity. For several years, it has been thought that these reentrant arrhythmias can often be associated with spiral waves (or scroll waves) [41, 65, 30]. Indeed, both models of cardiac tissue [38, 69, 12] and experimental preparations [13, 23, 10] have been shown to support spiral wave dynamics.

In order to induce spirals, there must be a mechanism that breaks the symmetry of the normal orderly wavefront that propagates through the heart. Experimentally spiral are induced by external premature electrical stimulation. However, the physiological mechanism involved in the autonomous induction of spiral waves is still unresolved. In many situations, the heterogeneity due to damaged tissue (by heart attacks for example) seems to be responsible for the symmetry breaking [66, 33, 69, 58]. Perhaps the most plausible mechanism proposed thus far involves curvature effects on the wavefronts as it tries to propagate around nonconducting regions of tissue [52, 9]. However, even this mechanism has problems if the non-

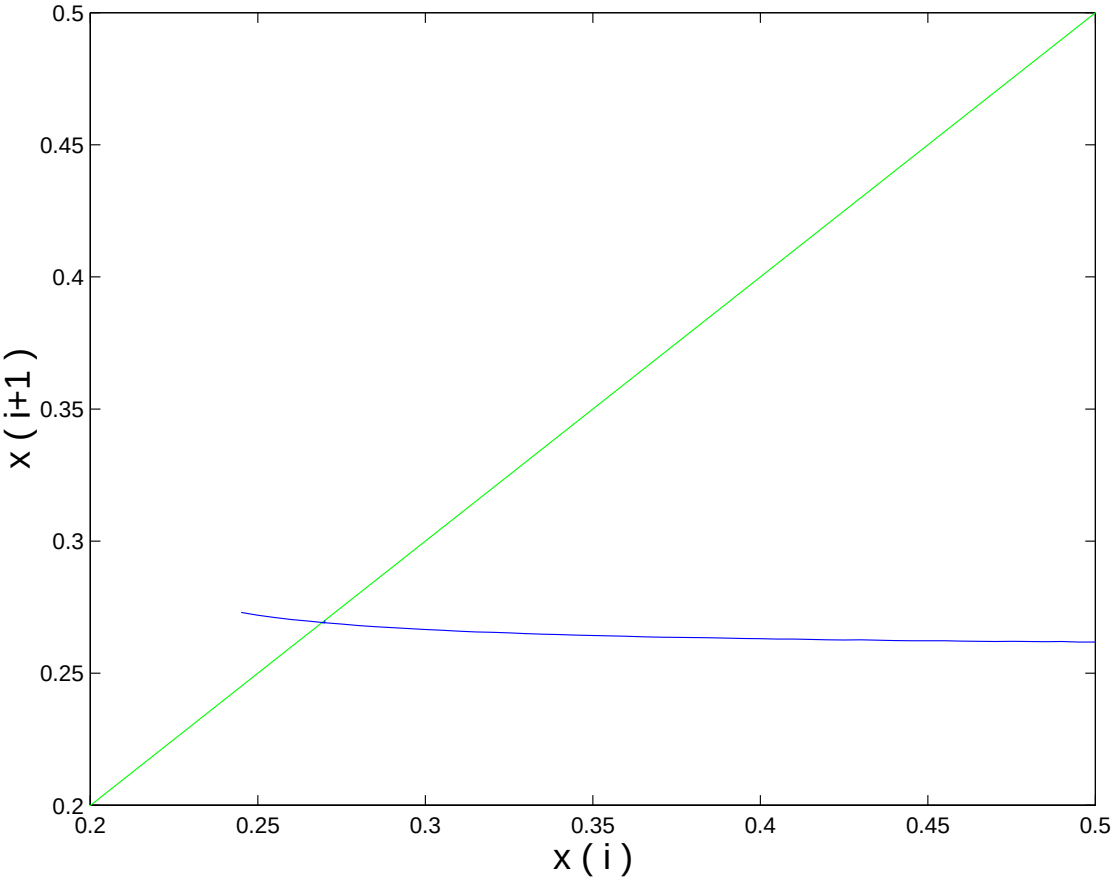

Figure 3.16. A portion of the one-dimensional return map showing a situation for c_g slightly large than a c_g^* where a heteroclinic bifurcation gave rise to a stable periodic orbit. Note that the slope of the map is between -1 and 0 everywhere. $c_g = 0.042$, $v_{min} = -0.1$, $v_{max} = 0.97$

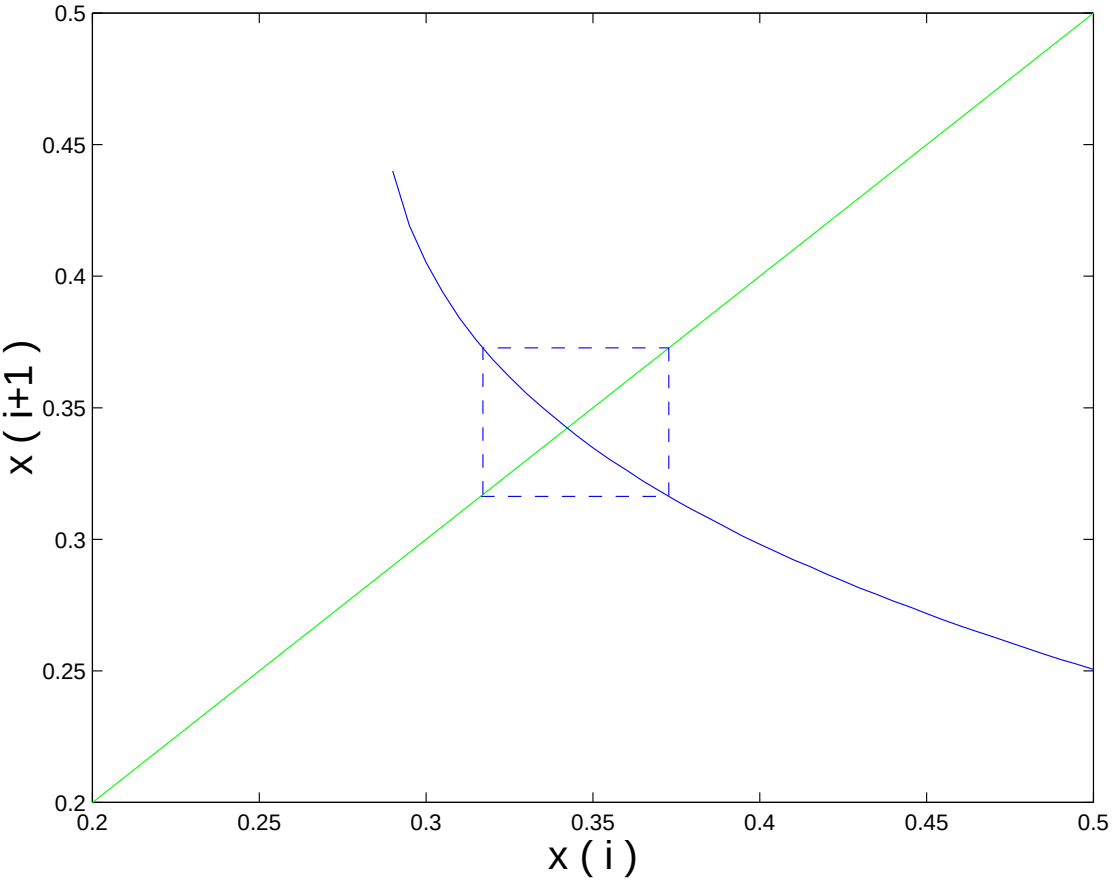

Figure 3.17. A portion of the one-dimensional return map showing unstable period-2 orbit and a stable period-1 orbit. $c_g = 0.063$, $v_{min} = -0.1$, $v_{max} = 0.91$

conducting tissue is due to damaged tissue. It is very reasonable to model the scar tissue resulting from heart attacks by a nonconducting medium. On the other hand, the mechanism requires wavefronts to experience a region of high curvature, and it seems unlikely that sharp enough corners would exist in scar tissue in order to give rise to such high wavefront curvature. Below, we suggest an alternative mechanism in which damaged tissue could induced spiral waves and that does not rely on sharp corners in the inhomogeneity in the medium. The mechanism involves a process that we will refer to as facilitated reflection which occurs in a two-dimensional version of the gap problem. To the best of our knowledge, this is the first time reflection has been shown to induce spiral wave via an autonomous mechanism.

We use a two-dimensional excitable medium with a region of pure diffusion in the middle. As discussed previously, this passive region is a simple model for ischemic tissue. The excitation dynamics are described by the Morris-Lecar model. A wave is started at an edge of the domain and it propagates towards the inhomogeneity. If the length and/or width of the nonexcitable domain is small, the wave is able to propagate through the medium without being significantly affected. If the diffusive region is long and wide, the wave is blocked and is unable to propagate through the diffusive area. As the wave hits the inhomogeneity, it breaks into two. These two waves propagate around the nonexcitable region and then reattatch at the far end of the region.

At intermediate sized passive domains, something interesting happens. Figures 3.18 and 3.18 show the results of a simulation in which the entire domain is 20x20 spatial units (i.e., $D = 1$) and the nonexcitable region is 15 units wide (i.e., the side parallel to the wavefront) and 4 units long. As the wave reaches the diffusive region, the portion of the wave immediately in front on the region stalls and begins to source current through the region. The portions of the wave that have excitable tissue in front of them continue to propagate, but are slowed by the portion of the wave that is lagging behind (see time=7ms). A combination of current from the stalled portion of the wave and the waves that propagate along the sides of the diffusive region is sourced into the excitable region distal to the gap-like

region and enable it to become excited. The result is that the wave reestablishes itself on the distal side of the diffusive region (see time 9ms). However, the delayed excitation of the distal side and the residual passive current in the diffusive region, reexcites the proximal side of the diffusive region. This reflection sets up the proper topology for spiral wave formation and in this case, the medium is large enough to support it. Thus, a pair of stable spiral waves are formed with their cores anchored in the diffusive region.

We call the reflective behavior that initiates the spiral facilitated reflection, because the length of passive region is longer than the gap length where reflection occurs in one-dimensional model. The reflection mechanism here relies partially on the waves propagating around the diffusive region helping to source enough current to excite the distal side and reexcite the proximal side of the gap-like region. This help, however, may not be necessary if the region is very wide but short in length.

3.6 Discussion

The work in this chapter has extended the current understanding of reflection and shows how it relates to a broad range of behaviors. By introducing a new simple model for excitable media and considering a pair of coupled cells with these dynamics, we demonstrate that an unstable orbit underlies transient reflections (without the same restriction of parameter space as Ermentrout and Rinzel [18]). Also, we answer the question first posed by Tyson [63] and show dynamical mechanisms for how stable reflection oscillations can arise. Finally, we describe a mechanism in which reflection can induce spiral waves.

We suggest several implications that our work has on problems in cardiac electrophysiology, in particularly on the generation of arrhythmias. Reflection has been hypothesized to be linked to several arrhythmias, but no solid explanation has ever been given. Transient reflections with more than one reflected wave appear to occur over a minute parameter range and thus, by themselves, cannot be a robust source of oscillatory behavior associated with AV nodal tachycardias or subsidiary pacemakers (ectopic foci) arising from zones of injury. However, if the unstable

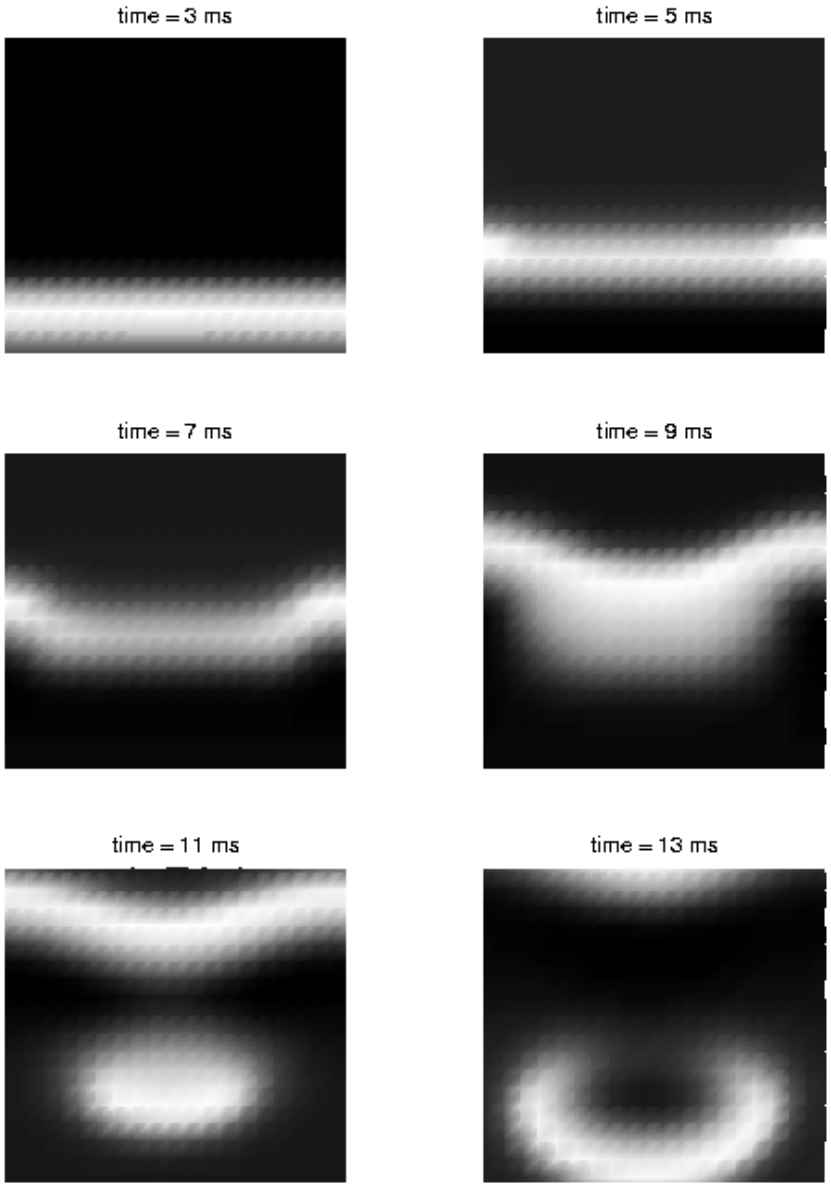

Figure 3.18. Numerical simulation of a two-dimensional sheet of tissue with a solely diffusive region. ML dynamics are used to describe the excitability. The light regions correspond to high u values. (a) The first six panels show a wave of excitation propagating towards the diffusive region, producing a reflected wave, and thus initiating a pair of spiral waves.

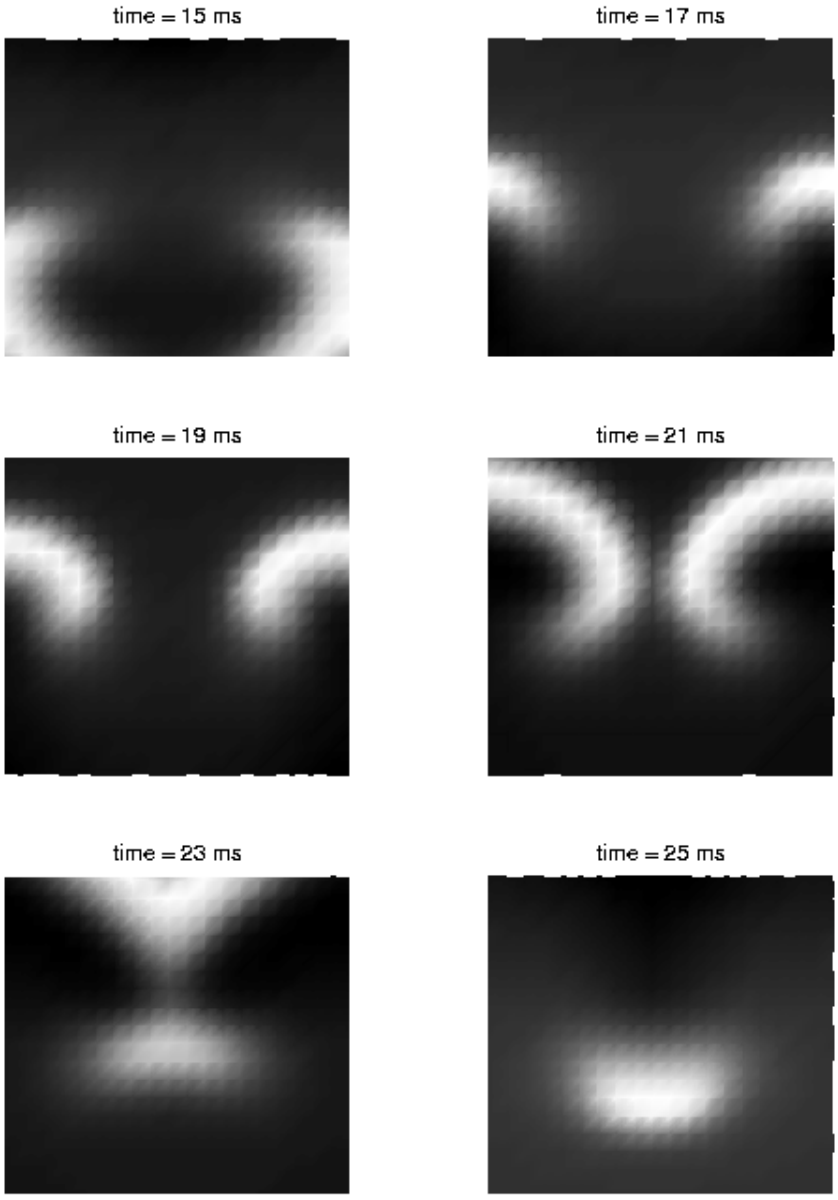

(b)

Figure 3.18. **(continued) (b)** The second six panels show the completion of a full rotation of the spiral waves. The size of the entire domain is 20x20 and the diffusive region is 15x4. The simulation was performed using a 2-D ADI method coupled to the 1-D implicit-explicit method of Hines [26] with $\Delta t = 0.01$ and $\Delta x = 0.05$

orbit underlying the transient reflection undergoes a period doubling bifurcation, robust stable oscillations could be produced. These stable oscillation are certainly a potential mechanism for the arrhythmic behavior mentioned above. Also, Because reentrant arrhythmias in the ventricular and atrial myocardium have been linked to spiral waves, the reflection mechanism for inducing spiral waves that we have demonstrated is a viable mechanism for producing these often fatal arrhythmias. In fact, it is perhaps the most viable mechanism to be proposed to date.

There is one possible point of contention concerning the applicability of our results on reflection to cardiac dynamics. Reflection seems to be exhibited much more readily in type I excitable systems than type II systems and it is generally considered that most ionic models of the electrical activity in cardiac tissue do not have type I excitability [4, 15, 44]. However, this is only definitely the case when the model is in its normal resting state. Slight modifications of these models (in order to mimic pathological changes in tissue or simply make them more realistic) may very well produce type I behavior. Also, the system could exhibit true threshold behavior in various states of recovery, and one only needs to study the response to premature stimulation to uncover this behavior. In fact, a numerical simulation of a sucrose gap experiment reflection demonstrated reflection using a slightly modified version of the Difrancesco-Noble model [8]. The simulated data showed the membrane potential on the distal side of the gap hovering around an apparent threshold prior to excitation in a way that is characteristic of type II excitability. Furthermore, this behavior was seen over larger parameter ranges following periodic stimulation. Therefore, before a definitive claim is made either way, a systematic study must be performed to classifying excitability dynamics in various ionic model under various conditions.

REFERENCES

[1] M. Akhtar, *Atrioventricular nodal reentry*, Circulation, 75 (1987), pp. III 26–30.

[2] J. C. Alexander, *Spontaneous oscillations in two 2-component cells coupled by diffusion*, J. Math. Biol., 23 (1986), pp. 205–219.

[3] D. G. Aronson and H. F. Weinberger, *Nonlinear diffusion in population genetics, combustion and nerve propagation*, in Lecture Notes in Mathematics, London, 1975, Springr-Verlag, pp. 5–49.

[4] G. W. Beeler and H. Reuter, *Reconstruction of the action potential of myocardial fibres*, J. Physiol. (London), 268 (1977), pp. 177–210.

[5] J. Belair and P. Holmes, *On linearly coupled relaxation oscillators*, Quart. Appl. Math., 42 (1984), pp. 193–219.

[6] J. Billette, F. Amellal, J. Zhao, and A. Shier, *Relationship between different recovery curves representing rate-dependent AV nodal function in rabbit*, J. Electrovasc. Electrophysiol., 5 (1994), pp. 63–75.

[7] J. J. C. Antzelevitch and G. K. Moe, *Characteristics of reflection as a mechanism of reentrant arrhythmias and its relationship to parasystole*, Circulation, 61 (1980), pp. 182–191.

[8] C. Cabo and R. C. Barr, *Reflection after delayed excitation in a computer model of a single fiber*, Circ. Res., 71 (1992), pp. 260–270.

[9] C. Cabo, A. M. Pertsov, J. M. Davidenko, W. T. Baxter, R. A. Gray, and J. Jalife, *Vortex-shedding as a precursor of turbulent ellecrical activity in cardiac muscle*, Biophys. J., 70 (1996), pp. 1105–1111.

[10] P. S. Chen, P. D. Wolf, E. G. Dixon, N. Danieley, D. W. Frazier, W. Smith, and R. Ideker, *Mechanism of ventricular vulnerability to single premature stimuli in open-chest dogs*, Circ. Res., 62 (1988), pp. 1191–1209.

[11] D. R. Chialvo and J. Jalife, *Nonlinear dynamics of cardiac excitation and impulse propagation*, Nature, 330 (1987), pp. 749–752.

[12] M. Courtemanche and A.T.Winfree, *Re-entrant rotating waves in a Beeler-Reuter-based model of 2-dimensional cardiac electrical activity.*, Int. J. Bif. and Chaos, 1 (1991), pp. 431–444.

[13] A. Davidenko, J.M. Pertsov, R. Salomontsz, W. Baxter, and J. Jalife, *Stationary and drifting spiral waves of excitation in isolated cardiac muscle*, Nature, 355 (1991), pp. 349–351.

[14] M. Delmar, L. Glass, D. C. Michaels, and J. Jalife, *Ionic basis and analytical solution of the Wenckebach phenomenon in guinea pig ventricular myocytes*, Circ. Res., 65 (1989), pp. 775–788.

[15] D. DiFrancesco and D. Noble, *A model of cardiac electrical activity incorporating ionic pumps and concentration changes*, Phil. Trans. R. Soc. B, 307 (1985), pp. 353–398.

[16] E. J. Doedel, *AUTO, a program for the automatic bifurcation analysis of autonomous systems*, Cong. Numer., 30 (1981), pp. 265–384.

[17] G. B. Ermentrout and J. Rinzel, *Waves in a simple excitable or oscillatory reaction-diffusion model*, J. Math. Bio., 11 (1981), pp. 269–294.

[18] ——, *Reflected waves in an inhomogeneous excitable medium*, SIAM J. Appl. Math., 56 (1996), pp. 1107–1128.

[19] P. C. Fife and J. B. McLeod, *The approach of solutions of nonlinear diffusion equations to traveling front solutions*, Arch. Rat. Mech. Anal., 65 (1977), pp. 335–361.

[20] P. C. Fife and L. A. Peletier, *Clines induced by variable selection and migration*, Proc. R. Soc. London Ser. B, 214 (1981), pp. 99–123.

[21] R. A. Fisher, *The wave advance of advantageous genes.*, Ann. Eugen., 7 (1937), pp. 355–369.

[22] S. S. Goldstien and W. Rall, *Changes of action potential shape and velocity for changing core conductor geometry*, Biophys. J., 14 (1974), pp. 731–757.

[23] R. Gray, J. Jalife, A. Panfilov, W. Baxter, C. Cabo, and A. Pertsov, *Non-stationary vortex-like reentrant activity as a mechanism of polymorphic ventricular tachycardia in the isolated rabbit heart*, Circulation, 91 (1995), pp. 2454–2469.

[24] M. R. Guevara, *Spatiotemporal patterns of block in an ionic model of cardiac Purkinje fibre*, in From Chemical to Biological Organization, M. Markus, S. Muller, and G. Nicolis, eds., Berlin, 1988, Springer, pp. 273–281.

[25] T. T. Harkins, T. J. Lewis, and J. E. Lindsley, *Pre-steady-state analysis of ATP by Saccharomyces cerevisiae DNA topoisomerase II: Kinetic mechanism for the sequential hydrolysis of two ATP*, Biochemistry, 20 (1998), pp. 7299–7312.

[26] M. Hines, *Efficient computation of branched nerve equations*, Int. J. Biomed. Comput., 15 (1984), pp. 69–76.

[27] J. F. Howe, W. H. Calvin, and J. D. Loeser, *Impulses reflected from dorsal root ganglia and from focal nerve injuries*, Brain Research, 116 (1976), pp. 139–144.

[28] H. Ikeda and M. Mimura, *Wave-blocking phenomena in bistable reaction-diffusion systems*, SIAM J. Appl. Math., 49 (1989), pp. 515–538.

[29] J. Jalife, *The sucrose gap preparation as a model of AV nodal transmission: Are dual pathways necessary for reciprocation and AV nodal echos?*, PACE, 6 (1989), pp. 1106–1122.

[30] J. Jalife and J. Davidenko, *Spiral waves as a mechanism of reentrant excitation in isolated cardiac muscle*, in Cardiac mapping, M. Shenasta, M. Borggrefe, and B. G., eds., Mount Kisko,NY, 1993, Futura, pp. 607–623.

[31] J. Jalife and G. K. Moe, *Excitation, conduction, and reflection of impulses in isolated bovine and canine Purkinje fibers*, Circ. Res., 49 (1981), pp. 233–247.

[32] M. J. Janse, *Reentry rhythms*, in The Heart and Cardiovascular System, H. Fozzard, E. Harber, R. Jenning, A. Katz, and H. Morgan, eds., New York, 1986, Raven Press, pp. 1203–1238.

[33] M. J. Janse and A. L. Wit, *Electrophysiological mechanisms of ventricular arrhythmias resulting from myocardial ischemia and infarction*, Physiol. Rev., 69 (1989), pp. 1049–1169.

[34] R. W. Joyner, *Mechanisms of unidirectional block in cardiac tissues*, Biophys. J., 35 (1981), pp. 113–125.

[35] Y. I. Kanel', *On the stabilization of solutions of the cauchy problem for equations arising in the theory of combustion.*, Mat. Sb., 59 (1962), pp. 245–288.

[36] J. Keener, *On cardiac arrhythmias: AV conduction block*, J. Math. Biol., 12 (1981), pp. 215–225.

[37] J. P. Keener, *Dynamic patterns in excitable media*, in Lecture Notes in Mathematics 55, S. Levin, ed., Berlin, 1984, Springr-Verlag, pp. 157–169.

[38] J. P. Keener and T. J. Lewis, *The biphasic mystery: Why a biphasic shock is more effective than a monophasic shock for defibrillation*, preprint, (1998).

[39] V. I. Krinskii and A. V. Kholopov, *Echo in excitable tissue*, Biophysics, 12 (1967), pp. 524–528.

[40] V. Krinsky, A. M. Pertsov, and A. N. Reshetilov, *Study of the mechanism of initiation of ectopic excitation centre on modified Hodgkin-Huxley equations*, Biophysics, 18 (1972), pp. 271–277.

[41] V. I. Krinsky, *Mathematical models of cardiac arrythmias (spiral waves)*,

Pharm. Ther. B., 3 (1978), pp. 539–555.

[42] M. Lewis and P. Grindrod, *One-way block in cardiac tissue: a mechanism for propagation failure in Purkinje fibres*, Bull. Math. Biol., 53 (1991), pp. 881–899.

[43] T. J. Lewis and M. R. Guevara, *Chaotic dynamics in a model of the propagated cardiac action potential*, J. theor. Biol., 146 (1990), pp. 407–432.

[44] C. Luo and Y. Rudy, *A model of the ventricular cardiac action potential. depolarization, repolarization, and their interaction*, Circ. Res., 68 (1991), pp. 1501–1526.

[45] O. P. M. Feingold, D. L. Gonzalez and H. Viturro, *Phase locking, period doubling, and chaotic phenomena in externally driven excitable systems.*, Phys. Rev. A, 37 (1988), pp. 4060–4063.

[46] G. R. Mines, *On circulating excitations in heart muscle and their possible relation to tachycardia and fibrillation*, Trans. Roy. Soc. Can., 4 (1914), pp. 43–53.

[47] W. Mobitz, *Uber die unvollstandjie storung der erregungs-uberleitung zwichen vorhof und kammer des menschlichen herzens*, Zeitsch. f. d. ges. exp. Med., 41 (1924), pp. 180–237.

[48] C. Morris and H. Lecar, *Voltage oscillations in barnacle giant muscle fiber*, Biophys. J., 35 (1981), pp. 193–213.

[49] D. Noble, *A modification of the Hodgkin-Huxley equations applicable to Purkinje fiber action and pacemaker potential*, J. Physiol., 160 (1962), pp. 317–352.

[50] T. Nordhaus, *Echo-Cycles in Coupled FitzHugh-Nagumo Equations*, PhD thesis, University of Utah, 1988.

[51] H. G. Othmer, *A continuum model for coupled cells*, J. Math. Biol., 17 (1983), pp. 351–369.

[52] A. V. Panfilov and J. P. Keener, *Effects of high frequency stimulation on cardiac tissue with an inexcitable obstacle*, J. Theor. Biol., 163 (1993), pp. 439–448.

[53] J. P. Pauwelussen, *Nerve impulse propagation in a branching nerve system: A simple model*, Physica D, 4 (1981), pp. 67–88.

[54] ——, *One way traffic of pulses in a neuron*, J. Math. Biol., 15 (1982), pp. 151–171.

[55] M. H. Protter and H. F. Weinberger, *Maximum Principles in Differential Equations*, Springer-Verlag, New York, 1984.

[56] F. Ramon, R. W. Joyner, and J. W. Moore, *Propagation of action potentials in inhomogeneous axon regions*, Federation Proc., 34 (1975), pp. 1357–1363.

[57] J. Rinzel and G. B. Ermentrout, *Analysis of neural excitability and oscillations*, in Methods in Neuronal Modeling: From Synapse to Networks, C. Koch and I. Segev, eds., Cambridge, Mass., 1989, MIT Press.

[58] P. Rohani, T. J. Lewis, D. Grunbaum, and G. D. Ruxton, *Spatial self-organization in ecology: pretty pictures or robust reality?*, Trends Ecol. Evol., 12 (1997), pp. 70–74.

[59] G. J. Rozanski, J. Jalife, and G. K. Moe, *Reflected reentry in nonhomogenous ventricular muscle as a mechnism of cardiac arrhythmias*, Circulation, 69 (1984), pp. 163–173.

[60] G. H. Sharp and R. W. Joyner, *Simulated propagation of the cardiac action potentials*, Biophys. J., 31 (1980), pp. 403–423.

[61] S. Smale, *A mathematical model of two cells via Turing's equation*, in Math. in the Life Sciences 6, 1974, pp. 15–26.

[62] J. Sneyd and J. Sherratt, *On the propagation of calcium waves in an inhomogeneous medium*, SIAM J. Appl. Math., 57 (1997), pp. 73–94.

[63] J. J. Tyson, *Oscillations, bistability, and echo-waves in models of the Beloousov-Zhabotinskii reaction*, in Mathematical Approaches to Cardiac Arrhythmias, Ann. New York Acad. Sci. 316, J. Jalife, ed., New York, 1979, New York Academy of Science, pp. 279–295.

[64] J. R. Wennemark and J. P. Bandura, *Microelectrode study of Wenckebach periodicity in canine Purkinje fibers*, Am. J. Cardiol., 33 (1974), pp. 475–488.

[65] A. T. Winfree, *Sudden cardiac death, a problem in topology*, Sci. Am., 248 (1983), pp. 114–161.

[66] A. L. Wit, S. M. Dillon, J. Coromilas, A. E. Saltman, and B. Waldecker, *Anisotropic reentry epicardial border zone of myocardial infarctions*, in Mathematical Approaches to Cardiac Arrhythmias, Ann. New York Acad. Sci. 591, J. Jalife, ed., New York, 1990, New York Academy of Science, pp. 86–108.

[67] M. Xie, H. G. Othmer, and M. Watanabe, *Resonance in excitable systems under step-function forcing. II. subharmonic solutions and persistence*, Physica D, 98 (1996), pp. 75–110.

[68] J. X. Xin and J. Zhu, *Quenching and propagation of bistable reaction-diffusion fronts in multidimnesional periodic media*, Physica D, 81 (1995),

pp. 94–110.

[69] A. Xu and M. R. Guevara, *Two forms of spiral-wave reentry in an ionic model of ischemic ventricular myocardium*, Chaos, 8 (1998), pp. 157–174.

[70] Y. Zhou and J. Bell, *Study of propagation along nonuniform excitable fibers*, Math. Biosci., 119 (1994), pp. 169–203.